

***In-vitro* digestion of fat crystal-stabilized water-in-oil emulsions**

By

Vivekkumar Patel

BSc, Ryerson University, Toronto, Ontario 2017

A thesis presented to

Ryerson University

in partial fulfilment of the requirements

for the degree of MSc

in the program of Molecular Science

Toronto, Ontario, Canada

© Vivekkumar Patel, 2019

The burning igneous chest sweating in rampant fear!

Boiling meteors scattered in the sky!

The waves are waiting for the earth to embrace!

The sun waits with patience to set in the sky!

Thunder and lightning are overriding the hillock!

Fate too shivers!

AUTHOR'S DECLARATION FOR ELECTRONIC SUBMISSION OF A THESIS

I hereby declare that I am the sole author of this thesis. This is a true copy of the thesis, including any required final revisions, as accepted by my examiners.

I authorize Ryerson University to lend this thesis to other institutions or individuals for the purpose of scholarly research

I further authorize Ryerson University to reproduce this thesis by photocopying or by other means, in total or in part, at the request of other institutions or individuals for the purpose of scholarly research.

I understand that my thesis may be made electronically available to the public.

In-vitro digestion of fat crystal-stabilized water-in-oil emulsions

Vivekkumar Patel - MSc, Molecular Science

Ryerson University, 2019

Abstract

The purpose of this research was to investigate the effect of surfactant type and presence of solid fat on the stability and release characteristics of water-in-oil (W/O) emulsions subjected to simulated gastrointestinal conditions. Emulsions consisting of a 20 wt% aqueous phase dispersed in canola oil were stabilized in one of four different ways: core-shell stabilization with glycerol monostearate (GMS), network stabilization using polyglycerol polyricinoleate and solid fat added to the continuous phase (PGPR-F), combined core-shell and network stabilization using glycerol monooleate and a continuous phase fat crystal network (GMO-F) and finally, a PGPR-based liquid emulsion with no added fat. The dispersed aqueous phase of all emulsions contained 1mM methylene blue (MB), which was used as a marker to quantify emulsion breakdown and release of aqueous phase cargo. Quiescent storage at 25 °C for 30 days revealed no phase separation for the GMS, GMO-F, and PGPR-F emulsions whereas the PGPR emulsion began to phase-separate 16 h following preparation. When subjected to gastric conditions, the PGPR-F emulsion showed the lowest MB release after 60 min (0.3 % of initial load) with the other emulsions showing ~ 12 % release. In duodenal conditions, the PGPR-F and GMS emulsions showed the lowest MB release after 120 min of exposure (~ 0.5 %) followed by the PGPR (9.4 %) and GMO-F (14.6 %) emulsions, respectively. Emulsion photomicrographs taken prior to, and after, contact with simulated gastric and intestinal fluids showed that emulsion microstructure was an important contributor to emulsion stability. Overall, the PGPR-F emulsion was the most stable in both gastric and intestinal fluids. These results have shown that fat phase structuring is an important contributor to W/O emulsion breakdown behaviour in simulated gastrointestinal conditions.

Acknowledgements

I would like to express my sincerest gratitude to my advisor professor D errick Rousseau for the guidance and help throughout the past three years. Thank you, D errick, for allowing me to join the Rousseau group, continued support through the years, mentoring, and the memories shared. It is your continued support and encouragement that has allowed me to grow out of my cocoon and spread my wings. I would also like to thank Jonathan Andrade. Without your continued support and patience, this thesis would not have been possible, thank you! Thank you for believing in me when others did not. I am forever grateful for the wisdom you provided me with, and I hope to continue to grow.

I would also like to thank my committee member for their continued support and encouragement. Thank you, professor Bryan Koivisto, for providing me with novel perspectives for this thesis without which I would be lost. Thank you professor Costin Antonescu, for your support and constructive feedback allowing me and this project to grow. Thank you Nick Bellissimo, for allowing me to use your lab space and asking the difficult questions during committee meetings allowing me to learn.

I'd like to thank my family for their continued moral support, unconditional love, and for always standing by my side through thick and thin. My father, Harshad Patel has always taught me to be honorable and has never stopped me from following my dreams to pursue education. My mother, Parul Patel has taught me kindness and respect, and my sister Bhavika Patel who always stood by my side through the toughest of times, I love you all. To all my friends, Hicran Ece Akkurt, Mohit Bhandari, and Anastasiya Boutko, thank you for being by my side when the going gets tough.

Finally, to all my lab mates, I'd like to thank Selvyn, Malek, Nicole, Auke, Qing, Adrian, Jessica, and Shweta. Without you, this lab space wouldn't have been the same. Thank you for being so welcoming and accepting of my weirdness. There are a lot of memories shared throughout my time here. Thank you!

Thank you, Ryerson University, being a Ram is the ultimate honor.

Table of Contents

Author’s declaration for electronic submission of a thesis	iii
Abstract	iv
Acknowledgements	v
List of Tables	viii
List of Structures	ix
List of Figures	x
List of Acronyms	xiii
1.0 Introduction.....	1
1.1 Emulsions	1
1.2 Emulsions as delivery systems.....	1
1.3 Surfactants.....	2
1.3.1 Glycerol monostearate	3
1.3.2 Glycerol monooleate.....	4
1.3.3 Polyglycerol polyricinoleate (PGPR).....	5
1.3.4 Food fats and oils.....	6
1.4 Emulsion stabilization with fat crystals	7
1.5 Emulsion destabilization processes	8
1.6 Methylene Blue	9
1.7 The matrix effect	10
1.8 The fat crystal matrix effect	11
1.9 Digestion	11
1.9.1 <i>In-vitro</i> digestion	13
2.0 Thesis Objectives and Hypotheses.....	15
3.0 Materials and Methods.....	16
3.1 Materials.....	16
3.2 Emulsion preparation	16

3.3 Emulsion stability.....	17
3.3.1 Droplet size determination.....	17
3.4 Recovery yield.....	18
3.5 Release during simulated <i>in-vitro</i> gastrointestinal digestion environments.....	19
3.6 Microscopy.....	22
3.7 Statistical analyses.....	22
4.0 Results and Discussion	23
4.1 MB, emulsion stability, and microstructure	23
4.2 Oral Digestion	27
4.3 Effect of environment on MB release	27
4.4 MB release from tests emulsions in SGF.....	38
4.5 MB release from tests emulsions in SIF.....	41
4.6 Mechanistic considerations	45
5.0 Overall conclusion	49
6.0 Future work.....	50
Appendix.....	51
Method development & Initial emulsion properties	51
Figures and photomicrographs	53
References.....	80

List of Tables

Table 1. Emulsion continuous oil phase composition of the test W/O emulsions..... 17

Table 2. Name and composition of conditions and release fluid used throughout this study. Note the incremental complexity of the fluids. Final test fluids are the SGF and SIF..... 21

Table 3. Comparison of the $D_{3,3}$ and sigma (σ) values of the unloaded and MB-loaded emulsions. All data are mean for $n = 3 \pm$ standard deviation. Statistical analyses (95% confidence) are shown for differences in droplet size and σ : within-column (ANOVA/Tukey, superscript letters) and between-column (Student's T test, superscript numbers). 25

Table 4. Recovery yield of MB from entrapped aqueous phase of emulsions on the day they were prepared. All data are means for $n = 3 \pm$ standard deviation. No statistical differences were observed (ANOVA $p > 0.05$ within emulsion types). 26

List of Structures

Structure 1. Chemical structure of glycerol monostearate. ⁴	4
Structure 2. Chemical structure of glycerol monooleate. ⁴	4
Structure 3. The molecular structure of a typical polyglycerol polyricinoleate molecule. ^{4,38}	5
Structure 4. The chemical structure of a typical TAG (SSS – tristearin) as commonly found in fully hydrogenated soybean oil. ⁴²	7
Structure 5. The chemical structure of thiazine dye methylene blue (MB). ⁵²	10

List of Figures

Figure 1. The 4 emulsion stabilization schemes used in the present study: (A) core-shell; (B) combined core-shell and continuous fat crystal network; (C) continuous phase fat crystal network only, and (D) liquid-state stabilization. ⁴	3
Figure 2. Surfactant vs. core-shell type emulsion stabilization.	7
Figure 3. Mechanisms by which an emulsion can destabilize. ⁶	8
Figure 4. Static <i>in-vitro</i> gastrointestinal set-up. Typical static sequential <i>in-vitro</i> gastrointestinal set-up where an emulsion is mixed with simulated oral fluid (SOF, 1:1 emulsion to SOF), gastric (1:1 SOF to SGF) and intestinal (1:3 SGF to SIF) digestion ensues. ¹⁸	13
Figure 5. Standard curve of absorbance of methylene blue at 664 nm as a function of concentration	19
Figure 6. Example of recovery yield determination of MB through aqueous phase extraction for a 4 wt.% GMS emulsion.....	19
Figure 7. The <i>in-vitro</i> MB release set-up where Falcon tubes are loaded with a) bolus and release medium.	20
Figure 8. Microstructure comparison of emulsions. Micrographs taken in brightfield light microscopy at RT - GMS (A), GMO-F (C), PGPR-F (E), and PGPR (G). The corresponding images in polarized light are also shown - GMS (B), GMO-F (D), PGPR-F (F), and PGPR (H). Insets are zoomed-in views of boxed areas. Scale bars = 50 μm	24
Figure 9. TSI of the four test emulsions. Statistically significant differences between fat phase compositions are denoted by different letters (ANOVA/Tukey, $p < 0.05$).	27
Figure 10. MB release from emulsions subjected to Condition 1 – SGF. All data are means based on $n = 3 \pm$ standard deviation. Between each fat phase composition, the letters denote significant differences within the same time point (30 or 60 min – lowercase and uppercase, respectively) (ANOVA/Tukey – $p < 0.05$). * denotes significant differences between time points (30 and 60 min) within the same fat phase composition (Student’s T-test, $p < 0.05$).	28
Figure 11. MB release from emulsions subjected to Condition 1 – SIF. All data are means based on $n = 3 \pm$ standard deviation. Between each fat phase composition, the letters denote significant differences within the same time point (30 or 60 min – lowercase and uppercase, respectively) (ANOVA/Tukey – $p < 0.05$). * denotes significant differences between time points (30 and 60 min) within the same fat phase composition (Student’s T-test, $p < 0.05$).	29

Figure 12. Microstructure post 60 minutes of the four test emulsions subjected to a 1:3 dilution (condition 1 – SIF). Images were captured in brightfield mode at 25 °C. GMS (A), GMO-F (B), PGPR-F (C), and PGPR (D). Scale bars = 50 μm. 30

Figure 13. MB release from emulsions subjected to Condition 2 – SGF. All data are means based on n = 3 ± standard deviation. Between each fat phase composition, the letters denote significant differences within the same time point (30 or 60 min – lowercase and uppercase, respectively) (ANOVA/Tukey – p < 0.05). * denotes significant differences between time points (30 and 60 min) within the same fat phase composition (Student’s T-test, p < 0.05). 31

Figure 14. MB release from emulsions subjected to Condition 2 – SIF. All data are means based on n = 3 ± standard deviation. Between each fat phase composition, the letters denote significant differences within the same time point (30 or 60 min – lowercase and uppercase, respectively) (ANOVA/Tukey – p < 0.05). * denotes significant differences between time points (30 and 60 min) within the same fat phase composition (Student’s T-test, p < 0.05). 32

Figure 15. Brightfield and polarized light microscopy of the PGPR-F emulsion subjected to Condition 2 – SGF for 60 min. Red arrow indicates coarse emulsification. (A) Brightfield; (B) PLM. Scale bars = 50 μm. 33

Figure 16. Brightfield and polarized light microscopy of the GMS emulsion subjected to Condition 2 – SGF (A, B) or Condition 2 – SIF (C, D) for 60 min. (A, C) Brightfield; (B, D) PLM. Scale bars = 50 μm. 34

Figure 17. MB release from emulsions subjected to Condition 3 – SGF. All data are means based on n = 3 ± standard deviation. Letters denote significant differences within the same time point (30 or 60 min) between each fat phase composition (ANOVA/Tukey – p < 0.05). * denotes significant differences between time points (30 and 60 min) within the same fat phase composition (Student’s T-test, p < 0.05). 35

Figure 18. MB release from emulsions subjected to Condition 3 – SIF. All data are means based on n = 3 ± standard deviation. Letters denote significant differences (ANOVA/Tukey p < 0.05) within the same time point amongst the fat phase compositions. 36

Figure 19. Brightfield microscopy of the 4 test emulsions subjected to Condition 3 – SIF for 30 minutes (left-hand column) or 120 min (right-hand column). A & B - GMS; C & D – GMO – F; E & F – PGPR-F; and G & H – PGPR. Red arrows in A and B indicate core-shell emulsion breakdown. Scale bars = 50 μm. 37

Figure 20. MB release from emulsions subjected to SGF. All data are means based on $n = 3 \pm$ standard deviation. Between each phase composition, the letters denote significant differences within the same time point (30 or 60 min – lowercase and uppercase, respectively) (ANOVA/Tukey – $p < 0.05$). * denotes significant differences between time points (30 and 60 min) within the same fat phase composition (Student’s T-test, $p < 0.05$). 39

Figure 21. Brightfield light microscopy of the 4 test emulsions subjected to SGF for 60 minutes. A - GMS; B – GMO-F; C – PGPR-F; and D – PGPR. Scale bars = 50 μm 40

Figure 22. MB release from emulsions subjected to SIF. All data are means based on $n = 3 \pm$ standard deviation. Letters denote significant differences (ANOVA/Tukey $p < 0.05$) within the same time point amongst the fat phase compositions. 41

Figure 23. Brightfield microscopy of the 4 test emulsions subjected to SIF for 30 minutes (left-hand column) or 120 min (right-hand column). A & B - GMS; C & D – GMO – F; E & F – PGPR-F; and G & H – PGPR. Scale bars = 50 μm 43

Figure 24. MB recovery as a function of time in bile salt solution over 120 minutes at 37 °C and 6 rpm. All data are means based on $n = 3 \pm$ standard deviation. 44

Figure 25. Possible mechanism of MB release in SGF for GMS (A), PGPR-F (B), GMO-F (C), and PGPR (D) emulsions. The symbol  at the interface represents GMS and GMO, and  represents MB. 46

Figure 26. Possible mechanism(s) of MB release in SIF for GMS (A), PGPR-F (B), GMO-F (C), and PGPR (D) emulsions. The symbol  at the interface represents GMS and GMO,  represents bile salts, and  represents MB. Micelles are shown as large for visualization only.. 47

List of appendices

Table A 1. Formulation parameters. Tabulated experimental and optimized phase compositions. 51

Figure A 1. 4 wt.% GMS emulsion with a ~ 60 μm average droplet size. Left is brightfield image taken on inverted light microscope with the corresponding polarized light image of the same field of view at right. Images were captured 25 °C. Scale bars = 50 μm 51

Figure A 2. W/O emulsions made with 1-4 wt% PGPR aged 16h at room temperature. Emulsions were prepared using magnetic stirring at 200-250 rpm. 52

Figure A 3. pfg-NMR aqueous droplet size distributions of test emulsions loaded with 1mM MB. All data are mean for $n = 3 \pm$ standard deviation (error bars are omitted for clarity)..... 53

Figure A 4. Vials of emulsions loaded with 1mM MB (top row) and unloaded emulsions (bottom row) stored at 25 °C for 30 days. 54

Figure A 5. Microstructure of GMS-based emulsion in Condition 1 taken in brightfield and polarized light microscopy at 25 °C at 30 minutes (A, C), and 60 minutes (B, D). Scale bars = 50 μm 55

Figure A 6. Microstructure of GMO-F emulsion in condition 1 taken in brightfield and polarized light microscopy at 25 °C at 30 minutes (A, C), and 60 minutes (B, D). Scale bars = 50 μm 56

Figure A 7. Microstructure of PGPR-F emulsion in condition 1 taken in brightfield and polarized light microscopy at 25 °C at 30 minutes (A, C), and 60 minutes (B, D). Scale bars = 50 μm 57

Figure A 8. Microstructure of PGPR emulsion in condition taken in brightfield and polarized light microscopy at 25 °C at 30 minutes (A), and 60 minutes (B). Scale bars = 50 μm 58

Figure A 9. Microstructure of GMS emulsion in condition 2 – SGF taken in brightfield and polarized light microscopy at 25 °C at 30 minutes (A, C), and 60 minutes (B, D). Scale bars = 50 μm 59

Figure A 10. Microstructure of GMS emulsion in condition 2 – SIF taken in brightfield and polarized light microscopy at 25 °C at 30 minutes (A, B), and 60 minutes (B, D). Scale bars = 50 μm 60

Figure A 11. Microstructure of GMO-F emulsion in condition 2 – SGF taken in brightfield and polarized light microscopy at 25 °C at 30 minutes (A, C), and 60 minutes (B, D). Scale bars = 50 μm 61

Figure A 12. Microstructure of GMO-F emulsion in condition 2 – SIF taken in brightfield and polarized light microscopy at 25 °C at 30 minutes (A, B), and 60 minutes (B, D). Scale bars = 50 μm.	62
Figure A 13. Microstructure of PGPR-F emulsion in condition 2 – SGF taken in brightfield and polarized light microscopy at 25 °C at 30 minutes (A, C), and 60 minutes (B, D). Scale bars = 50 μm.	63
Figure A 14. Microstructure of PGPR-F emulsion in condition 2 – SIF taken in brightfield and polarized light microscopy at 25 °C at 30 minutes (A, B), and 60 minutes (B, D). Scale bars = 50 μm.	64
Figure A 15. Microstructure of PGPR emulsion in condition 2 – SGF taken in brightfield and polarized light microscopy at 25 °C at 30 minutes (A, B), and 60 minutes (B, D). Scale bars = 50 μm.	65
Figure A 16. Microstructure of PGPR emulsion in condition 2 – SIF taken in brightfield and polarized light microscopy at 25 °C at 30 minutes (A, B), and 60 minutes (B, D). Scale bars = 50 μm.	65
Figure A 17. Microstructure of GMS emulsion in condition 3 – SGF taken in brightfield and polarized light microscopy at 25 °C at 30 minutes (A, B), and 60 minutes (B, D). Scale bars = 50 μm.	66
Figure A 18. Microstructure of GMO-F emulsion in condition 3 – SGF taken in brightfield and polarized light microscopy at 25 °C at 30 minutes (A, B), and 60 minutes (B, D). Scale bars = 50 μm.	67
Figure A 19. Microstructure of PGPR-F emulsion in condition 3 – SGF taken in brightfield and polarized light microscopy at 25 °C at 30 minutes (A, B), and 60 minutes (B, D). Scale bars = 50 μm.	68
Figure A 20. Microstructure of PGPR emulsion in condition 3 – SGF taken in brightfield and polarized light microscopy at 25 °C at 30 minutes (A, B), and 60 minutes (B, D). Scale bars = 50 μm.	69
Figure A 21. Microstructure of GMS emulsion in condition 3 – SIF taken in brightfield and polarized light microscopy at 25 °C at 30 minutes (A, D), 60 minutes (B, E), and 120 minutes (C, F). Scale bars = 50 μm.	70

Figure A 22. Microstructure of GMO-F emulsion in condition 3 – SIF taken in brightfield and polarized light microscopy at 25 °C at 30 minutes (A, D), 60 minutes (B, E), and 120 minutes (C, F). Scale bars = 50 μm.	71
Figure A 23. GMO-F destabilization via condition 3 – SIF showing separation of an oil layer.	71
Figure A 24. Microstructure of PGPR-F emulsion in condition 3 – SIF taken in brightfield and polarized light microscopy at 25 °C at 30 minutes (A, D), 60 minutes (B, E), and 120 minutes (C, F). Scale bars = 50 μm.	72
Figure A 25. Microstructure of PGPR emulsion in condition 3 – SIF taken in brightfield and polarized light microscopy at 25 °C at 30 minutes (A, D), 60 minutes (B, E), and 120 minutes (C, F). Scale bars = 50 μm.	72
Figure A 26. Microstructure of GMS emulsion in SGF taken in brightfield and polarized light microscopy at 25 °C at 30 minutes (A, C), 60 minutes (B, D). Scale bars = 50 μm.	73
Figure A 27. Microstructure of GMO-F emulsion in SGF taken in brightfield and polarized light microscopy at 25 °C at 30 minutes (A, C), 60 minutes (B, D). Scale bars = 50 μm.	74
Figure A 28. Microstructure of PGPR-F emulsion in SGF taken in brightfield and polarized light microscopy at 25 °C at 30 minutes (A, C), 60 minutes (B, D). Scale bars = 50 μm.	75
Figure A 29. Microstructure of PGPR emulsion in SGF taken in brightfield and polarized light microscopy at 25 °C at 30 minutes (A), 60 minutes (B). Scale bars = 50 μm.	76
Figure A 30. Microstructure of GMS emulsion in SIF taken in brightfield and polarized light microscopy at 25 °C at 30 minutes (A, D), 60 minutes (B, E), and 120 minutes (C, F). Scale bars = 50 μm.	77
Figure A 31. Microstructure of GMO-F emulsion in SIF taken in brightfield and polarized light microscopy at 25 °C at 30 minutes (A, D), 60 minutes (B, E), and 120 minutes (C, F). Scale bars = 50 μm.	78
Figure A 32. Microstructure of PGPR-F emulsion in SIF taken in brightfield and polarized light microscopy at 25 °C at 30 minutes (A, D), 60 minutes (B, E), and 120 minutes (C, F). Scale bars = 50 μm.	79
Figure A 33. Microstructure of PGPR emulsion in SIF taken in brightfield and polarized light microscopy at 25 °C at 30 minutes (A), 60 minutes (B), and 120 minutes (C). Scale bars = 50 μm.	79

List of Acronyms

BS – Bile Salts

DSD – Droplet Size Distribution

FHSO – Fully Hydrogenated Soybean Oil

GMO – Glycerol Monooleate

GMO-F – Glycerol Monooleate with Fully Hydrogenated Soybean Oil

GMS – Glycerol Monostearate

MB – Methylene Blue

O/W – Oil-in-Water

PGPR – Polyglycerol Polyricinoleate

PGPR-F – Polyglycerol Polyricinoleate with Fully Hydrogenated Soybean Oil

SOF – Simulated Oral Fluid

SGF – Simulated Gastric Fluid

SIF – Simulated Intestinal Fluid

TSI – Turbiscan Stability Index

W/O – Water-in-Oil

1.0 Introduction

1.1 Emulsions

Emulsions are defined as colloidal systems where two or more immiscible liquids are combined to form a dispersion where one is dispersed as droplets within the other.¹⁻³ Oil-in-water (O/W) emulsions (dairy cream, salad dressings, etc.) are generally fluid and may contain a crystalline fat phase whereas food-related water-in-oil (W/O) emulsions (e.g., butter and margarine) are oil-continuous and often solid-like. This latter type of emulsion is increasingly being sought given its potential to encapsulate labile, water-soluble compounds such as amino acids, vitamins, aromas, flavours, and peptides.^{4,5}

In its simplest form, a quiescent mixture of oil and water will form a phase-separated system with the lower density oil atop the water as this configuration minimizes the thermodynamically unfavourable contact area between the two phases. To assist in emulsion formation and subsequent stabilization, surface-active molecules that lower the interfacial tension between the oil and water phases and reduce droplet-droplet encounters are commonly used.^{3,6-9} Their properties are discussed in section 1.3.

1.2 Emulsions as delivery systems

It is well established that emulsion-based delivery systems can provide significant protection to bioactive ingredients against degradation due to oxidation (photo-, air or otherwise) and passage through the gastrointestinal tract (GIT).¹⁰⁻¹² As a result, the use of emulsions for the delivery of labile aqueous compounds along with controllable digestion behaviour is increasingly being sought out.¹³ Emulsions of the W/O and O/W types may be used as delivery vehicles for aqueous and lipid-soluble compounds, respectively. The latter can be used for the delivery of lipophilic materials, for the slow and sustained release of active materials within the bloodstream, and for delivery to targeted tissues in the body whereas W/O emulsions are used for the delivery of water-soluble bioactive compounds, as presently studied. The key properties that emulsions must offer as delivery systems include: i) tailored controlled release properties, ii) the protection of emulsified material (e.g., against oxidation) and iii) the lengthy (ideally +1 year) kinetic stability of the emulsion. Some advantages of emulsions as delivery systems include the possibility of high

entrapment rates of active substances and simple preparation using a single dispersion step, which can easily be scaled-up for industrial production.

Double emulsions are systems in which both W/O and O/W emulsions exist simultaneously. In case of water-in-oil-in-water ($W_1/O/W_2$) emulsions, the initial aqueous phase (W_1) is dispersed in a continuous oil phase and it is stabilized with a lipophilic surfactant residing within the oil. This initial W_1/O emulsion is subsequently dispersed (aided by hydrophilic surfactants) throughout a larger outer aqueous phase (W_2).¹⁴⁻¹⁶ In $W_1/O/W_2$ emulsions, nutrients, flavonoids, drugs, and other labile compounds can be effectively encapsulated within the internal aqueous or oil phases while being protected from harsh gastrointestinal conditions (e.g., changes in pH, ionic strength or presence of bile salts).¹⁷⁻²⁰ In this regard, numerous compounds such as salts, sugars, acids, bases,²⁰ vitamin D₃²¹, and vitamin B₁₂¹⁶ have been explored. Multiple emulsions can be used as delivery systems as they provide protection of the inner encapsulated compounds (in W_1) by minimizing contact with other hydrophilic ingredients, and the possibility of controllable release based on changes in local environment (e.g., in temperature, pH, etc.).^{22,23} The W/O emulsions in the present study were coarsely emulsified into double emulsions of the $W_1/O/W_2$ type, as discussed later.

1.3 Surfactants

Surfactants are amphiphilic molecules that consist of polar and non-polar moieties, which render them surface-active. This implies that they preferentially adsorb to the oil-water interface, with their polar groups oriented towards the aqueous droplet surface and nonpolar groups residing in the oil phase. There are numerous categories of small-molecule surfactants that differ based on compositional factors such as hydrophile-lipophile balance (HLB), molecular weight, molecular shape, radius of gyration, surface activity, critical packing parameter, and critical micelle concentration (CMC). Depending on the application, surfactants will be used to: i) lower the interfacial tension at the oil-water interface thereby greatly facilitating emulsion formation, and/or ii) stabilize the resulting emulsion by preventing droplet coalescence, creaming/sedimentation and subsequent phase separation.⁷

Surfactants are classified by their HLB value, which is a semi-empirical scale ranging from 1 to 20 that quantifies the contributions of the hydrophilic and lipophilic moieties of the molecule^{24,25}. The HLB value can aid in determining where surfactants will be located (i.e., water, oil, or

interface) and by extension, which type of emulsion is favoured (W/O for low HLB and O/W for high HLB).²⁶ The HLB value is calculated based on the following:

$$\text{HLB} = 7 + \sum(\text{hydrophilic group numbers}) - (\text{lipophilic group numbers}) \quad (1)$$

Surfactants for W/O systems have low HLB values, meaning they are mainly lipophilic and will promote the formation of oil-continuous emulsions.²⁷ In the present study, three low HLB surfactants were selected - these differed in molecular weight and melting point. The monoacylglycerols (MAGs) glycerol monostearate (GMS) and glycerol monooleate (GMO) were both used, these differing in melting point. The polymeric surfactant polyglycerol polyricinoleate (PGPR) was also used. In addition, fully hydrogenated soybean oil (FHSO) was used to add solid fat to the continuous oil phase for emulsions containing GMO or PGPR (Figure 1). These four systems provided emulsions that were either stabilized as a core-shell type emulsion (Figure 1A), a combined core-shell and continuous fat crystal network (Figure 1B), a continuous phase network only (Figure 1C) and a fully liquid emulsion with no solid species (Figure 1D). A brief description of the components used in the 4 formulations are presented in the following sections.

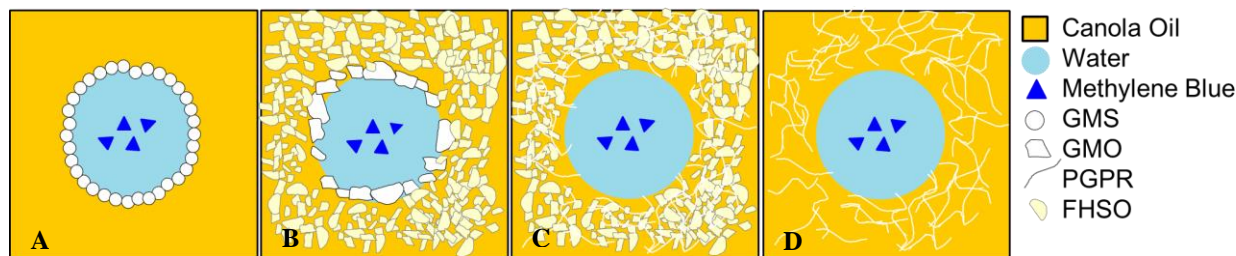
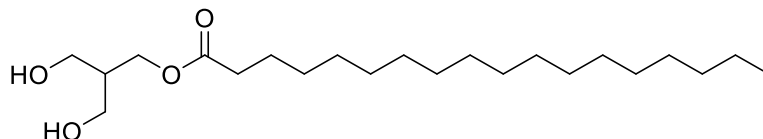


Figure 1. The 4 emulsion stabilization schemes used in the present study: (A) core-shell; (B) combined core-shell and continuous fat crystal network; (C) continuous phase fat crystal network only, and (D) liquid-state stabilization.⁴

1.3.1 Glycerol monostearate

GMS is a MAG consisting of stearic acid esterified at the sn-1, 2 or 3 position that is solid at room temperature (Structure 1).²⁸ Given the dominance of the hydrophobic stearic acid over that of the hydrophilic glycerol, its HLB value is ~ 4.^{28,29}

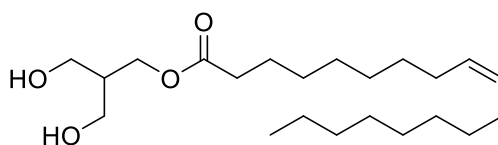


Structure 1. Chemical structure of glycerol monostearate.⁴

GMS has been used as a lubricant, emollient, protective coating in hygroscopic powders, solidifier, dispersant, and for drug release in applications for the pharmaceutical, cosmetics, plasticizer, and other industries.^{28,30} The amphiphilic nature of GMS as well as its small molecular weight enables it to readily self-assemble at the oil-water interface and form a number of mesophases.^{31,32} The solid crystal phase formed by GMS allows it to form highly-stable core-shell type emulsion droplets where dispersed aqueous droplets are surrounded by a crystalline shell.^{26,33} When present at the oil-water interface, GMS molecules are organized with the polar head group oriented towards the water, and acyl chain towards the oil, thereby lowering the interfacial tension.^{30,34} Bulk GMS readily solidifies and can exist in different crystalline phases, with melting points at ~ 30 °C, and ~ 50 °C, and 75 °C.³⁵

1.3.2 Glycerol monooleate

Pure GMO (melting point $35\text{--}37$ °C) consists of an oleic acid esterified to glycerol at the sn-1, 2 or 3 position. It differs from GMS due to the presence of oleic acid, which has a *cis* double bond on the n-9 carbon (Structure 2), which confers a much lower melting point (~ 35 °C) than its stearic acid-based counterpart.³⁶



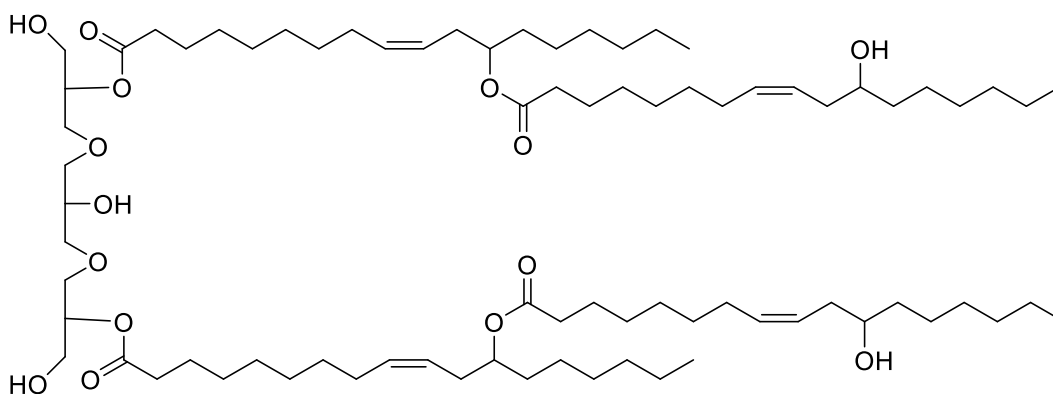
Structure 2. Chemical structure of glycerol monooleate.⁴

GMO is generally synthesized via esterification of glycerol with oleic acid in the presence of catalytic aluminum oxide.³⁷ The two free -OH groups on the glycerol provide polarity to the headgroup allowing for hydrogen bond formation in aqueous environments during emulsification.³⁶ The acyl chain (hydrocarbon backbone) is lipophilic and dominates the properties of GMO, namely its ability to be solubilized in vegetable oil and its low HLB (3-4).³⁶ GMO is

generally recognized as safe (GRAS - 21CFR184.1324) due to its nontoxicity, biocompatibility and biodegradability.³⁶

1.3.3 Polyglycerol polyricinoleate (PGPR)

PGPR is a powerful emulsifier that readily lowers the oil-water interfacial tension to values near 1 mN/m even when used at low concentrations. Given its dominant lipophilic character, it has a low HLB value and is readily soluble in oil. Its key food application is in confectionery applications where it is used in lower-quality chocolates for its ability to reduce the viscosity of molten chocolates. It is also used to prepare industrial margarines, given its ability to generate W/O emulsions with micron-scale droplets.^{38,39}



Structure 3. The molecular structure of a typical polyglycerol polyricinoleate molecule.^{4,38}

PGPR is a non-ionic surfactant consisting of a mixture of esters varying in the degree of polymerization (MW ~ 1500 g/mol), degree of esterification, position of esterification, and is synthesized when the fatty acids in castor oil are condensed with polyglycerol.³⁸ PGPR has been deemed safe for consumption (GRAS - GRN 000179) and can be considered ideal for certain food applications (e.g., low fat margarine systems with higher water content).

Given its polymeric nature, PGPR enhances emulsion stability by lowering the interfacial tension and by providing effective steric stabilization due to its long polymer strands.^{2,4,21} PGPR's ability to stabilize emulsions has been studied extensively.^{21,40} For example, Su et al. demonstrated the synergistic effects of PGPR in the presence of dairy protein that resulted in lowered concentrations of PGPR needed for effective emulsion stability. Previously, it was demonstrated that PGPR

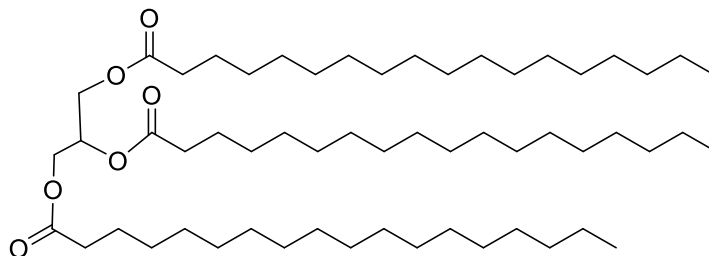
interacts with proteins by changing the oil-water interfacial tension and elasticity.²¹ The combination of solid fat and PGPR has been used to stabilize W/O emulsions.^{41,42}

1.3.4 Food fats and oils

Triacylglycerols (TAGs) are the dominant lipid form in food lipids, these consisting of three fatty acids esterified to a glycerol backbone. The nature of the constituent fatty acids (acyl chain length, degree of unsaturation) and their positional distribution (sn-1, 2 or 3) will dictate their physical properties, digestibility and impact on human health.

Food fats and oils are incorporated into different processed foods as ingredients (e.g., milkfat in yogurt and cheese, vegetable oil in salad dressing and animal fat in sausages), during food preparation as bulk materials (frying oil or butter on toast) or exist in naturally-occurring foods in the form of emulsions where oil droplets are encased within a continuous liquid or solid matrix (e.g., dairy milk, seeds, and nuts). Fats and oils thus exist in a variety of forms in the bulk or within a food matrix.

Interesterification, hydrogenation, and fractionation are three processes available to food manufacturers to tailor the physical, and chemical properties of food lipids. Each operation is based on different principles to attain its goal. Fractionation is a physical separation process based on the distinct crystallization temperature of different TAGs; thus, crystallization at a set temperature is used to separate TAGs that have solidified from those that remain liquid.⁴² Hydrogenation is a chemical process leading to the saturation of double bonds present in fatty acids in the presence of hydrogen gas and a metal catalyst to harden fats for use as margarine and shortening base stocks, but also almost always results in the formation of *trans* unsaturated fatty acids. The usage of hydrogenated fats is declining due to the negative health effects (e.g., heart disease) of hydrogenated fats enriched in *trans* fatty acids and governmental pressures to reduce *trans*-fat levels in food product. Finally, interesterification causes a fatty acid redistribution within and among TAGs, which can lead to substantial changes in lipid functionality such as melting point or profile. Fractionation and/or interesterification are common unit operations for the production of a low or “zero-*trans*” fats with desirable physical properties (e.g., a higher melting point). The fat used in this study, fully hydrogenated soybean oil (FHSO), primarily consists of TAGs based on stearic acid and palmitic acid, and combinations thereof (Structure 4).⁴²



Structure 4. The chemical structure of a typical TAG (SSS – tristearin) as commonly found in fully hydrogenated soybean oil.⁴²

1.4 Emulsion stabilization with fat crystals

Fat crystals may stabilize W/O emulsions in one of three ways: interfacially-bound crystals, network stabilization, and a combination thereof.^{6,43} Core-shell type emulsion stabilization is an extension of Pickering stabilization where solid particles replace amphiphilic surfactants at the interface (Figure 2).^{8,44} This form of stabilization often results from direct solidification of high-melting surfactants at the oil-water interface and/or interfacial crystallization of TAGs to result in the formation of a shell around the droplet.⁴⁴ Core-shell stabilized emulsions typically show higher resilience against coalescence when compared to emulsions stabilized by amphiphilic molecules such as phospholipids.⁴⁵

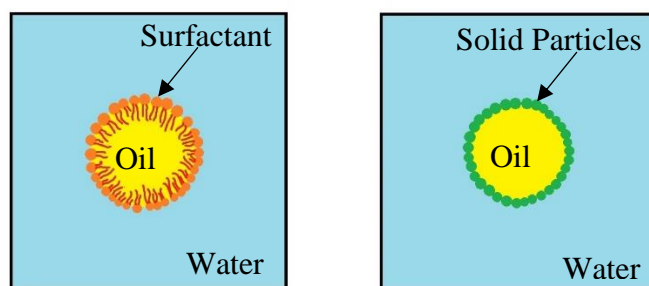


Figure 2. Surfactant vs. core-shell type emulsion stabilization.

Network stabilization results from the presence of a fat crystal network dispersed throughout the continuous phase, and is typically based on commercial fats that will partly crystallize during the processing regime that an emulsion is subjected to.⁴⁶ In such networks, the emulsions are stabilized by encasing the dispersed water droplets within a continuous structure crystalline fat

network.⁴⁷ The fat crystal network, therefore, hinders emulsion breakdown by restricting movement of the dispersed phase, but does not directly interact with the droplets.⁴⁶ Finally, it is possible to have a combination of both core-shell and network stabilization, where crystals will be adsorbed to the oil-water interface and also be present as a continuous fat crystal network.⁴⁸ Their combined presence typically imparts additional rigidity and enhanced stabilization.⁴¹

1.5 Emulsion destabilization processes

Emulsions typically destabilize through i) creaming and sedimentation; ii) flocculation and coalescence; iii) Ostwald ripening, and iv) phase inversion (Figure 3).^{6,7}

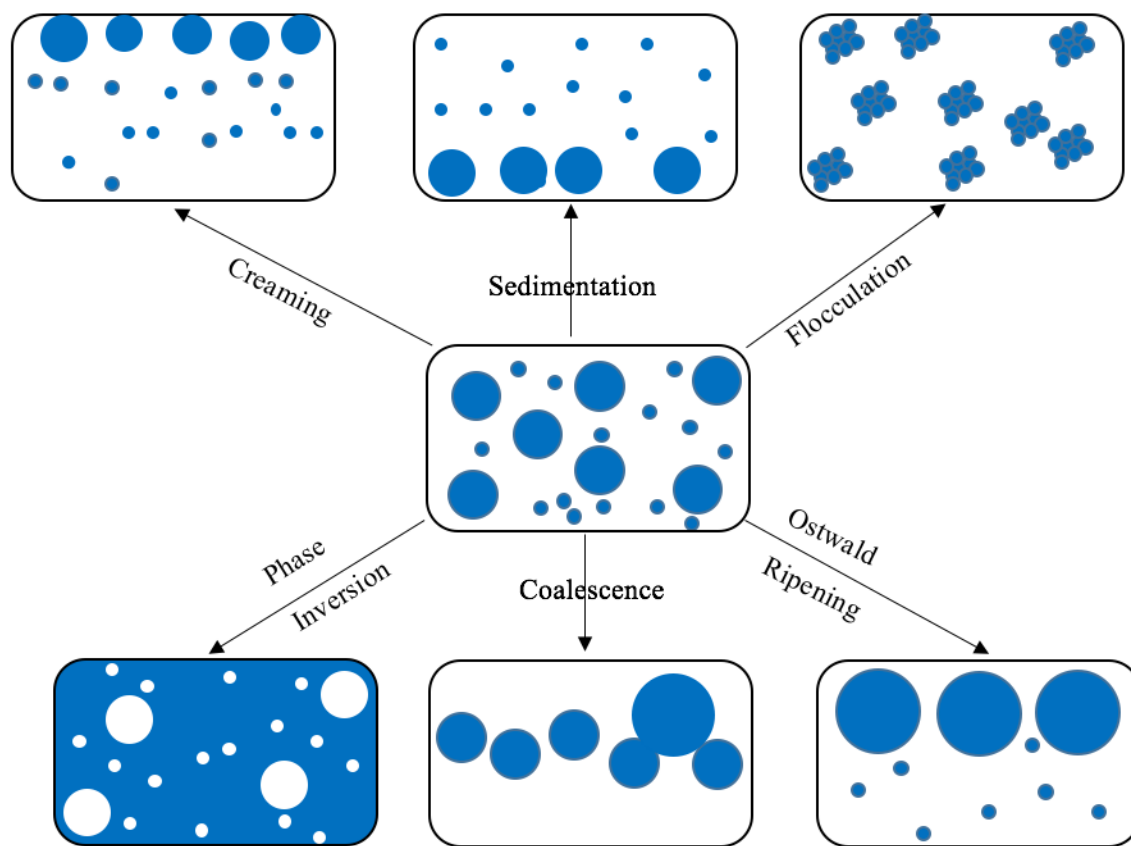


Figure 3. Mechanisms by which an emulsion can destabilize.⁶

Creaming and sedimentation occur due to the density difference between the dispersed and continuous phases, and arise due to the influence of gravity.⁷ When the dispersed droplets have a lower density than the continuous phase, they will rise, thereby resulting in creaming. Conversely, sedimentation occurs when the dispersed droplets have a higher density and as result, will settle

towards the bottom of an emulsion^{6,7} Creaming and sedimentation ultimately lead to phase separation given enough time.⁶

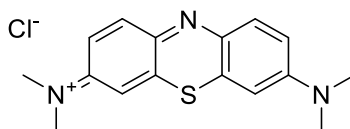
Flocculation is result of attractive and repulsive forces present within the emulsion (namely van der Waals/London dispersion forces) where droplet collisions can cause aggregation (flocculation).⁶ Dependent upon the interfacial film/structure of the emulsions, droplet collisions can cause coalescence, which is the merging of two individual droplets into a larger single droplet as a result of the interfacial film between neighbouring droplets rupturing.^{6,7}

In Ostwald ripening, mass transfer of the dispersed phase occurs from smaller droplets to larger droplets via passage through the continuous phase.⁴⁹ Large droplets therefore grow in size whereas small droplets become smaller and may disappear. The basis of Ostwald ripening is related to the solubility gradient that exists between larger and smaller droplets, that is to say, the solubility of the material within a spherical droplet increases as the droplet decreases in size.⁴⁹ The effect of this process is minimal when the mutual solubility of the oil and water phases is low enough to render the rate of mass transfer negligible, as in most food applications.^{6,7}

In the process of phase inversion, an O/W emulsion transforms into a W/O emulsion or vice-versa. The production of some foods such as butter or margarine is based on this process, while in other products, the effects of phase inversion may be undesirable. A number of factors may trigger phase inversion. These may be related to alterations in the composition or environmental conditions, such as the dispersed-phase volume fraction, the type and concentration of the emulsifier, the solvent conditions, presence of electrolytes, temperature or mechanical agitation.⁷

1.6 Methylene Blue

Water-soluble thiazine dyes such as methylene blue (MB) are used in applications such as staining/dying, release studies (from $W_1/O/W_2$ emulsions) ¹⁶, and as a visualization agent in biomedical applications.^{50,51} MB has a distinct blue colour that is easily detected both visually and spectroscopically (absorbance at 664 nm), making it an appropriate candidate for release studies (Structure 5).⁵⁰



Methylene Blue

Structure 5. The chemical structure of thiazine dye methylene blue (MB).⁵²

MB is widely studied and its spectroscopic profile is well-understood.⁵³ MB is synthesized via the oxidation of dimethyl-4-phenylenediamine in the presence of sodium thiosulfate.⁵⁴ MB has unique spectroscopic properties that are dependent upon its molecular aggregation, which will be influenced by concentration, presence of salts, and dielectric constants, pH, temperature, and the nature of the solvent.^{51,52} MB can form dimers that give it a unique spectroscopic absorption bands at 293 nm ($\pi - \pi^*$ transition) and 664 nm ($n - \pi^*$ transition) in dilute aqueous solutions.⁵¹ The spectral behaviour of MB has been extensively studied in media such as aqueous solutions containing human serum albumin, sodium lauryl sulfate, etc.^{16,51,53} Here, it was used as an aqueous marker within the W/O emulsions that were studied.

1.7 The matrix effect

The structure (or matrix) of a food is defined as the organization of its constituent molecules at multiple spatial length scales. It plays a vital role in how food interacts with the gastrointestinal tract (GIT) (e.g., bodily fluids and receptors) and the resulting release and uptake of nutrients. Most foods are complex, heterogeneous materials composed of structural elements or domains (co-)existing as solids, liquids and/or gases where length scales span < 1 nanometre to millimetres. The structure of all foods is provided by nature or imparted during processing and preparation. Food structure design is the dedicated conception and fabrication of foods in such a way as to attain specific structures, functions or properties. Beyond contributing to texture, sensory properties, shelf life and stability, control of food structure can alter the kinetics and extent of food digestion (e.g., lipid digestion). For example, nutrient absorption in peanuts in different physical forms has been found, with less fat absorbed from nuts than the butter or oil. From a food product design standpoint, lipid digestion, which largely determines the absorption of fatty acids and other

lipophilic nutrients/bioactives, can be modulated by controlling the access of lipases onto the oil-water interface via alteration of the surrounding food matrix.

1.8 The fat crystal matrix effect

The presence of fat crystals at the oil-water interface is an important consideration in the formation and stabilization of many emulsion-containing foods such as butter, margarine, and ice cream. Some studies have explored the ability of fat crystals to stabilize O/W emulsions. Of note, Kurukji et al. investigated O/W emulsions stabilized by sodium stearyl lactylate aggregates 200 nm in size adsorbed to the oil-water interface, which resulted in Pickering-type stabilization.^{55,56} Zafeiri et al. investigated the ability of O/W emulsions stabilized by solid lipid particles to withstand coalescence.⁵⁷ Our group developed surface-active solid nanoparticles using a high-melting citrated monoacylglycerol, and found that O/W emulsions stabilized by these particles were stable against coalescence for 6 months.⁵⁸

In W/O emulsions, aqueous droplets can be stabilized either by interfacially-bound fat crystals present as discrete, adsorbed particles or via an interfacial, crystalline film. The former originates from the attachment of pre-solidified crystals to the oil-water interface and the latter consists of species such as TAG or emulsifiers directly crystallized onto the droplet surface.^{4,55,59}

A growing area of interest is the use of such solids-stabilized W/O emulsions for encapsulation and release of aqueous compounds sensitive to light, air or other compounds (Melle, Lask, & Fuller, 2005), as these have shown improved encapsulation potential over surfactant-stabilized emulsion droplets.^{4,62,63} Emulsions with crystalline fat at the interface have been used to encapsulate salt within the dispersed aqueous phase of W/O emulsions.^{4,62} Nadin et al. found that GMS-stabilized droplets were more effective for retaining salt than PGPR⁴, as the former resulted in a solid interfacial layer. Release was triggered by an increase in temperature, which melted the fat at the interface, promoting droplet destabilization and subsequent release of encapsulated cargo. The present study builds upon the work of Nadin et al.⁴

1.9 Digestion

Digestion consists of a series of physicochemical and biochemical events that begins in the oral cavity where food first encounters saliva, mechanical forces, and surfaces such as the palate, teeth,

tongue, cheeks, and throat.^{20,64–67} Saliva is a mixture of buffers, salts, enzymes (amylase), and biopolymers (mucin) in an aqueous media at neutral pH.^{20,64,66} Oral processing takes place when food first encounters saliva within the oral cavity and experiences forces related to chewing whilst movement of the tongue ensures proper mastication.^{20,64,66} Subsequently, food is transported down to the esophagus into the stomach where it is exposed to the gastric fluid.^{64,66,67} Gastric fluid is highly acidic and contains digestive enzymes and salts.^{20,64,66} In the gastric environment, the proteinaceous material of a food is broken down into peptides, and the peristaltic action of the stomach finely grinds the food into smaller digestible particulates that can move to the intestines.^{64,66,67} The pyloric sphincter controls the rate at which partially digested food enters the small intestine from the stomach.^{64,66} Intestinal fluid consisting of bile salts, phospholipids, protease, pancreatic lipase, colipase, and other alkaline fluids interacts with gastric chyme (the food mixture with gastric fluid).^{64,66} In the case of digestion of a food emulsion, at this point, the lipase and colipase can adhere to oil with the aid of bile salts and phospholipids, causing the hydrolysis of TAGs into free fatty acids and formation of mixed micelles, which will aid the absorption of the digested material by the intestinal cells. There are a significant number of studies describing the relationship between food structure and bioavailability of nutrients and micro-nutrient.⁶⁷

In the context of emulsion digestion and release behaviour, the retention and release of encapsulated biomarkers is dependent on not only mass transport, but also on the contributions of the gastrointestinal physiological conditions, as well as the properties of emulsion interfacial films, if present.²³ Numerous physiological changes occur during transit through the GIT, namely with pH, dilution, ionic strength, and enzymatic activity. Additionally, temperature, mechanical force, presence of surface-active compounds (i.e., bile salts, and pancreatic lipase), as well as food particle size/structure will result in physical changes in the emulsions.^{23,64,66,68–71}

In contrast to O/W emulsions, ingestion of a W/O emulsion begins with the formation of a coarse double emulsion with the initial W/O emulsion being incorporated within saliva. In parallel, the constituents within saliva begin to break down the emulsion constituents such as oil and protein (if present).^{23,64,66} With passage to the stomach, the low-pH environment results in some lipid hydrolysis and further emulsion breakdown. During the ensuing duodenal passage, the fat present in the emulsion will be hydrolyzed to partial acylglycerols and MAGs. The pH that an emulsion is

exposed to will change from the oral cavity (pH ~ 7) to the gastric environment (pH ~ 2) and small intestine (pH ~ 7).^{23,64,66} The integrity of the oil-water interfacial film and solid fat crystal network (if present) will likely be affected due to the combined action of the mixing and changes in local composition.^{23,64,66} For example, acid hydrolysis in the stomach may reduce the electrostatic repulsion between droplets.^{23,64,66} Furthermore, the GIT contains a number of surface-active substances such as bile salts, phospholipids, proteins, and biological surfactants that may readily adsorb to the oil-water interface.^{23,64,66} Digestive enzymes secreted in the GIT can cause severe damage to the emulsion causing any encapsulated material within aqueous droplets to degrade and/or be released.^{23,64,66}

1.9.1 *In-vitro* digestion

Numerous existing *in-vitro* digestion models (both static and dynamic) may be used to simulate *in-vivo* digestion conditions.⁶²⁻⁶⁵ (Figure 4).

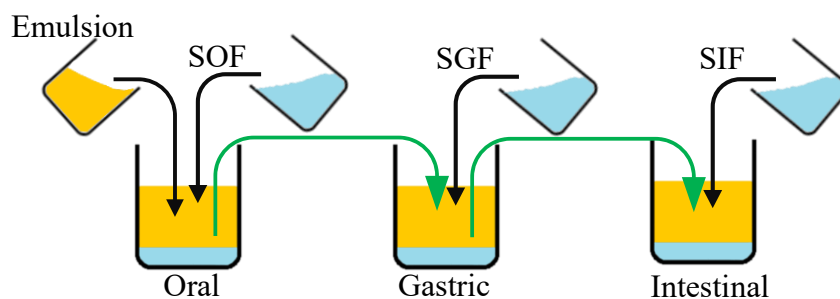


Figure 4. Static *in-vitro* gastrointestinal set-up. Typical static sequential *in-vitro* gastrointestinal set-up where an emulsion is mixed with simulated oral fluid (SOF, 1:1 emulsion to SOF), gastric (1:1 SOF to SGF) and intestinal (1:3 SGF to SIF) digestion ensues.¹⁸

Dynamic digestion models employ the use of one or more reaction chambers that contain different digestion components.⁷⁴ A number of models such as the Dynamic Gastric Model (DGM), TNO Gastro-Intestinal Model (TIM), and Simulator of the Human Intestinal Microbial ecosystem (SHIME) exist, and allow exploration of *in-vitro* digestion at specific part of the GIT with very specific conditions (i.e., digestion in accordance with a certain age).⁷⁴ Drawbacks for dynamic digestion models include improper mechanical feedback mechanisms, mismatch in the re-creation of *in-vivo* peristaltic movement, lack of hormonal activities, and are more time consuming compared to static models.⁷⁵

When compared to the *in-vivo* models (typically animal models, or human volunteers), *in-vitro* static models are relatively inexpensive, less labour-intensive, more controllable and come with no ethical restrictions.⁷¹ Static models typically focus on a simpler approach of oral, gastric, and intestinal digestion within a single static reaction chamber (e.g., beaker or bioreactor). These are simple models that provide superior control to answer research questions such as microstructure evolution/breakdown, and interfacial lipolysis.⁷⁵ For example, a pH-stat titration model allows for exploration of lipolysis within duodenal conditions. This is a simple well-described method in which free fatty acids produced through lipolysis are titrated against a basic solution while maintaining neutral pH.^{76,77} Limitations also exist for static *in-vitro* digestion models as there is little literature validating accuracy of *in-vitro* results *in-vivo*.¹⁸

The *in-vitro* digestion model used in this study was adopted from the one proposed by Minekus *et al.*, along with modifications based upon work by Guo *et al.*, for a simple digestion protocol.^{18,77} This modified model allows for testing the impact of each individual digestion phase to determine where (and perhaps how) emulsion breakdown occurs. Here, the ability of solid and crystalline interfaces (with/without a solid fat network) to slow or retard marker (MB) diffusion/transport from the dispersed aqueous phase of W/O emulsions was studied. It was imperative that a non-sequential digestion protocol be developed to focus on the evolution of microstructure using controls of increasing compositional complexity and eventually gastrointestinal digestion conditions. The structure-function relationship linking W/O emulsion breakdown/stability in the simulated gastrointestinal fluids, and the role of emulsifiers and solid fat used in their formation and stabilization, remains largely unexplored.

2.0 Thesis Objectives and Hypotheses

Objective 1: To establish the encapsulation capacity of W/O emulsions stabilized with different fat phase compositions.

Hypothesis 1: Different fat phase compositions will provide different initial MB encapsulation capacities, with core-shell emulsion stabilization providing the highest retention of MB following exposure to various environments. The presence of a solid fat network stabilizing a W/O emulsion will provide an additional barrier against release, when used with both liquid-state and solid-state surfactant.

Objective 2: To determine the emulsion breakdown and release profile of an encapsulated marker from within W/O emulsions in the presence of environments that simulate the gastric and duodenal stages of *in-vitro* digestion.

Hypothesis 2: Time, dilution and the complexity of *in-vitro* gastric and duodenal environments will affect the marker release profiles of the emulsions.

3.0 Materials and Methods

3.1 Materials

Canola oil (acid value < 0.1 %) was purchased from a local grocery and stored at room temperature (RT) until usage. PGPR with a 90% purity was donated by Danisco (Copenhagen, Denmark). The monoacylglycerols (MAGs) glycerol monostearate (GMS, 95% MAG) and glycerol monooleate (GMO, 90% MAG) were kindly supplied by BASF (Ludwigshafen, Germany). Fully hydrogenated soybean oil (FHSO) (acid value < 0.1%) was obtained from Bunge Oils (Bunge international, Mississauga, ON, Canada). Ultrapure water (18.2 MΩ.cm at 25 °C) produced by an E-pure water purification system (Thermo Scientific, Waltham, MA, USA) was used for all experiments. Pepsin (P7000) and bile extract (total bile salt content of 49 wt.%, with 10-15% glycodeoxycholic acid, 3-9% taurodeoxycholic acid, 0.5-7% deoxycholic acid, and 5 % phospholipids) were obtained from Sigma Chemicals (Oakville, Ontario, Canada). Porcine pancreatin (enzyme activity equivalent to 4x USP specifications) was also obtained from Sigma Chemicals (Oakville, Ontario, Canada). Hydrochloric acid (12 M) was purchased from Fisher Scientific (Mississauga, ON, Canada). All other chemicals were of analytical grade and purchased from local suppliers.

3.2 Emulsion preparation

The emulsions were prepared using the oil phase compositions shown in

Table 1. The constituent of all emulsions were heated at > 85 °C to ensure all components remained liquid during emulsification. The constituents of the oil phase (80 g / 100 g) (Table 1) and the aqueous phase (which consisted of water only) (20 g / 100 g) were heated for 15 mins and then emulsified. The MAG-based emulsions were mixed with a roto/stator (Polytron PT 2500 E, Kinematica, Inc. Bohemia, NY, USA) at 12,000 rpm for 5 mins. The PGPR and PGPR-F emulsions were mixed with an overhead mixer (Caframo, Georgian Bluffs, On., Canada) at 250 rpm for 15 mins for the former and at 300 rpm for 10 mins for the latter emulsion. All emulsions were cooled to 25 °C ± 5 °C with continuous stirring (750 rpm) in an ice bath.

Table 1. Emulsion continuous oil phase composition of the test W/O emulsions.

Name	Oil phase composition (g/100g canola oil)	Stabilization mechanism⁴
GMS	4 GMS	Core-shell
GMO-F	4 GMO + 10 FHSO	Combined core-shell and continuous phase fat crystal network
PGPR-F	2 PGPR + 10 FHSO	Continuous phase fat crystal network
PGPR	2 PGPR	Steric stabilization (liquid-state surfactant only)

3.3 Emulsion stability

Emulsion samples were transferred to glass vials (h = 50 mm) and stored at 25 °C for at least 4 weeks. Stability was assessed via visual examination, sedimentation, brightfield and polarized light microscopy and pulsed NMR for droplet size analysis.

3.3.1 Droplet size determination

The emulsion droplet size distribution of freshly-prepared and aged emulsions was measured using a Bruker Minispec Mq pulsed field gradient nuclear magnetic resonance (pfg-NMR) unit. The principle of operation is based on the restricted diffusion measurements of hydrogen nuclei that allows for unimodal fitting of emulsion droplet size distributions.⁷⁸ Average droplet sizes were reported as the volume-weighted geometric mean diameter ($d_{3,3}$) and breadth of the distribution (σ).⁴ This technique detects size increase in the droplet themselves because it relies on the molecular movement of water molecules within the droplet.⁴ Hence, measurements are of the droplets themselves and not clusters, which allows for the differentiation of coalescence from flocculation/coagulation.⁴

3.3.2 Emulsion phase separation

Emulsion sedimentation was characterized using a vertical scan analyzer (Turbiscan LAb, Formulacion, L'Union, France). The turbidity of samples was characterized by measuring the backscattering of incident light ($\lambda = 880$ nm) along the height of an optical glass tube by two

synchronous detectors. The backscattering detector was set at an angle of 45 °. Samples were prepared by filling glass vials (20 mm diameter) up to a 40 mm mark and then sealing with a cap. The entire length of a given sample was scanned and the turbidity profiles were analyzed with Turbiscan LAb Turbisoft LAb EXPERT software v 1.14.0. All samples were analyzed at 25 °C. The Turbiscan Stability Index (TSI) was calculated based on the differences in intensity at each height in the sample for a given scan and the one preceding it. The emulsions loaded with MB were examined on days 0 and 30 to assess differences in their stability over time, with TSI being calculated as:

$$\text{TSI} = \frac{\sum |\text{scan}_i(h)_{\text{day } 30} - \text{scan}(h)_{\text{day } 0}|}{H} \quad (1)$$

where h is the height in the sample, and H is the total sample height.

3.4 Recovery yield

The recovery yield of the MB was measured as the MB recovered from the dispersed aqueous phase post-emulsification compared with the amount initially added to the emulsion preparation. To recover MB from both the internal droplets and external aqueous phase, syringe extraction was performed. Samples were subsequently subjected to centrifugation (to remove possible contaminants, namely oil/surfactants) at $500 \times g$ for 15 min at 4 °C, with the supernatants collected and centrifuged at $10,000 \times g$ for 30 min at 4 °C. The recovery yield [Ry (%)] was calculated as follows:

$$\text{Ry}(\%) = \text{Cm}_{\text{OAP}(t)} \times \frac{100}{\text{Cm}_b} \quad (2)$$

where $\text{Cm}_{\text{OAP}(t)}$ is the outer aqueous phase marker concentration at time t

Cm_b is the initial concentration added to inner aqueous phase.

MB concentration was calculated based on its absorbance at 664 nm (UV-1900 spectrophotometer, Shimadzu, Kyoto, Japan), using the standard curve shown in Figure 5. This concentration was compared to the initial MB concentration in the freshly-prepared emulsions to obtain Ry.

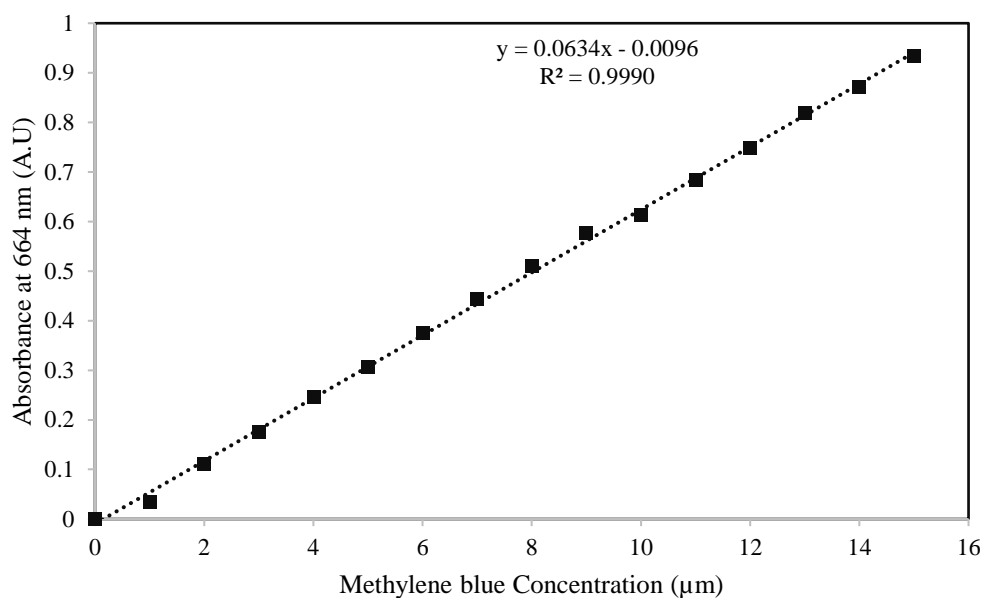


Figure 5. Standard curve of absorbance of methylene blue at 664 nm as a function of concentration.

Emulsions containing fat crystals in bulk or at the interface were heated to 70 °C to melt all crystals and centrifuged at 10,000 × *g* for 30 min. After aqueous phase extraction using a syringe, secondary centrifugation again at 10,000 × *g* for 30 min was performed to separate impurities (oil/surfactants, Figure 6).

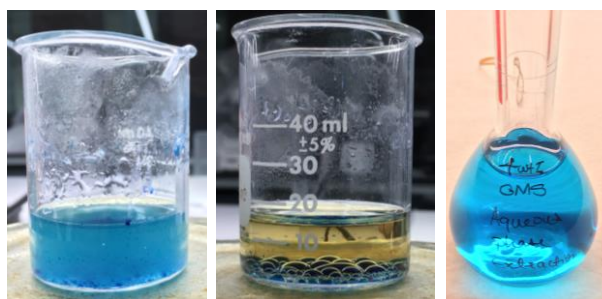


Figure 6. Example of recovery yield determination of MB through aqueous phase extraction for a 4 wt.% GMS emulsion.

3.5 Release during simulated *in-vitro* gastrointestinal digestion environments

Emulsion *in-vitro* digestion was separated into three phases: oral, gastric, and intestinal. Simulated saliva stock solution (500 mL) for the oral phase contained KCl (0.9 g), KSCN (0.2 g), NaH₂PO₄ · 2H₂O (1.2 g), Na₂SO₄ (0.57 g), NaCl (0.3 g), NaHCO₃ (1.60 g), and urea (0.2 g). The pH was

adjusted to 6.8 using standardized stock solutions of NaOH (0.05 M, 0.1 M, or 1.0 M). Sodium bicarbonate (0.08 g) was added to the simulated saliva stock solution (25 g). Simulated saliva (20 g) was then mixed with emulsion (20 g) and incubated at 37 °C for 2 minutes.⁷¹

The simulated gastric fluid stock solution (1L) contained NaCl (8.775 g) and pH was adjusted to 2.5 (with 1 M HCl). Pepsin (3.2 g/L pepsin, enzyme activity of 456 U/mg) was added to simulated gastric fluid. Emulsion (20 g) was then mixed with SGF (20 g), and the pH was adjusted to 2.0. All samples were placed in a mechanical incubator with a rotating arm (Figure 7) at 37 °C using a rotational speed of 6 RPM for 60 minutes, with sampling at 30 minute intervals (Robbins Scientific, Model 2000 Micro-Hybridization incubator, Sunnyvale, CA, USA).^{71,77}



Figure 7. The *in-vitro* MB release set-up where Falcon tubes are loaded with a) bolus and release medium.

The simulated intestinal fluid stock solution (1L) contained NaCl (150 mM). Calcium chloride (10 mM) and pancreatin (1.5 g/L, 4x USP specifications) were added to the SIF and bile extract mixture, mixed for 5 min and the pH was adjusted to 7. The bile extract (7.2 mM) was added to SIF stock solution (40 g) and mixed (~ 60 minutes), with the pH adjusted to 7 (2 drops 5M NaOH). Emulsion samples (10 g) were mixed with SIF (30 g) in Falcon tubes and incubated as above for 120 min (37 °C, 6 rotations/min).⁷¹

In order to evaluate the role of each of the constituents on the release behaviour of the starting emulsions, three sets of conditions (Conditions 1, 2 and 3) were tested, along with the full SGF and SIF. For Condition 1, the test emulsions were diluted with water adjusted to pH 7 either at 1:1 as per the gastric tests or at 1:3 as per the intestinal release tests. With Condition 2, NaCl was added at the same concentration (150 mM) as that of SGF and SIF. Thereafter, in Condition 3, the gastric environment pH was reduced to 2 while in the intestinal environment, pH was kept neutral, but bile salts were added. Finally, the representative *in-vitro* gastric and intestinal digestion fluid were tested.

Table 2. Name and composition of conditions and release fluid used throughout this study. Note the incremental complexity of the fluids. Final test fluids are the SGF and SIF.

Release medium	Gastric conditions (1:1 emulsion:medium)	Intestinal conditions (1:3 emulsion:medium)
Condition 1	Water	Water
Composition	pH 7 (pH adjusted)	pH 7 (pH adjusted)
Condition 2	Salt water	Salt water
Composition	pH 7, 150 mM NaCl	pH 7, 150 mM NaCl
Condition 3	pH-adjusted salt water	Salt water with bile salts
Composition	pH 2, 150 mM NaCl	pH 7, 150 mM NaCl, 7.2 mM bile salts
Test fluid	Gastric fluid (SGF)	Intestinal fluid (SIF)
Composition	pH 2, 150 mM NaCl, pepsin (3.2 g/L)	pH 7, 150 mM NaCl, 7.2 mM Bile Salts, 10 mM CaCl ₂ , pancreatin (1.5 g/L)

Characterization of MB release under the different gastric and duodenal conditions (i.e., Conditions 1-3 and test fluids) followed the method of Giroux et al.⁷⁹ Samples containing MB were subjected to gastrointestinal digestion environments using the above-mentioned protocols, with external aqueous phase samples taken at 0, 30 and 60 min for gastric digestion and 0, 15, 30, 60 and 120 min for duodenal digestion. The samples were then centrifuged at $500 \times g$ for 15 min at 4 °C, after which the supernatant was collected and centrifuged at $10,000 \times g$ for 30 min at 4 °C.

The concentration of MB in the aqueous phase was determined by characterizing absorbance at 664 nm. The total concentration of marker released from the emulsions was reported as Ry.

3.6 Microscopy

Brightfield and polarized light microscopy (PLM) were both used to characterize emulsion microstructure before and after exposure to the different release media. Samples were taken at the same time intervals as the release experiments and examined. Samples were deposited on viewing slides (Fischer Scientific, Ottawa, ON, Canada) at room temperature (~ 25 °C), covered with a coverslip (Fischer Scientific, Nepean, ON, Canada) and analyzed. Image analysis (contrast/brightness matching, scalebars, etc..) post microscopy was performed with ImageJ.⁸⁰ ImageJ was used to estimate the effect of digestion on the droplet size evolution by measuring the mean area of the aqueous droplets. Over 100 droplets per micrograph were measured for all treatments (conditions 1-4 for both SGF and SIF) at all time points, with the exception of the freshly-prepared emulsions analyzed via pulsed NMR. Further calculations were carried out using OriginPRO 2015.

3.7 Statistical analyses

All experiments were performed in triplicate measurements, and three independent experiments were performed prior to statistical analysis. When analyzed pair-wise, data were tested with Student's T-test. The differences in group mean values were tested using analysis of variance (ANOVA). Tukey's HSD post-hoc test was carried out when significant differences among groups were obtained. All statistical tests were performed with 95 % of significance. The statistical analysis was performed using the free software [R] (www.r-project.org) (libraries: stats and agricolae), MS-Excel and OriginPRO 2015.

4.0 Results and Discussion

4.1 MB, emulsion stability, and microstructure

The surfactants glycerol monostearate (GMS), glycerol monooleate (GMO) and polyglycerol polyricinoleate (PGPR) were used to generate W/O emulsions, with fully hydrogenated (FHSO) added in the test emulsions containing either GMO or PGPR. The four systems consisted of emulsions that were either stabilized as a core-shell type emulsion (GMS), a combination of core-shell and continuous fat crystal network stabilization (GMO-F), a continuous phase fat crystal network only (PGPR-F) and a fully liquid emulsion with no solid fat present (PGPR). Emulsions stabilized solely with GMO (≤ 2 wt.% GMO) were not sufficiently stable to carry out any stability studies. Methylene blue (MB) was the probe of choice as its absorption at 664 nm did not overlap with the absorption of other components (CaCl₂, bile salts and pancreatin) present in the emulsions.

The GMS-based emulsions were stabilized by interfacial solid shells englobing the dispersed aqueous droplets, based on the droplet deformation in Figure 8A and crystals visible under polarized light in Figure 8B. During post-emulsification cooling, the GMO promoted the interfacial crystallization of the FHSO. The resulting emulsion was stabilized by a combination of GMO and FHSO fat crystals (Figures 8C and D).²⁷ The PGPR-F emulsion consisted of solid fat present only in the continuous phase, with no signs of solid fat adsorbed at the oil-water interface (Figure 8E and F). Deformation of aqueous droplets in the PGPR-F emulsions due to close proximity of solid fat network and droplets was visible in photomicrographs Figure 8E and F. As discussed below, the presence of solid fat in the continuous phase was expected to impair the movements of the water droplets of W/O emulsion and improve stability to coalescence.^{45,46} Lastly, stabilization of the PGPR emulsions was strictly due to the emulsifying ability of the PGPR given the absence of solid fat crystals (Figure 8G and H). PGPR is known as an effective emulsifier and forms W/O emulsions with minimal, or even no shear.⁸¹ By contrast, the MAG-based emulsions required much higher shear environments for their preparation. Other than the PGPR-only emulsion, all emulsion droplets showed some evidence of aggregation. Coalescence was not

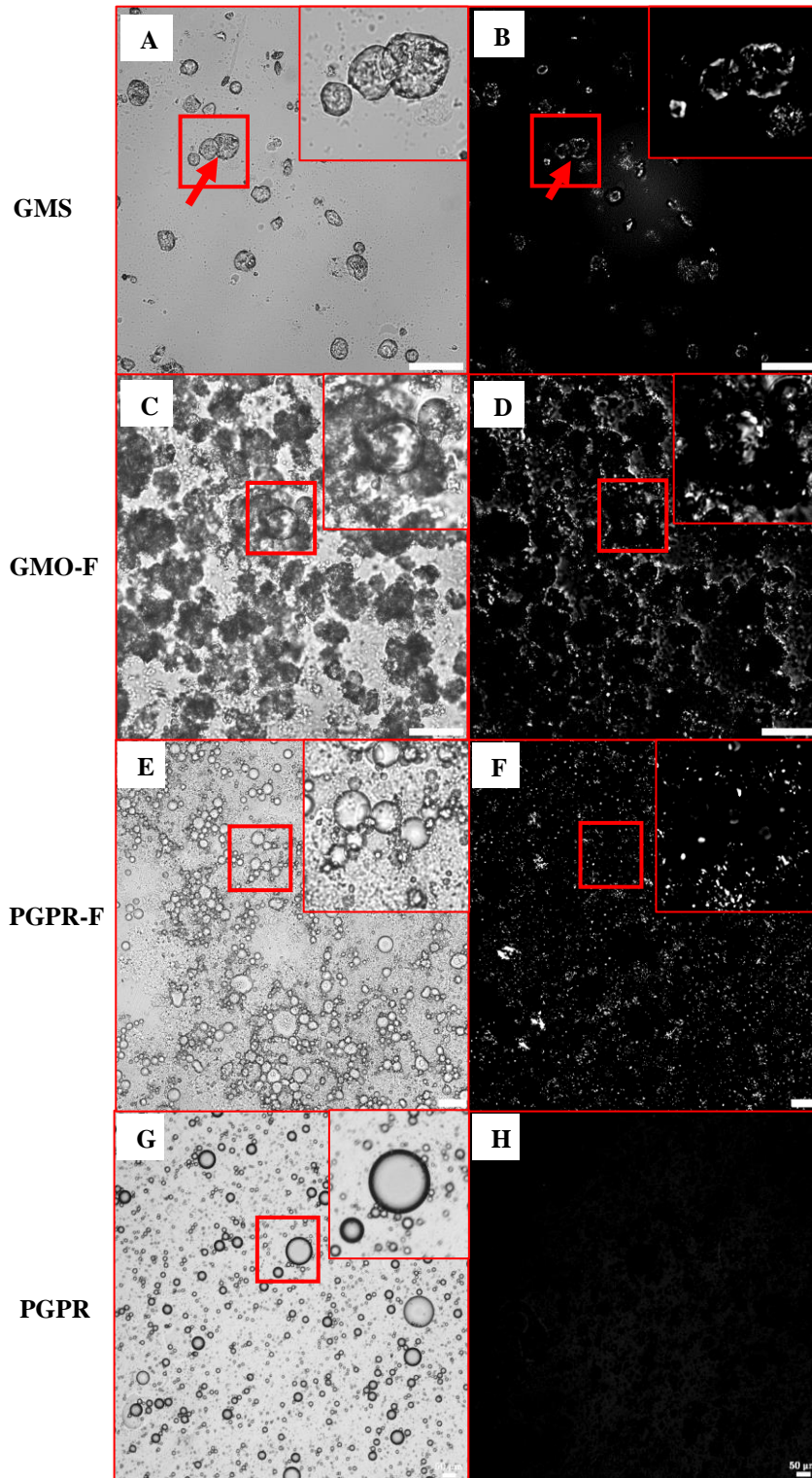


Figure 8. Microstructure comparison of emulsions. Micrographs taken in brightfield light microscopy at RT - GMS (A), GMO-F (C), PGPR-F (E), and PGPR (G). The corresponding images in polarized light are also shown - GMS (B), GMO-F (D), PGPR-F (F), and PGPR (H). Insets are zoomed-in views of boxed areas. Scale bars = 50 μm .

observed for these emulsions partly due to the presence of the solid fat and/or surfactant present acting as a cement between the droplets.

All emulsions were designed to have similar droplet sizes in order to remove this confounding factor from the release experiments. All emulsions were formulated with or without 1 mM MB dissolved in the dispersed aqueous phase and evaluated for phase separation, microscopy and droplet size analysis using pfg-NMR. Droplet size distributions were roughly matched for all emulsions (Table 3). Once added, the MB resulted in different average emulsion droplet sizes (Table 3). The shift in size, though statistically significant in some cases (GMO-F and PGPR-F) was considered acceptable due to difficulties associated with achieving smaller droplet sizes (namely with GMS emulsions). The dye was determined to be surface-active based on the small changes in emulsion droplet size (Table 3). Upon addition of MB, the difference in σ was only statistically significantly different for the GMO-F ($p < 0.05$). Measured immediately after preparation, pfg-NMR showed unimodal droplet size distributions (Appendix, Figure A 3) for both the MB-loaded and unloaded emulsions.

Table 3. Comparison of the $D_{3,3}$ and sigma (σ) values of the unloaded and MB-loaded emulsions. All data are mean for $n = 3 \pm$ standard deviation. Statistical analyses (95% confidence) are shown for differences in droplet size and σ : within-column (ANOVA/Tukey, superscript letters) and between-column (Student's T test, superscript numbers).

Emulsion	Droplet size ($D_{3,3}$ μm)		Width of distribution curve (σ)	
	Unloaded	Loaded	σ (Unloaded)	σ (Loaded)
GMS	$16.8 \pm 0.8^{a,1}$	$18.7 \pm 1.8^{a,1}$	$0.44 \pm 0.04^{a,1}$	$0.43 \pm 0.02^{a,1}$
GMO-F	$11.8 \pm 1.5^{b,1}$	$8.7 \pm 0.4^{b,2}$	$0.62 \pm 0.07^{b,1}$	$0.53 \pm 0.02^{b,2}$
PGPR-F	$12.6 \pm 2.5^{ab,1}$	$9.1 \pm 0.1^{b,2}$	$0.84 \pm 0.03^{ab,1}$	$0.82 \pm 0.06^{c,1}$
PGPR	$12.2 \pm 1.1^{b,1}$	$13.6 \pm 1.3^{c,1}$	$0.54 \pm 0.04^{b,1}$	$0.56 \pm 0.03^{d,1}$

Table 4 relates the recovery yield (Ry) values of MB of the freshly-prepared emulsions. Ry was defined as the proportion of MB initially dispersed within the aqueous phase of emulsions that was subsequently separated from the system and recovered. This was a necessary step to ensure that the ensuing release results would not be impacted by the extraction and recovery method. Recovery of MB (Table 4, > 99.7% for all emulsion types) from freshly-prepared emulsions confirmed that

the dye was completely recovered from oil, solid fat, and emulsifiers present in the system. There were no significant differences between emulsion type, and recovery yields between freshly-prepared emulsions and those aged 24 h (ANOVA, $p > 0.05$). Regan et al. showed similar encapsulation efficiencies of MB within their freshly-prepared W/O/W emulsions.¹⁶

Table 4. Recovery yield of MB from entrapped aqueous phase of emulsions on the day they were prepared. All data are means for $n = 3 \pm$ standard deviation. No statistical differences were observed (ANOVA $p > 0.05$ within emulsion types).

Emulsion type	Recovery yield (%)
GMS	99.9 ± 0.1
GMO-F	99.8 ± 0.1
PGPR-F	99.8 ± 0.1
PGPR	99.7 ± 0.1

Figure 9 compares the Turbiscan stability index (TSI) between days 0 and 30 of the four test emulsions. The GMS emulsion showed the lowest extent of destabilization followed by the GMO-F, PGPR-F and PGPR emulsion, which began to show signs of destabilization within 16-24h of formulation. The structure of the continuous phase played an important role on the sedimentation stability of the emulsions, with the core-shell type stabilization of the GMS conferring the greatest stability. Lack of fat in the PGPR emulsion further demonstrated the important stabilizing role that

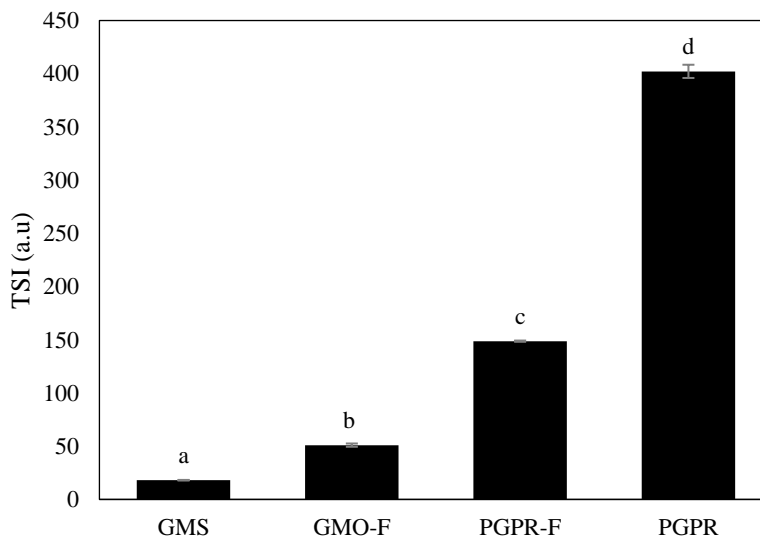


Figure 9. TSI of the four test emulsions. Statistically significant differences between fat phase compositions are denoted by different letters (ANOVA/Tukey, $p < 0.05$).

fat plays on emulsion stability. These results were in line with those of Tran et al., who reported that emulsions made with GMS or GMO combined with fat were resistant to sedimentation.⁴⁶ Similarly, Rafanan and Rousseau spoke of the effectiveness of solid fat networks in regards to stabilization against sedimentation for W/O emulsions employing PGPR, GMO, and GMS as emulsifiers.²⁷ Nadin et al., however, reported that in the absence of solid fat, PGPR-stabilized emulsions readily broke down.⁴ These results were further borne out visually (Appendix, Figure A 4).

4.2 Oral Digestion

All emulsions mixed with simulated oral fluid (SOF) showed no MB release following 2 mins of mixing. As a result, no further experiments with SOF were performed.

4.3 Effect of environment on MB release

Figure 10 shows the extent of MB released from the 4 emulsion types as a result of 1:1 dilution with unbuffered water at pH 7 (Condition 1 - SGF). The GMO-F emulsion showed the highest extent of MB release at both 30 and 60 min, followed by GMS, PGPR-F, and PGPR, respectively. The GMS emulsions released $1.8 \pm 0.3\%$ MB at 30 min, and $6.0 \pm 0.1\%$ at 60 min ($p < 0.05$) whereas release from the GMO-F emulsions was greater at $9.4 \pm 0.1\%$ MB at 30 min and $10.5 \pm 0.1\%$ at 60 min ($p < 0.05$), respectively. MB release from the PGPR-F and PGPR emulsions was lowest, with values of $2.2 \pm 0.1\%$ and $3.5 \pm 0.3\%$ at 30 and 60 minutes for the former ($p < 0.05$) and $1.7 \pm 0.2\%$ MB and $6.00 \pm 0.06\%$ at 30 and 60 min for the latter, respectively ($p < 0.05$). These results demonstrated the poor emulsifying capability of the GMO compared to PGPR, which was best able to withstand changes in environmental conditions.

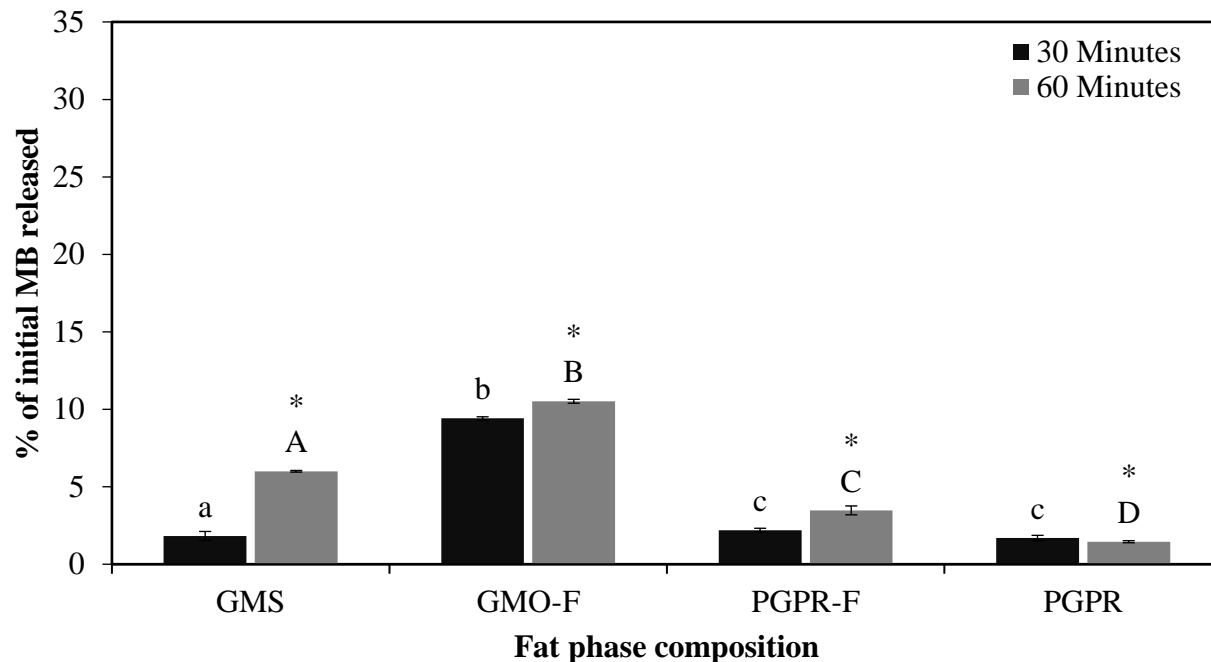


Figure 10. MB release from emulsions subjected to Condition 1 – SGF. All data are means based on $n = 3 \pm$ standard deviation. Between each fat phase composition, the letters denote significant differences within the same time point (30 or 60 min – lowercase and uppercase, respectively) (ANOVA/Tukey – $p < 0.05$). * denotes significant differences between time points (30 and 60 min) within the same fat phase composition (Student’s T-test, $p < 0.05$).

When subjected to a 1:3 dilution (Condition 1 – SIF, Figure 11), there was greater MB release observed in all emulsions, except for the GMO-F and PGPR-F emulsions which both showed similar MB release as in the Condition 1 - SGF. The GMS emulsion released 12.1 ± 0.1 % MB at 30 minutes and 29.9 ± 0.4 % at 60 minutes ($p < 0.05$) whereas the GMO-F displayed 4.5 ± 0.1 % MB release at 30 minutes and 6.1 ± 0.1 % at 60 minutes ($p < 0.05$). The PGPR-F emulsion released 2.1 ± 0.1 % MB at 30 minutes and 2.6 ± 0.4 % at 60 minutes ($p < 0.05$), and the PGPR emulsion saw release of 8.3 ± 0.4 % and 11.1 ± 0.2 % MB at 30 and 60 minutes, respectively ($p < 0.05$).

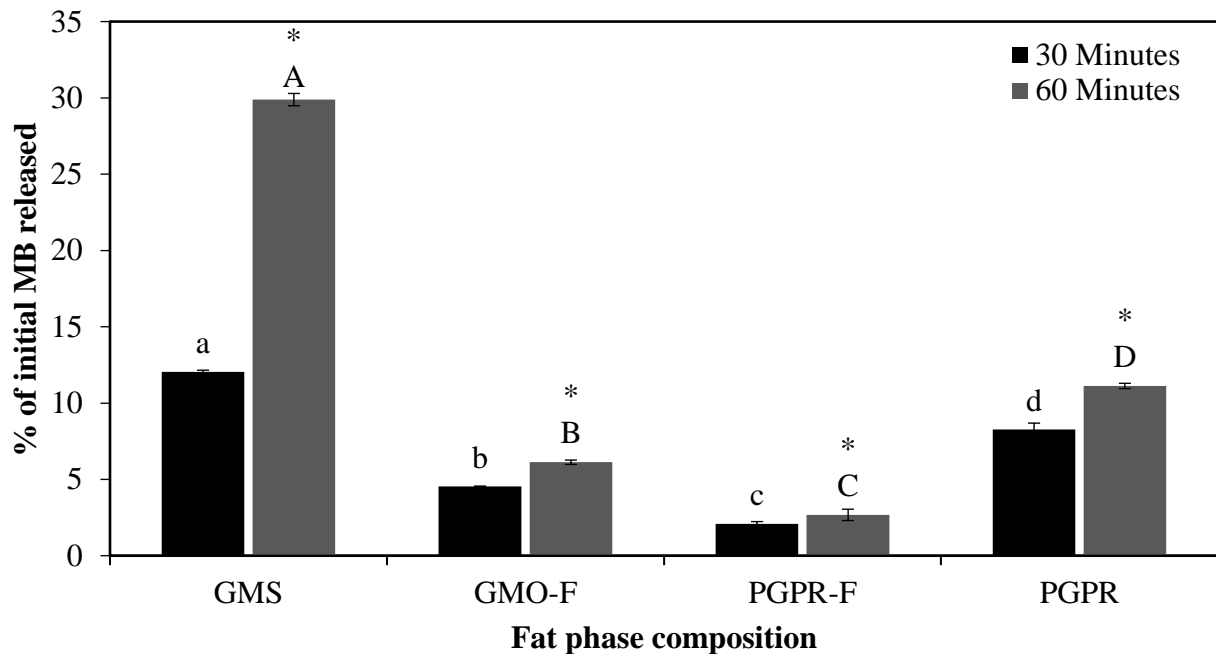


Figure 11. MB release from emulsions subjected to Condition 1 – SIF. All data are means based on $n = 3 \pm$ standard deviation. Between each fat phase composition, the letters denote significant differences within the same time point (30 or 60 min – lowercase and uppercase, respectively) (ANOVA/Tukey – $p < 0.05$). * denotes significant differences between time points (30 and 60 min) within the same fat phase composition (Student’s T-test, $p < 0.05$).

Figure 12 shows the microstructure of the 4 emulsions subjected to 60 min of contact with a 1:3 dilution (Condition 1- SIF). Generally speaking, the observed microstructure was similar to when the emulsions were exposed to a 1:1 dilution, with the average droplet size increasing with time. It was expected that the core-shell stabilization offered by the GMS would confer significant stabilization to the emulsion, however, this was not the case. In contrast to Figure 8, Figure 12A revealed that the GMS-covered dispersed aqueous droplets were malformed, and larger ($93.3 \pm 6.1 \mu\text{m}$), following 2 h of mixing. This was in contrast to previous efforts from our group⁴, where it was shown that GMS shells effectively halted NaCl release over a 2 h period, with little change in microstructure. It may be that the different mixing conditions were responsible for this discrepancy, given the head-over-head mixing used in the present study vs. the stir bar mixing in our previous work. The presence of a continuous fat crystal network in the GMO-F and PGPR-F was most effective at limiting release over 2 h, even when possible melting (or at least weakening) of GMO crystals occurs at physiological conditions (GMO melting point $\sim 35 \text{ }^\circ\text{C}$). This was

evident in the microscopy images, which showed that the solid fat network (GMO-F and PGPR-F) remained largely intact following 1:3 dilution and subsequent mixing (Figure 12B and C, respectively). A rise in droplet size was evident based on the average droplet size of $87.2 \pm 4.7 \mu\text{m}$

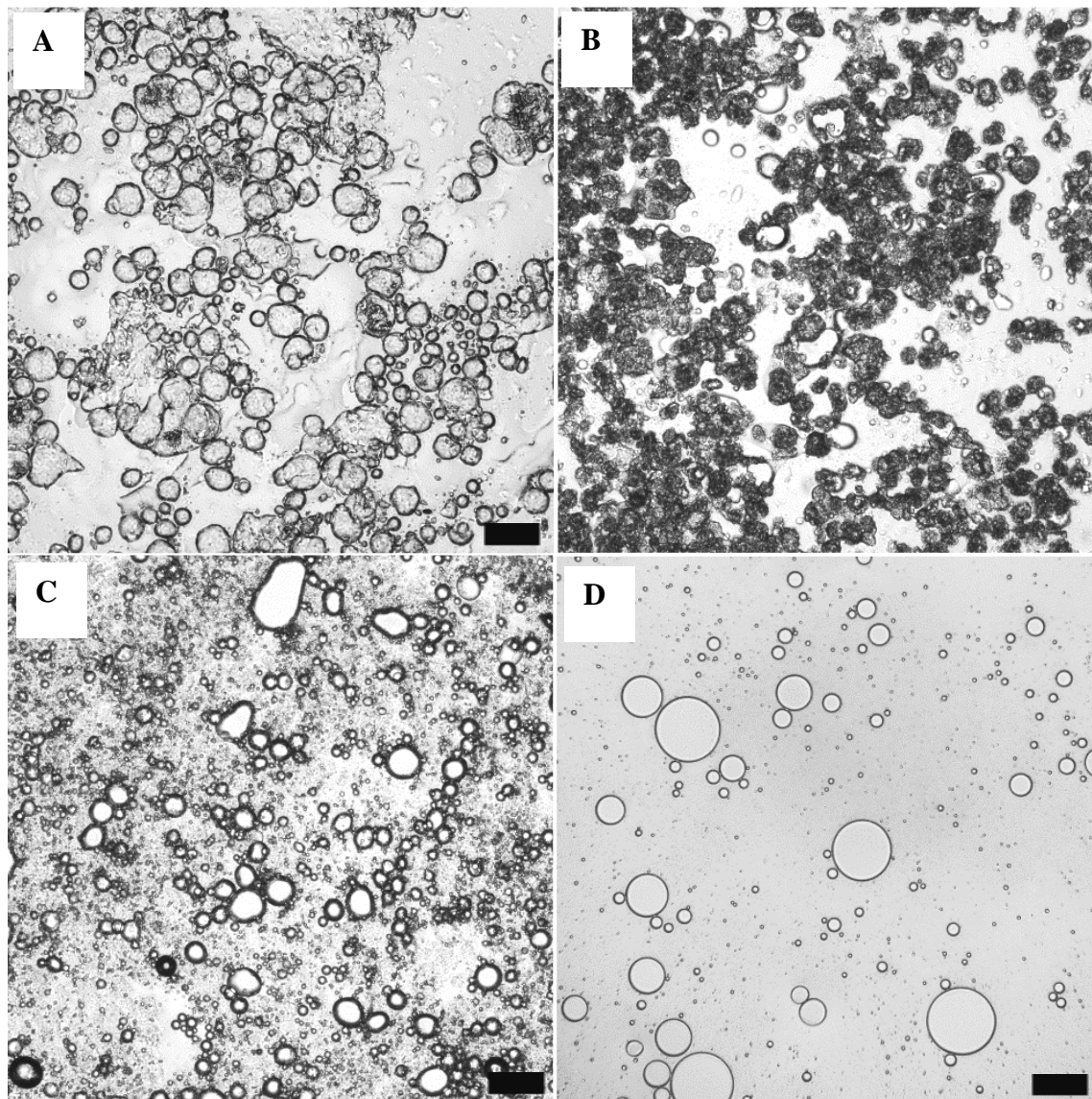


Figure 12. Microstructure post 60 minutes of the four test emulsions subjected to a 1:3 dilution (condition 1 – SIF). Images were captured in brightfield mode at 25 °C. GMS (A), GMO-F (B), PGPR-F (C), and PGPR (D). Scale bars = 50 μm .

for GMO-F and $71.7 \pm 4.7 \mu\text{m}$ ($p < 0.05$) for PGPR-F emulsions (Figure 12B and C, respectively). The release results were on par with the literature confirming the ability of solid fat networks to retain aqueous droplets when paired with PGPR.^{4,82} Finally, the PGPR-only emulsion showed significant emulsion breakdown based on the increase in average droplet size due to rapid

coalescence ($276.3 \pm 6.5 \mu\text{m}$ at 120 minutes). This likely contributed to the greater release seen in the 1:3 vs. the 1:1 emulsion, and also suggested the possibility of droplet swelling as a contributor to emulsion breakdown.⁸¹

Exposure of all emulsions to Condition 2 (Figure 13 – SGF, Figure 14 - SIF), where there was added NaCl at the molarity corresponding to the SGF and SIF (150 mM), did not significantly alter the release profiles and microstructure compared to the dilution results in Figure 10 and Figure 11. The osmotic gradient via addition of NaCl was initially thought to enhance release, however, no

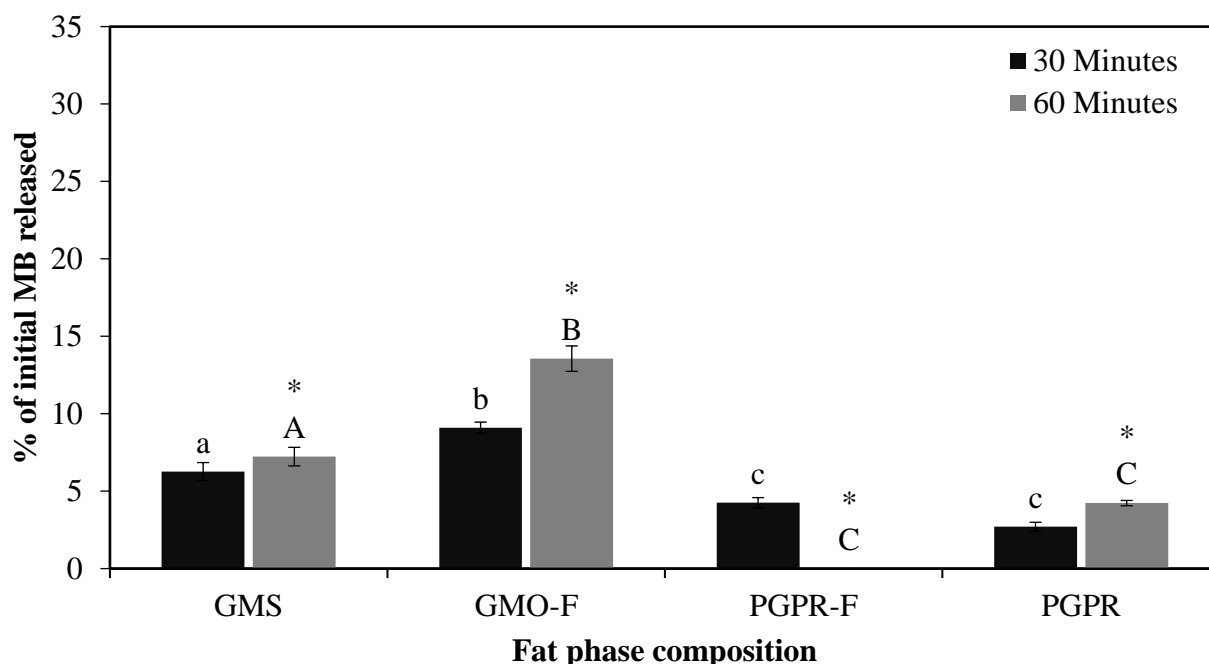


Figure 13. MB release from emulsions subjected to Condition 2 – SGF. All data are means based on $n = 3 \pm$ standard deviation. Between each fat phase composition, the letters denote significant differences within the same time point (30 or 60 min – lowercase and uppercase, respectively) (ANOVA/Tukey – $p < 0.05$). * denotes significant differences between time points (30 and 60 min) within the same fat phase composition (Student’s T-test, $p < 0.05$).

such effect was observed (Figure 13 and Figure 14). Generally speaking, in both SGF and SIF environments, exposure of the emulsions to Condition 2 followed release trends similar to the respective water controls, albeit at slightly higher MB concentrations ($p > 0.05$) resulting in no significant differences. Amongst the stabilization methods, the PGPR-based emulsion showed lower release in Condition 2 vs. Condition 1. This was likely related to the ability of the interfacial

PGPR film to resist droplet swelling, unlike the MAG-based emulsions. Even with the apparent destabilization of the PGPR-F emulsion (Figure 15), where clear separation of the emulsion and fat crystal network was seen, these emulsions saw only limited MB release. NaCl has been shown to improve the stability of PGPR films, likely via ion-dipole interactions through the interface.⁸³

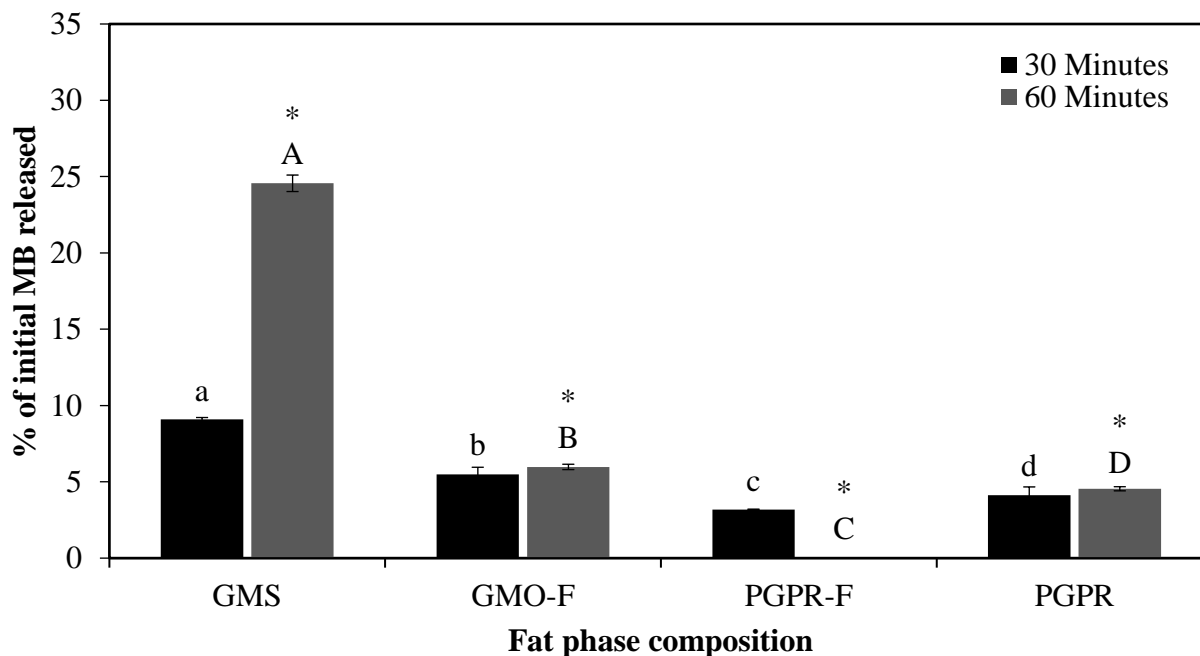


Figure 14. MB release from emulsions subjected to Condition 2 – SIF. All data are means based on $n = 3 \pm$ standard deviation. Between each fat phase composition, the letters denote significant differences within the same time point (30 or 60 min – lowercase and uppercase, respectively) (ANOVA/Tukey – $p < 0.05$). * denotes significant differences between time points (30 and 60 min) within the same fat phase composition (Student’s T-test, $p < 0.05$).

As well, in the presence of PGPR, a coarse secondary W/O emulsion formed, but only when salt was present in the aqueous phase. This was apparent in PGPR emulsions with and without solid fat (PGPR alone, and PGPR-F).^{14,83}

By contrast, the MAG-based emulsions saw MB release values as high as $29.9 \% \pm 0.4 \%$ in the presence of salt, possibly due to the osmotic gradient present (Figure 16).⁴ Microstructurally, the GMS emulsion subjected to both Condition 2 media (i.e., SGF and SIF) exhibited significant breakdown (Figure 16), based on the large droplet size increase ($73.4 \pm 10.1 \mu\text{m}$ for SGF, and $81.7 \pm 3.0 \mu\text{m}$ for SIF at 60 min) and generally distorted core-shell structures, which was particularly

evident with the Condition 2 – SIF (Figure 16C and D). It is apparent that emulsion core-shell crystallization could not effectively retard MB release nor could the GMO-F emulsions, strongly suggesting that MAGs, irrespective of physical state, were ineffective at controllably releasing MB

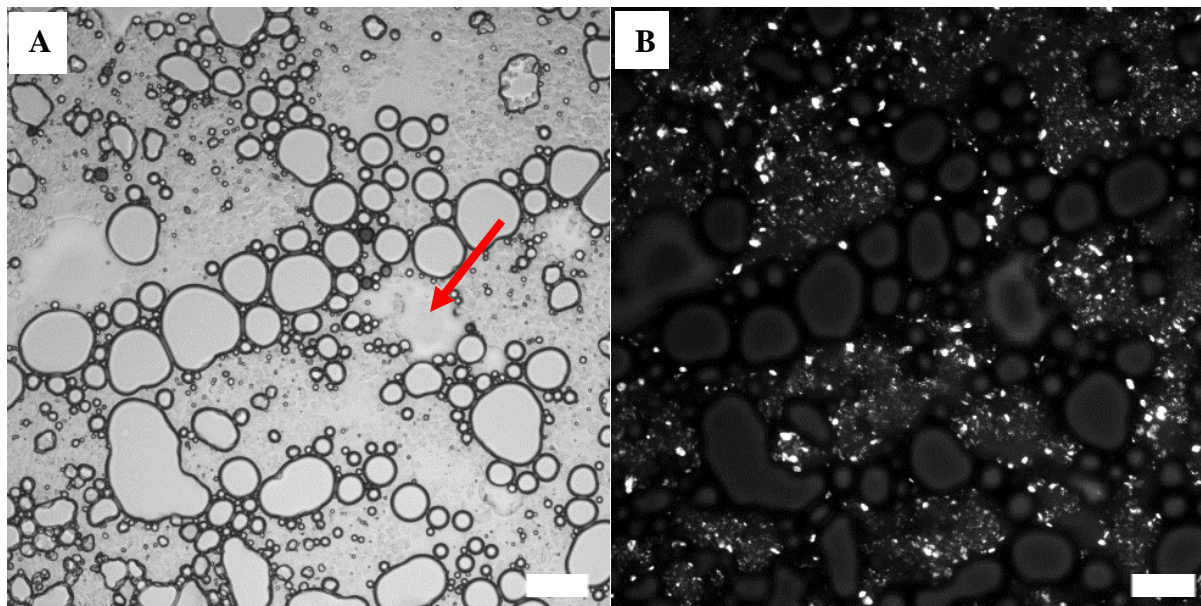


Figure 15. Brightfield and polarized light microscopy of the PGPR-F emulsion subjected to Condition 2 – SGF for 60 min. Red arrow indicates coarse emulsification. (A) Brightfield; (B) PLM. Scale bars = 50 μm .

under these experimental conditions. The overall higher MB release observed for Condition 2 (SGF and SIF) may be explained by the increase in average droplet size over 60 min when compared to the freshly-prepared emulsions. The average droplet size of the GMO-F was $87.1 \pm 4.5 \mu\text{m}$ in the SGF and $102.8 \pm 11.2 \mu\text{m}$ in the SIF after 60 mins ($p < 0.05$). The PGPR-F emulsion average droplet size was $35.7 \pm 4.1 \mu\text{m}$ in the SGF, and $59.7 \pm 8.8 \mu\text{m}$ in the SIF after 60 min ($p < 0.05$) whereas for the PGPR-stabilized emulsion, the average droplet size was $87.4 \pm 7.0 \mu\text{m}$ in the SGF and $134.6 \pm 5.3 \mu\text{m}$ in the SIF after 60 min ($p < 0.05$) in Condition 2. Overall, statistically significant differences existed between all time points in same system and between systems ($p < 0.05$).

Compositionally, Condition 3 – SGF was similar to Condition 2 – SGF except that the pH was adjusted to 2, similar to what would be found in the stomach. For Condition 3 – SIF, the pH was maintained at 7, but bile salts (7.2 mM) were added. Together, these 2 factors helped to further isolate the individual effects of pH and bile salts on the release of MB from the emulsions and any

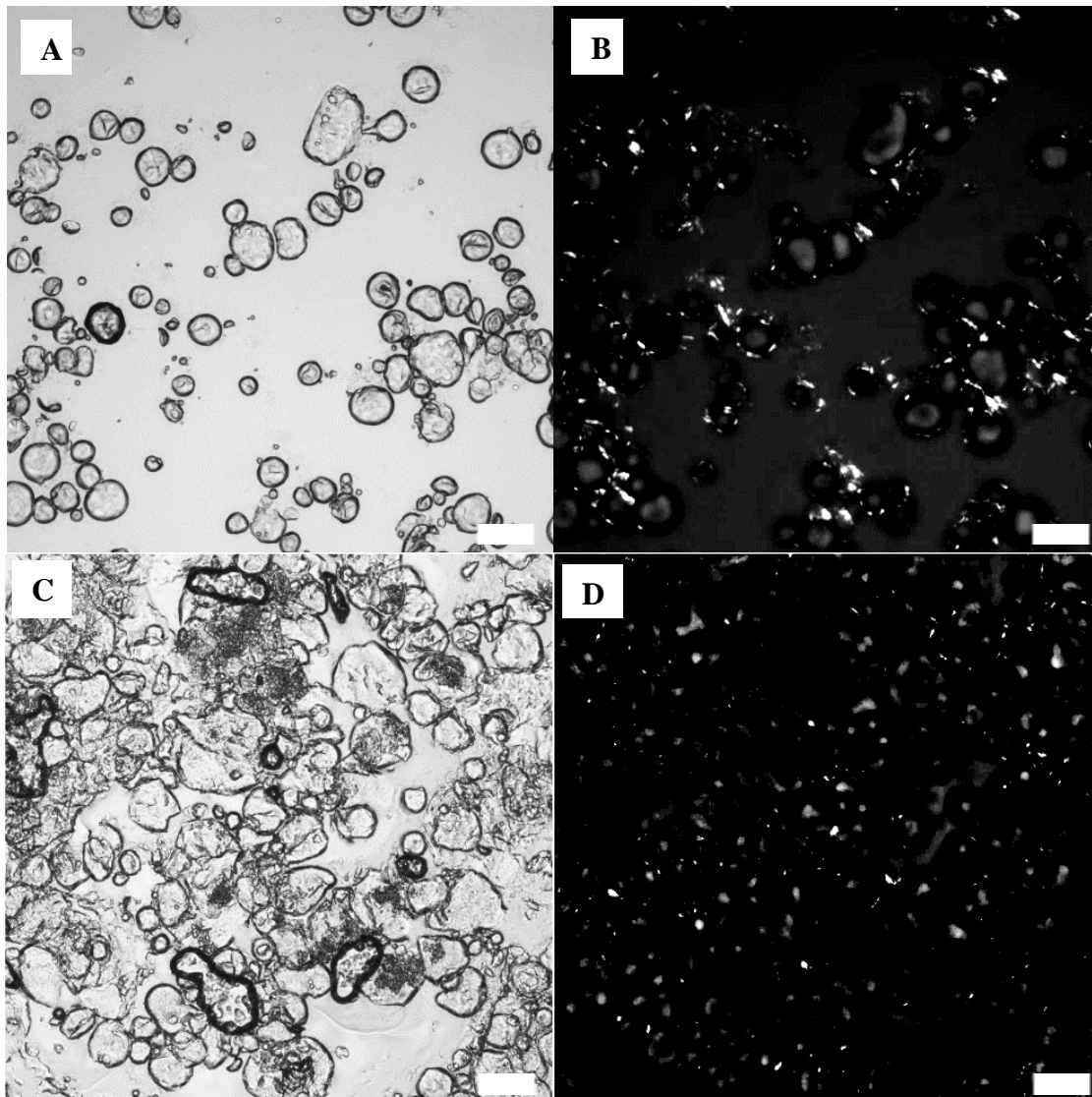


Figure 16. Brightfield and polarized light microscopy of the GMS emulsion subjected to Condition 2 – SGF (A, B) or Condition 2 – SIF (C, D) for 60 min. (A, C) Brightfield; (B, D) PLM. Scale bars = 50 μm .

contributing role of fat microstructure.

Figure 17 shows the MB release from the 4 test emulsions subjected to Condition 3 – SGF, where similar trends and release concentrations to controls 1 and 2 were apparent. The GMO-F emulsion released the largest MB concentration (5.0 ± 0.3 % MB at 30 minutes, 14.2 ± 0.3 % at 60 minutes) ($p < 0.05$) followed by GMS (2.6 ± 0.4 % MB at 30 minutes, 7.2 ± 0.6 % at 60 minutes) ($p < 0.05$), and PGPR (2.5 ± 0.2 % MB at 30 minutes, 4.0 ± 0.3 % at 60 minutes) ($p < 0.05$). Interestingly, the

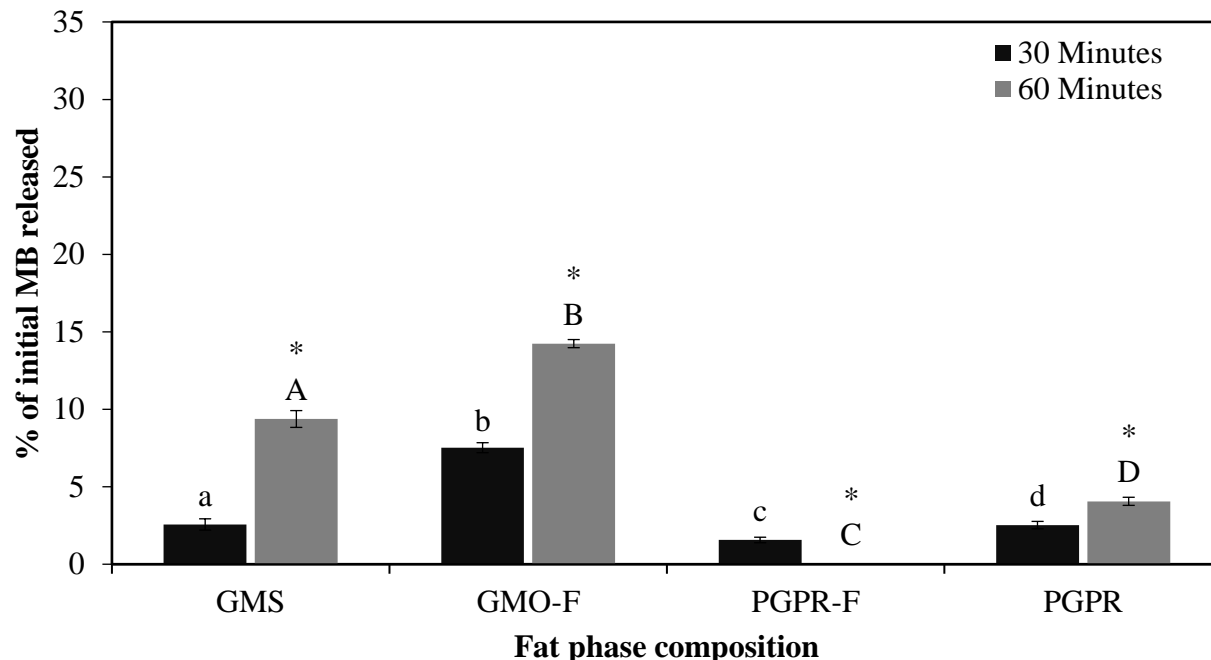


Figure 17. MB release from emulsions subjected to Condition 3 – SGF. All data are means based on $n = 3 \pm$ standard deviation. Letters denote significant differences within the same time point (30 or 60 min) between each fat phase composition (ANOVA/Tukey – $p < 0.05$). * denotes significant differences between time points (30 and 60 min) within the same fat phase composition (Student’s T-test, $p < 0.05$).

PGPR-F emulsions only showed little release after 30 minutes (1.6 ± 0.2 % MB) with no subsequent release at 60 minutes. Therefore, a change in pH from 7 to 2 resulted in little to no change in MB release from these emulsions. Microstructurally, there was little change compared to that observed with controls 1 and 2 (Appendix, Figure A 5 - Figure A 16).

Emulsion exposure to Condition 3 – SIF showed substantial changes in release (Figure 18). The GMS emulsions released 23.1 ± 0.1 % MB within 30 minutes, with no release at 60 and 120 minutes. The GMO-F emulsion completely broke down within seconds of contact with Condition 3 – SIF, clearly demonstrating the substantial effect of bile salt on emulsion stability. By contrast, both the PGPR-F and PGPR-only emulsions continued to release MB during the 2 h experimental timeframe. The PGPR-F emulsion released 22.5 ± 0.5 % of its initial MB cargo within 120 minutes whereas the PGPR-only emulsion released less (15.2 ± 0.2 %). There were statistically significant differences in release at the various time points for all emulsions ($p < 0.05$, for every emulsion but

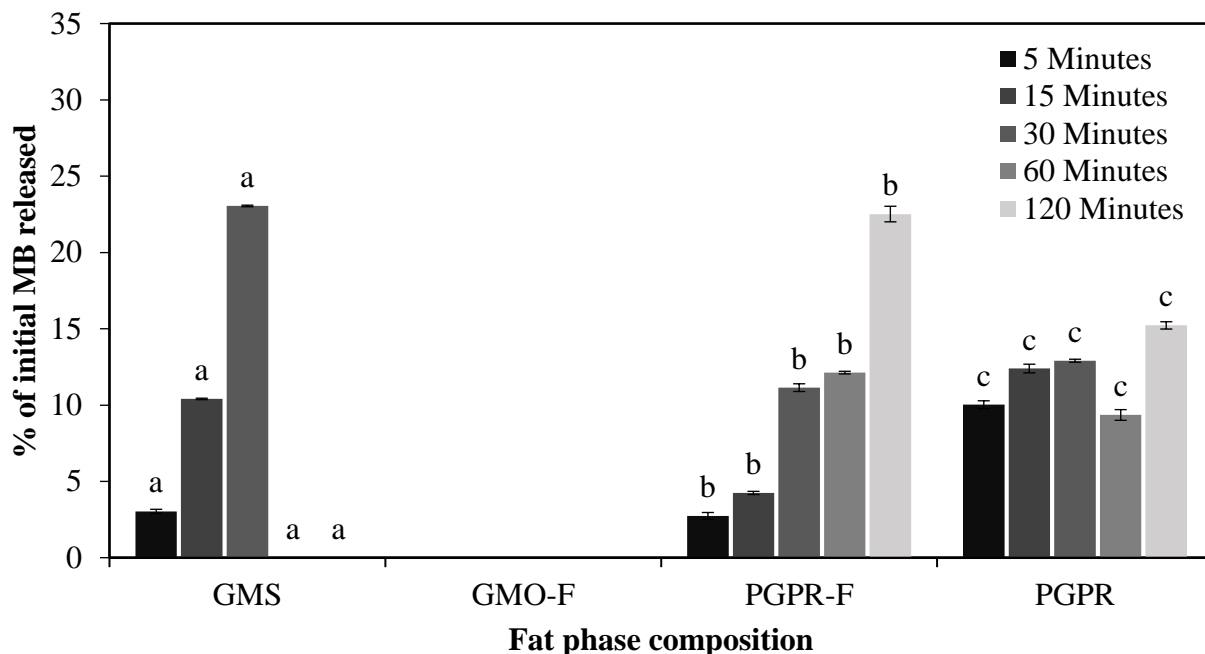


Figure 18. MB release from emulsions subjected to Condition 3 – SIF. All data are means based on $n = 3 \pm$ standard deviation. Letters denote significant differences (ANOVA/Tukey $p < 0.05$) within the same time point amongst the fat phase compositions.

not GMO-F, which was not considered in the analysis). **Figure 19** shows brightfield microscopy images of the emulsions subjected to Condition 3 – SIF for 30 and 120 min. There was a significant increase in MB release in all emulsions resulting from degradation of the interfacial film by the bile salts.^{51,71,73,84} Bile extract contains glycodeoxycholic acid, taurodeoxycholic acid, deoxycholic acid, and phospholipids⁷⁷, all of which interact with emulsions.^{18,77} Phospholipids, in particular, are known to compete for the oil-water interface, which may have resulted in displacement of interfacial crystals or other surface-active species.^{51,71,73,84} This phenomenon was particularly visible for the GMS and GMO-F emulsions as remnants of empty GMS shells were observed (Figure 19A and B (red arrows)], suggesting evidence of emulsion breakdown. The corresponding polarized light photomicrographs showed no fat crystals (Appendix, Figure A 21). There were two possible mechanisms to explain the lower MB release results of the GMS and GMO-F emulsions: i) the heterocyclic aromatic face of MB may chelate with carboxylic acids present in bile salt solutions⁵¹ or ii) the MB remained encapsulated within the inner aqueous phase of the emulsion.

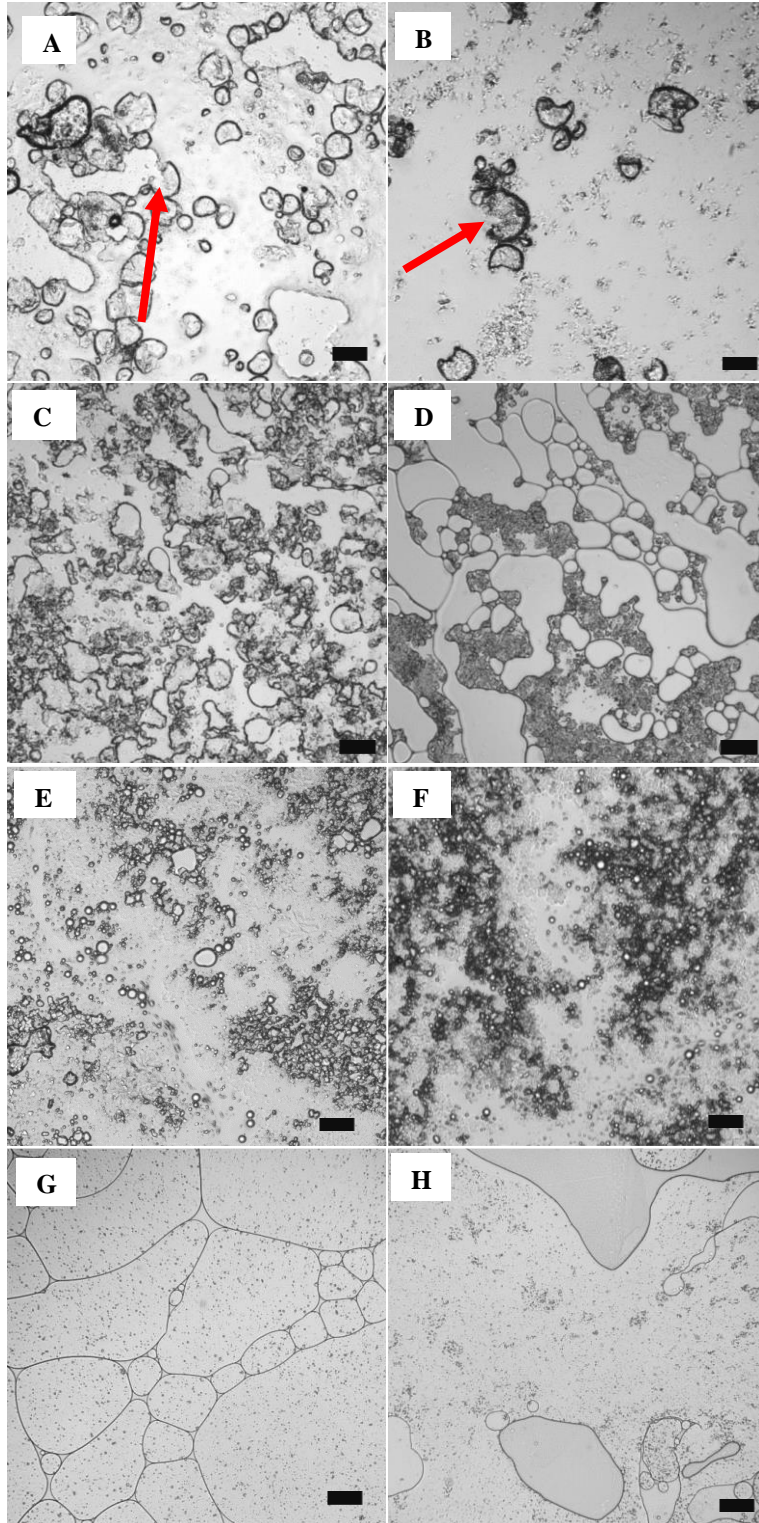


Figure 19. Brightfield microscopy of the 4 test emulsions subjected to Condition 3 – SIF for 30 minutes (left-hand column) or 120 min (right-hand column). A & B - GMS; C & D – GMO – F; E & F – PGPR-F; and G & H – PGPR. Red arrows in A and B indicate core-shell emulsion breakdown. Scale bars = 50 μ m.

The microstructure of the PGPR-F emulsion showed evidence of emulsion droplets even after 120 min of contact the Condition 3 – SIF (Figure 19F), though there was also extensive aggregation, suggesting that the fat crystal network was effective at protecting the dispersed phase from attack by the bile salts. It has been reported that bile salts interact with fats, emulsifying them and facilitating their breakdown into MAGs and free fatty acids via pancreatic lipase.^{73,77,85–87} Hence, the release trends seen in Figure 18 may be explained by the slow breakdown of fat facilitated by the bile salts over time, especially for the fat-containing emulsions (GMO-F and PGPR-F). This was not the case with the PGPR-only emulsion, where after 60 and 120 minutes, complete emulsion breakdown had taken place (Figure 19G and H), a further testament to the stabilizing role of the fat crystal network.

The overall release trends were as follows: i) in the presence of solid fat, whether at the interface (GMS) or in the continuous phase (PGPR-F), there was slower MB release initially. Following the destabilization of emulsion via bile salt competition^{71,73,87}, a greater release of MB was observed; ii) the GMO-F emulsion did not show any release, given its immediate and total breakdown once in contact with bile salts; iii) in the absence of solid fat (PGPR), the initial MB release was high, followed by a plateau. Results presented were in accordance with previous literature on bile salt activity presented by multiple research groups.^{32,51,70,73}

4.4 MB release from tests emulsions in SGF

Emulsion exposure to SGF is shown in Figure 20. In short, contact with SGF resulted in similar release profiles to that observed in Conditions 1, 2 and 3. The GMS emulsion released 3.7 ± 0.1 % MB at 30 minutes and 11.6 ± 0.6 % at 60 minutes ($p < 0.05$), with the GMO-F emulsion releasing 11.4 ± 0.4 % MB at 30 minutes and 12.0 ± 0.7 % at 60 minutes, respectively ($p > 0.05$). The PGPR-F emulsion released 2.3 ± 0.1 % MB at 30 minutes, but only 2.7 ± 0.04 % MB at 60 minutes ($p < 0.05$). Finally, the PGPR emulsion released 3.2 ± 0.1 % MB at 30 minutes and 12.3 ± 0.2 % at 60 minutes ($p < 0.05$).

The GMS emulsion was greatly influenced by contact with the SGF, with large misshapen droplets present in the emulsions (92.4 ± 5.7 μm at 60 min). The acidic conditions present in the SGF likely hydrolyzed the MAGs resulting in their displacement from the interfacial film (Figure 21A),^{20,88} with the mechanical mixing upping the collision frequency between the GMS-covered droplets, which further contributed to MB release.^{20,88}

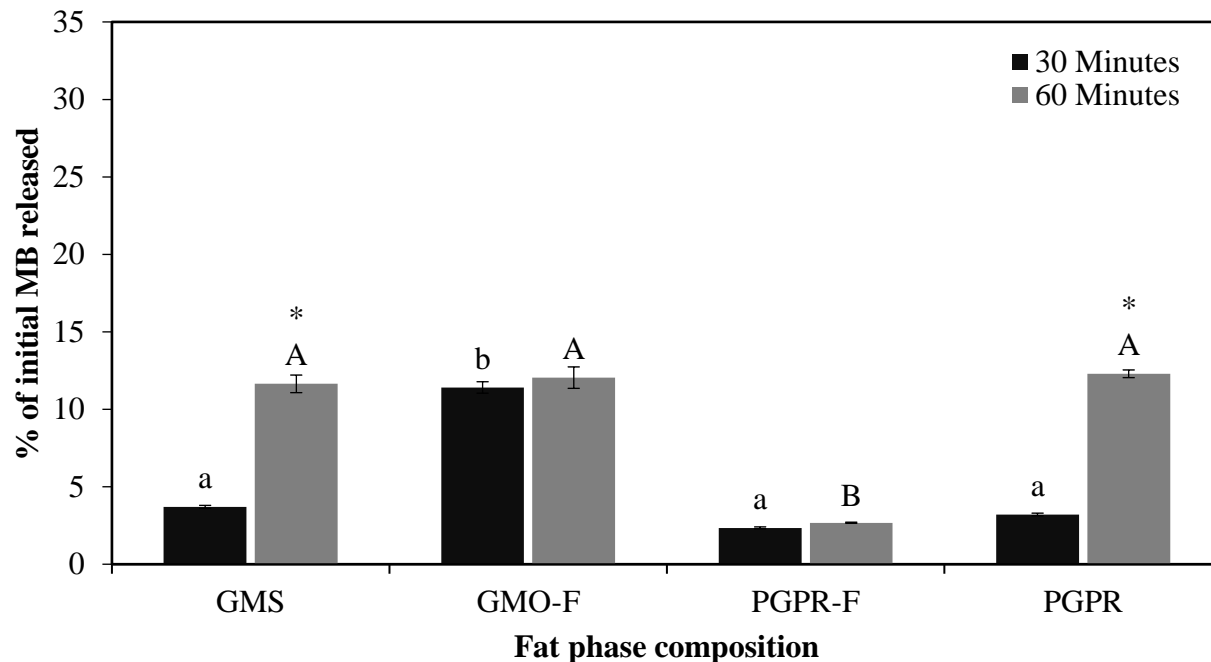


Figure 20. MB release from emulsions subjected to SGF. All data are means based on $n = 3 \pm$ standard deviation. Between each phase composition, the letters denote significant differences within the same time point (30 or 60 min – lowercase and uppercase, respectively) (ANOVA/Tukey – $p < 0.05$). * denotes significant differences between time points (30 and 60 min) within the same fat phase composition (Student’s T-test, $p < 0.05$).

After 60 min of contact with SGF, the GMO-F emulsion showed similar MB release as the GMS-stabilized emulsion. However, this was not necessarily borne out by the microstructure, which showed a distinct morphology that differed from that of the GMS emulsion. The GMO-F emulsion was still populated by large aqueous droplets ($86.7 \pm 5.3 \mu\text{m}$ at 60 min, Figure 21B), suggesting that the fat crystal network was effectively contributing to stabilization of the emulsion. Statistically, there were no significant differences between GMS and GMO-F emulsions after 60 minutes of digestion in SGF ($p > 0.05$).

The lowest extent of release occurred with the PGPR-F emulsion, which appeared able to resist the effects of the acid, osmotic gradient and mechanical mixing (Figure 21C). These results agreed with the findings of Howes et al., who described the low digestibility of PGPR within gastric conditions in animal models.⁸⁹ Therefore, the combined presence of PGPR and a solid fat network

was responsible for the limited release. The average droplet size ($55.2 \pm 5.5 \mu\text{m}$) at 60 min was smaller than with the GMO-F emulsion.

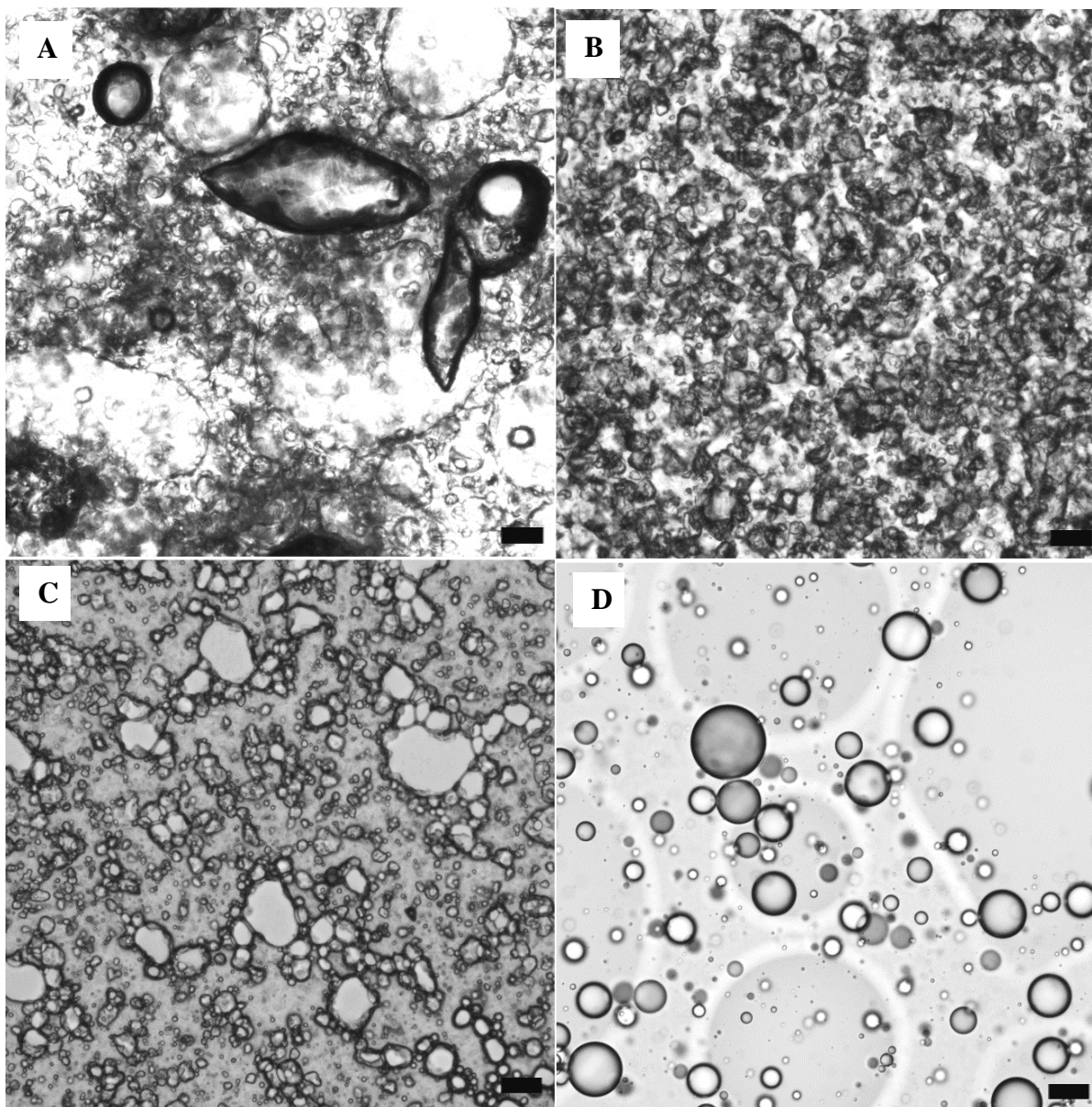


Figure 21. Brightfield light microscopy of the 4 test emulsions subjected to SGF for 60 minutes. A - GMS; B – GMO-F; C – PGPR-F; and D – PGPR. Scale bars = 50 μm .

Finally, the PGPR-only emulsion showed low initial release similar to the PGPR-F emulsion. However, this was followed by a greater extent of release. Figure 21D shows the presence of spherical droplets ($118.9 \pm 3.1 \mu\text{m}$ at 60 min), an average twice that of the PGPR-F emulsion. These results suggested that this surfactant, though affected by the SGF, was not completely

degraded. Expectedly, the presence of pepsin in SGF did not contribute to MB release as the overall release profile remained similar to Conditions 1, 2 and 3 for all emulsifiers.

4.5 MB release from tests emulsions in SIF

Emulsion exposure to SIF is shown in Figure 22. For each emulsion type, increased exposure time resulted in significant differences in MB release ($p < 0.05$). Maximum release with GMS occurred at 15 minutes ($10.7 \pm 0.8 \%$), after which the extent of release diminished to $5.2 \pm 0.2 \%$ at 120 minutes ($p < 0.05$). The GMO-F emulsion showed the highest extent of release of all emulsions, with maximum release seen at 15 minutes ($26.0 \pm 0.4 \%$), after which the extent of release also started to drop, reaching $14.6 \pm 0.3 \%$ at 120 minutes ($p < 0.05$). Overall, the PGPR-F emulsion showed the lowest extent of release, with the maximum extent reaching $5.8 \pm 0.1 \%$ of MB at 60 minutes. Finally, the PGPR emulsion plateaued at 60 minutes ($18.7 \pm 0.9\%$), dropping thereafter ($9.4 \pm 0.4 \%$ at 120 minutes).

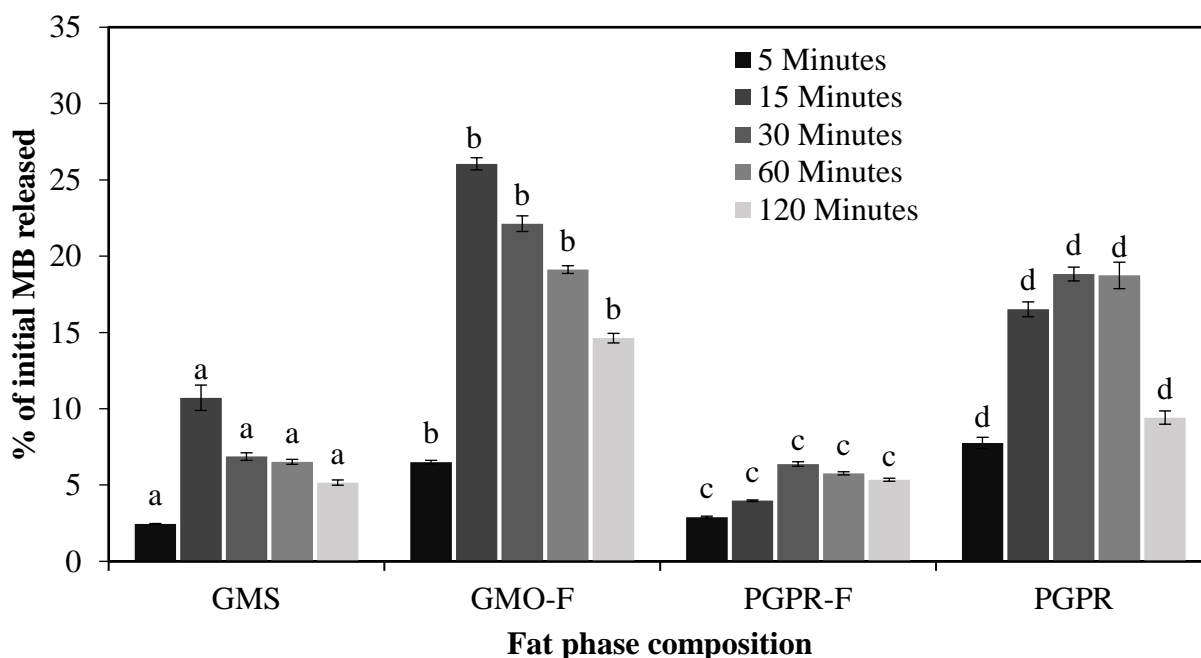


Figure 22. MB release from emulsions subjected to SIF. All data are means based on $n = 3 \pm$ standard deviation. Letters denote significant differences (ANOVA/Tukey $p < 0.05$) within the same time point amongst the fat phase compositions.

Microstructurally, there remained undigested GMS core-shells that contained still encapsulated MB after 30 minutes of contact with SIF (Figure 23A). However, after 2 h of contact, the emulsion had fully broken down (Figure 23B), which was not borne out by the release results, however. Overall, release with GMS was slow and generally limited. This was in agreement with the study of Yasmin et al., who stated that the presence of solid-state GMS slowed digestion in drug release studies.⁸⁸ Alternatively, following the maximum release at 15 minutes, MB was slowly micellized along and/or complexed with SIF media.^{32,73,90,91} A similar phenomenon was observed by Aditya et al., where during 2 h of intestinal digestion, curcumin was micellized.⁹⁰ The highest MB release likely corresponded to breakdown of the interfacial film followed by a subsequent decrease in release due to MB being micellized and no longer measurable.⁵¹

The greatest extent of MB release was with the GMO-F emulsion, which indicated that the GMO-based emulsion broke down in SIF, irrespective of the presence of solid fat (Figure 23C and D). In fact, the oil-water interface in the GMO-F emulsion underwent rapid breakdown within 5 min of contact with SIF (Appendix, Figure A 23). It is likely that the bile salt competed for the interface, with pancreatin aiding in displacement of emulsifier/fat from the interface.^{10,71} Zhou et al. determined that GMO micellizes with bile salts, which would support the present observations.⁷³

The PGPR-F emulsion yielded the lowest release, with only a gradual increase in droplet size with time ($63.3 \pm 4.5 \mu\text{m}$ at 120 min) (Figure 23E and 23F). Marquez et al. found that NaCl and CaCl₂ enhanced the stability of emulsions formulated with PGPR. The low MB release showed that the combined presence of PGPR and a fat crystal network provided resistance against digestion in SIF. Finally, the PGPR-only emulsion showed a release pattern between that of the GMO-F and PGPR-F. Microstructurally, however, significant breakdown was seen after 30 minutes of contact with SIF (Figure 23G). By 120 min, the emulsion had fully broken down (Figure 23H). Though the PGPR demonstrated increased resistance compared to the GMO-based emulsion, the absence of a surrounding fat crystal network resulted in a higher release than in the PGPR-F emulsion.

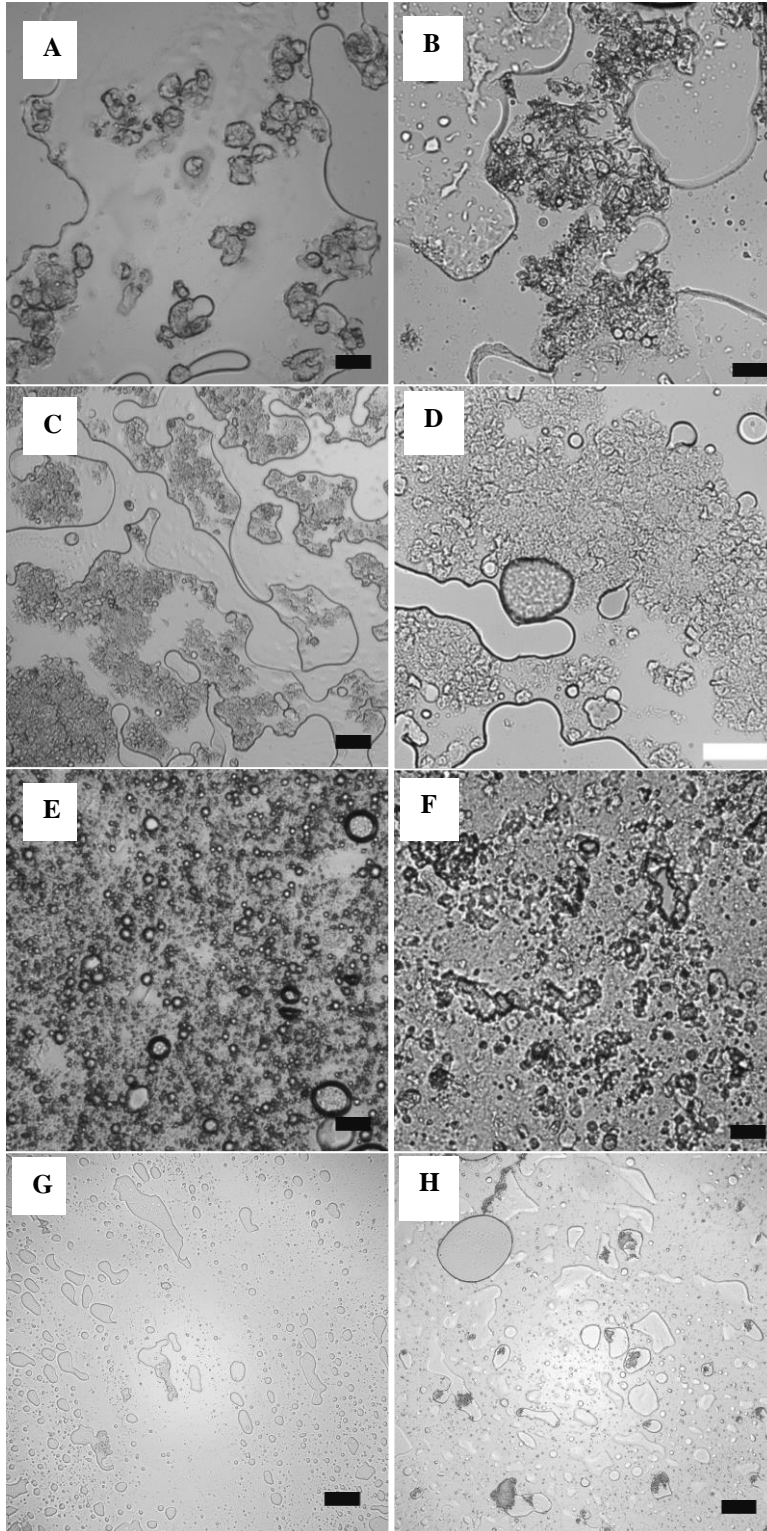


Figure 23. Brightfield microscopy of the 4 test emulsions subjected to SIF for 30 minutes (left-hand column) or 120 min (right-hand column). A & B - GMS; C & D - GMO - F; E & F - PGPR-F; and G & H - PGPR. Scale bars = 50 μ m.

Overall, these results suggested that the effect of bile salts as an interfacial competitor diminished in SIF (Figure 22) compared to Condition 3 – SIF (Figure 18). The release profiles in Condition 3 – SIF showed increasing release with time whereas in SIF, a decrease in MB release was observed following an initial peak in MB release. In Condition 3, the bile salts competed for the oil-water interface thereby displacing the surfactant and destabilizing the emulsion.³² Interactions between bile salts and MB may have led to the lower MB release observed. A study by Werawatganone and Muangsiri showed that formation of micelles and reverse micelles decreased the absorbance intensity of the dyes bromothymol blue and neutral red, which resulted in lower overall detectable concentrations.⁹¹

To further explore the MB release behaviour in Figure 22, and the role bile salt played in emulsion destabilization, the recovery yield of MB in a bile salt solution was determined. Selvam et al. previously explored association of bile salt with MB, showing that it becomes micellized.⁵¹ Here, MB was exposed to a bile salt solution and processed using the same conditions as SIF (37 °C at 6 rpm for 120 mins). Similar to Selvam et al., the % MB recovery linearly decreased with contact time, with 100% at 5 minutes dropping to 82% at 120 minutes (Figure 24),⁵¹ strongly hinting at

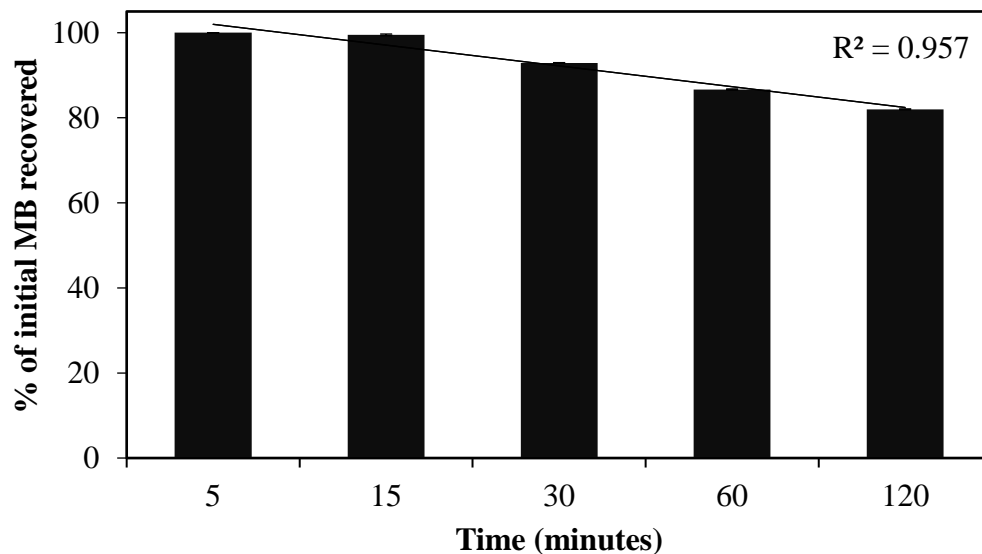


Figure 24. MB recovery as a function of time in bile salt solution over 120 minutes at 37 °C and 6 rpm. All data are means based on $n = 3 \pm$ standard deviation.

bile salt-MB interactions limiting recovery. Interaction between MB with bile salts and perhaps free fatty acids may have contributed to lower overall release in SIF conditions when compared to Condition 3 - SIF.

4.6 Mechanistic considerations

The observed differences in MB release arose from the compositional and structural differences of the four test emulsions. The proposed mechanisms by which MB release occurred are shown in Figure 25 for SGF and Figure 26 for SIF.

All test emulsions containing solid fat crystals (GMS, GMO-F and PGPR-F – Figure 25A - C) experienced an increase in droplet size when subjected to each of the SGF Conditions 1-3. This effect may have been due to the osmotic pressure gradient between the release medium and dispersed phase and/or mechanical stress during mixing. Andrade et al. stated that the differences in ionic strength between the inner and outer aqueous phases of double emulsions induced vitamin B12 release, irrespective of the presence of solid fat in the oil phase.⁹² In parallel, mixing favoured collisions between droplets contributing to the breakdown of core-shells and/or weakened the solid fat network. Both suggested mechanisms would ultimately favour coalescence and release of the entrapped MB. Finally, in the system where solid fat was absent (PGPR, Figure 25D), MB release may have occurred as a result of droplet migration due to swelling (and gravity), and mechanical stress causing flocculation, coalescence and subsequent release.^{45,48,93} In SIF conditions 1 and 2, the behaviour of all test emulsions was similar to SGF conditions 1 and 2. Therefore, the mechanisms regarding the release of MB would presumably also be similar.

In the presence of bile salts alone (not shown), there was noticeable destabilization of the GMS emulsion (Figure 26A), with presence of solid droplets and half-degraded shells (**Error! Reference source not found.**) leading to higher MB release (Figure 18). In case of GMO-F emulsion, although destabilization was observed, no release was measured potentially due to formation of bile salt micelles containing or chelating MB⁵¹ (Figure 24).

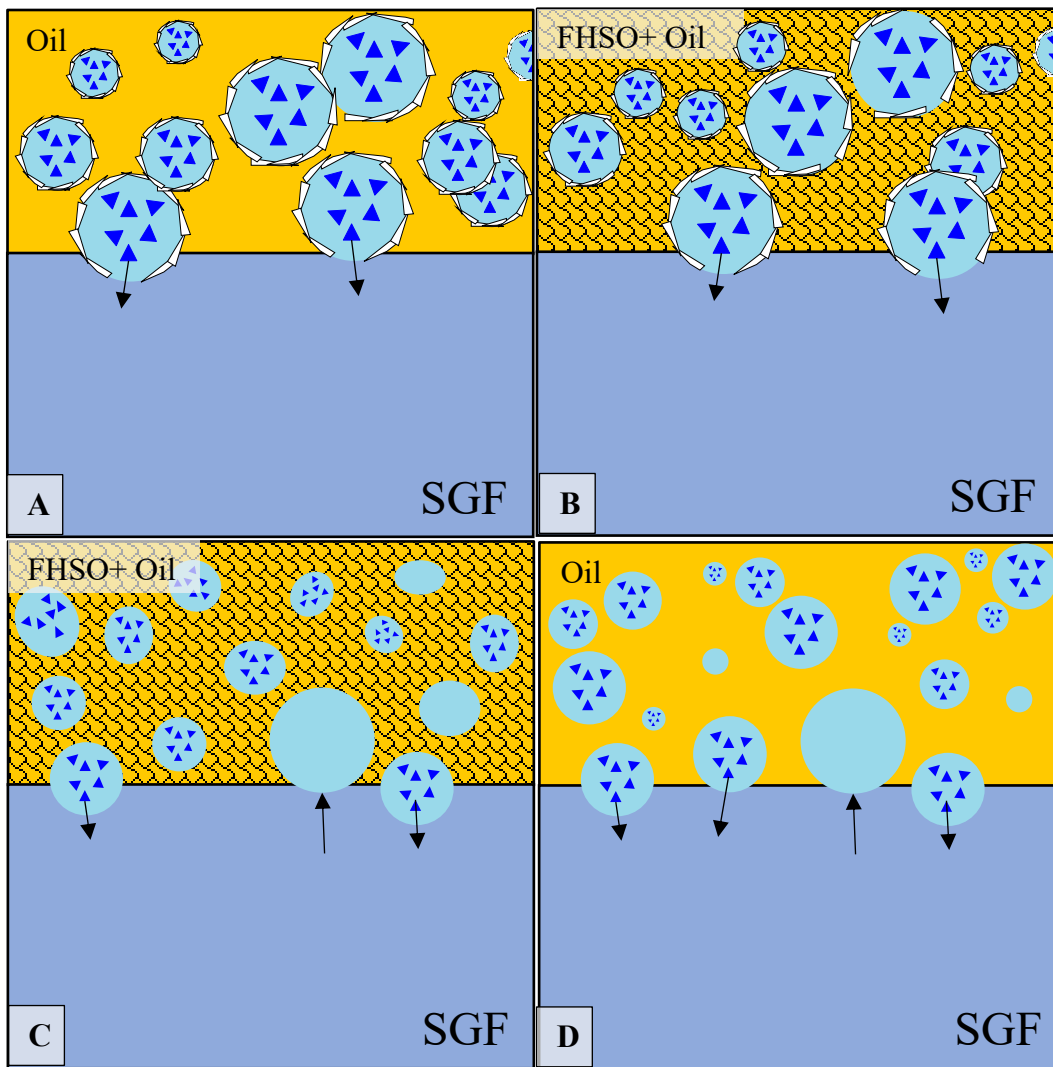


Figure 25. Possible mechanism of MB release in SGF for GMS (A), PGPR-F (B), GMO-F (C), and PGPR (D) emulsions. The symbol \triangle at the interface represents GMS and GMO, and \blacktriangle represents MB.

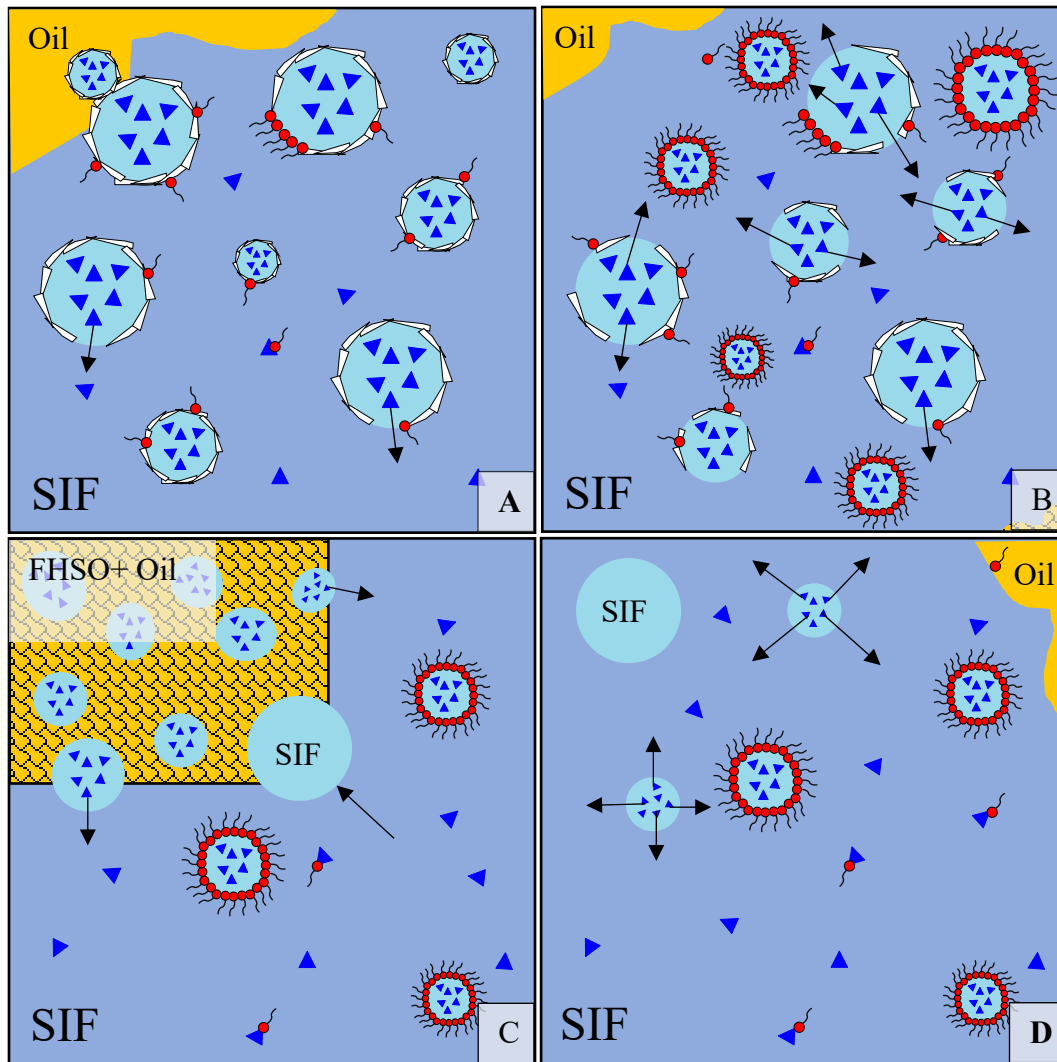


Figure 26. Possible mechanism(s) of MB release in SIF for GMS (A), PGPR-F (B), GMO-F (C), and PGPR (D) emulsions. The symbol \triangle at the interface represents GMS and GMO, \circ represents bile salts, and \blacktriangle represents MB. Micelles are shown as large for visualization only.

The proposed mechanism of MB release in SIF for all fat phase compositions is as follows (Figure 26):

- i) in the presence of solid fat, bile salts may act on the interface or structured fat phase in bulk oil, displacing the emulsifiers that contribute to the barrier that prevents flocculation, coalescence and therefore release (Figure 26B and C);
- ii) absence of solid fat may allow for direct release as a result of lipolysis of surrounding bulk oil, and differences in osmotic pressure (Figure 26A and D);

- iii) MB interacts with bile salts and is micellized⁵¹ potentially lowering the overall absorbance readings and decreasing the intensity of the absorbance peak, therefore, the release readings are lower (Figure 26A – D).
- iv) Throughout the intestinal digestion, mixed micelles containing bile salts and free fatty acids are formed encapsulating MB and SIF in the process (Figure 26A – D).⁹⁰

5.0 Overall conclusion

Kinetically-stable W/O emulsions generated with different fat phase compositions were evaluated for their ability to encapsulate and release MB in gastric and intestinal conditions. Irrespective of the emulsifier present, initial MB encapsulation capacities were near identical. Time, dilution rates and the incremental environment complexity all affected MB release. Core-shell emulsions (GMS and GMO-F) displayed the highest release of MB in both gastric and intestinal fluids, which contrasted with our null hypothesis that core-shell emulsions would provide the highest retention of MB (GMS), and that the presence of FHSO would provide an additional barrier against release (GMO). The PGPR-based emulsions, both with and without stabilized fat, showed a lower extent of MB release. As well, irrespective of surfactant type, the presence of a solid fat network may have restricted droplet migration but did not delay breakdown. The emulsion consisting of PGPR and a surrounding fat crystal network showed the lowest overall extent of release. Therefore, the type of surfactant and solid fat stabilization scheme may be used to control the release behaviour of an encapsulated aqueous compound.

6.0 Future work

Future research efforts should explore additional W/O emulsion systems such as GMS-based emulsions that also contain a surrounding fat crystal network or perhaps GMO-based emulsions that are kinetically stable. As well, changes in composition such as using different solid fats or oils as well as altering the aqueous phase composition should be considered. This may allow for further elucidation of the structure-function relationship that is responsible for emulsion stability in the presence of the digestive fluids. Unusual features such as outer aqueous phase reincorporation as a coarse emulsion in the PGPR-F and PGPR emulsions may warrant scrutiny, especially in regards to the role of salts on PGPR interfacial behaviour. Finally, competitive behaviour between the emulsifiers, solid fat crystals and components from the digestive fluids at the oil-water interface should be further investigated. A deeper understanding of these various factors would allow for the creation of highly-tunable emulsion-based release systems.

Appendix

Method development & Initial emulsion properties

Formulation parameters to attain similar droplet size distributions for all emulsions were determined using the starting compositions shown in **Error! Reference source not found.** along with optimization of homogenization, cooling rate, post-cooling stirring, and water:oil ratios.

Table A 1. Formulation parameters. Tabulated experimental and optimized phase compositions.

Emulsifier / Fat Combinations	Experimental oil phase compositions (g/100g canola oil)	Ideal oil phase compositions (g/100g canola oil)
GMS	2, 2.5, 3, 3.5, 4.5, 5 GMS	4 GMS
GMO – FHSO	2, 2.5, 3, 3.5, 4.5, 5 GMO	4 GMO, 10 FHSO
PGPR – FHSO	0.5, 1, 1.5, 2, 2.5, 4 PGPR	2 PGPR, 10 FHSO
PGPR	0.5, 1, 1.5, 2, 2.5, 4 PGPR	2 PGPR

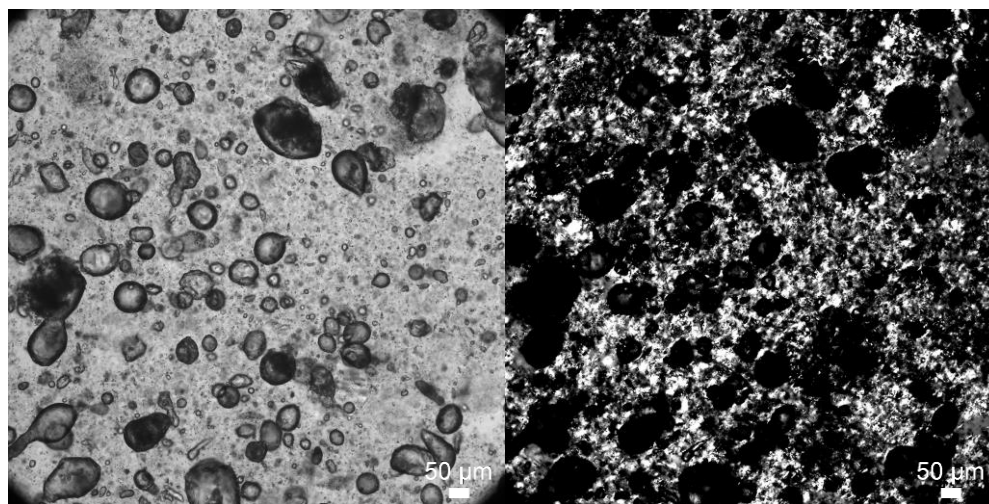


Figure A 1. 4 wt.% GMS emulsion with a $\sim 60 \mu\text{m}$ average droplet size. Left is brightfield image taken on inverted light microscope with the corresponding polarized light image of the same field of view at right. Images were captured 25°C . Scale bars = $50 \mu\text{m}$.



Figure A 2. W/O emulsions made with 1-4 wt% PGPR aged 16h at room temperature. Emulsions were prepared using magnetic stirring at 200-250 rpm.

Figures and photomicrographs

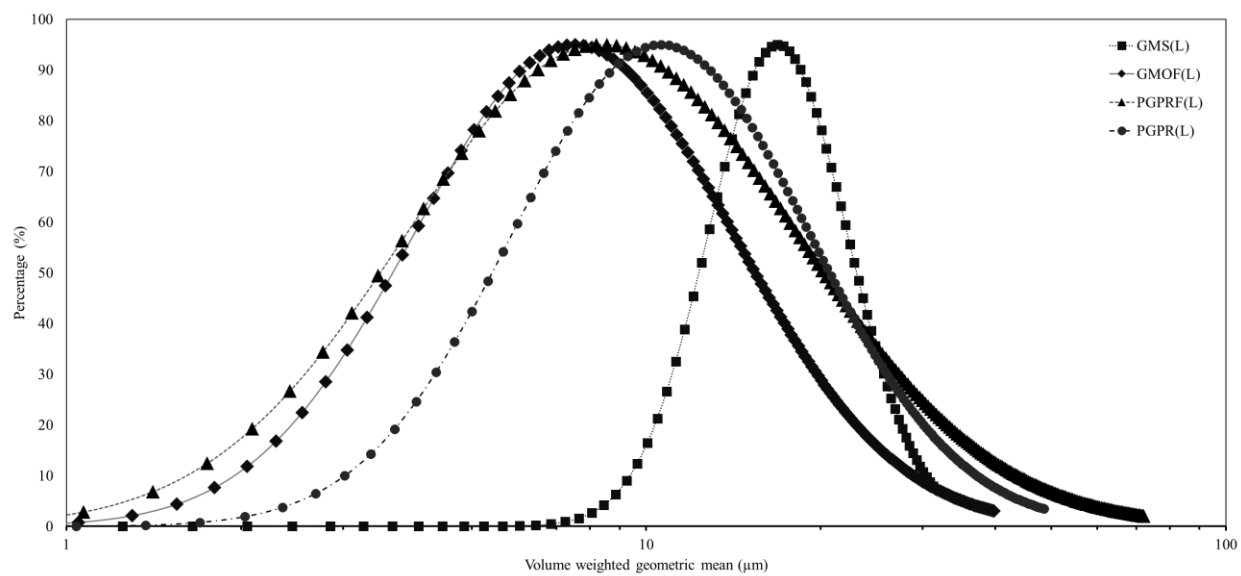


Figure A 3. pfg-NMR aqueous droplet size distributions of test emulsions loaded with 1mM MB. All data are mean for $n = 3 \pm$ standard deviation (error bars are omitted for clarity).

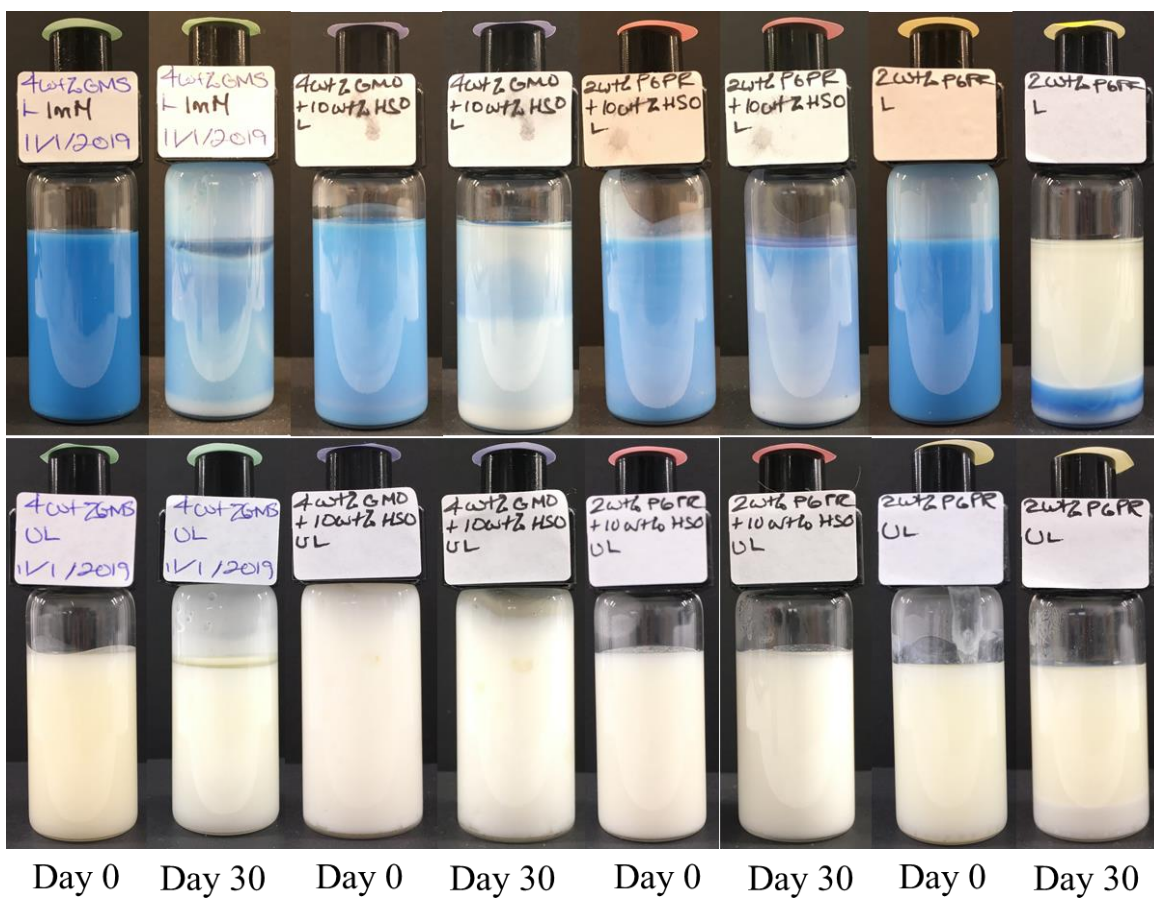


Figure A 4. Vials of emulsions loaded with 1mM MB (top row) and unloaded emulsions (bottom row) stored at 25 °C for 30 days.

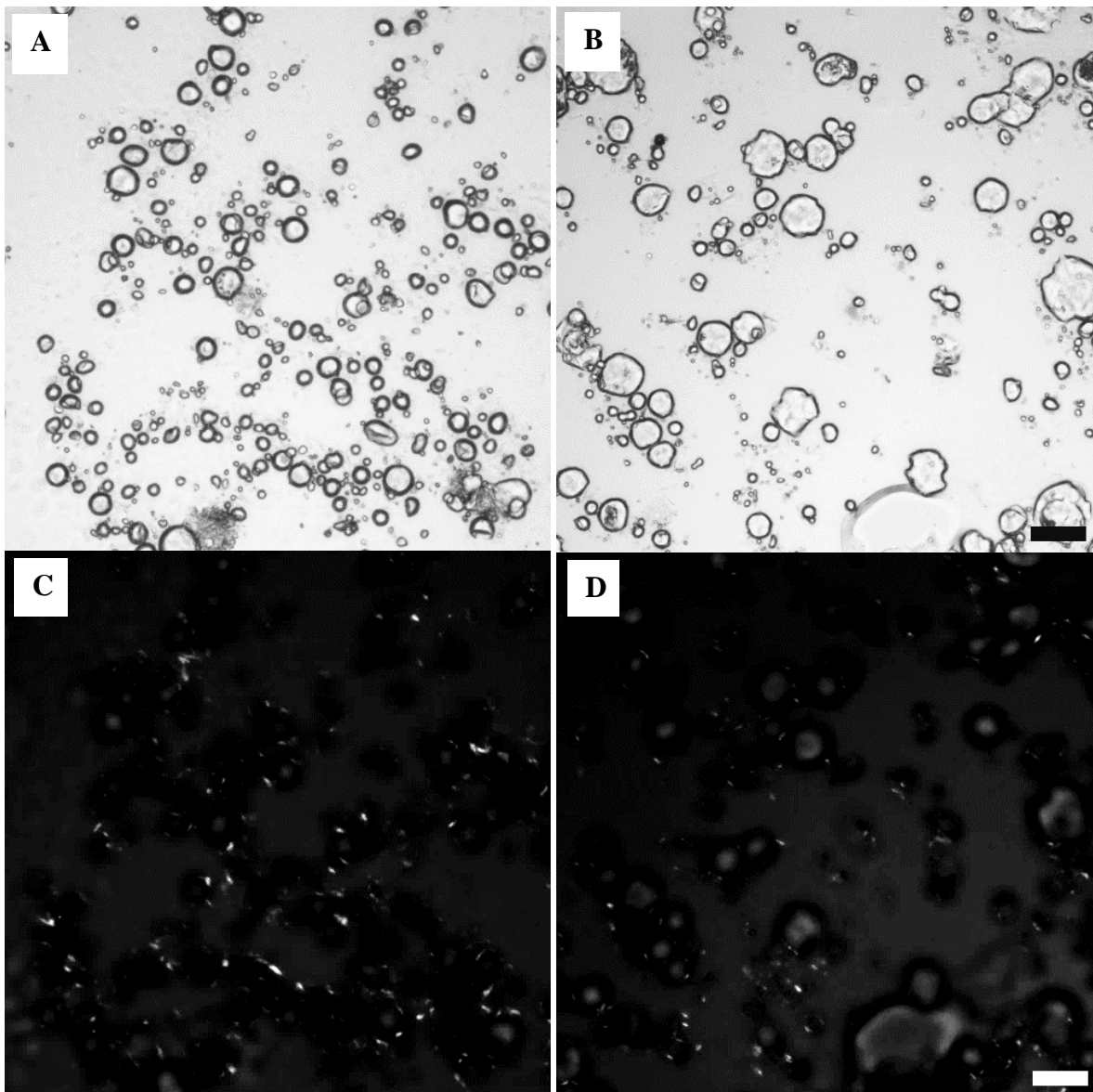


Figure A 5. Microstructure of GMS-based emulsion in Condition 1 taken in brightfield and polarized light microscopy at 25 °C at 30 minutes (A, C), and 60 minutes (B, D). Scale bars = 50 μm .

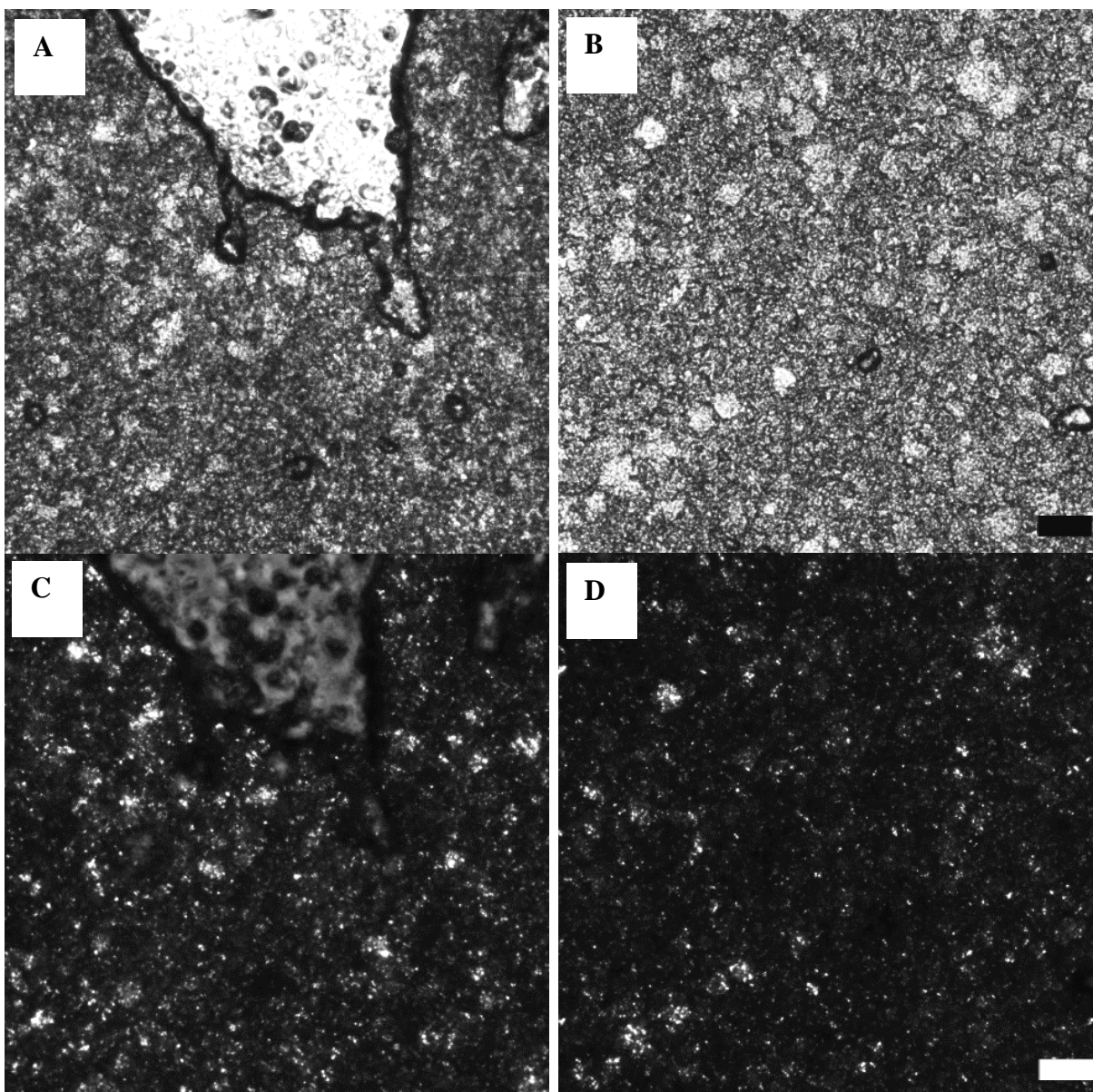


Figure A 6. Microstructure of GMO-F emulsion in condition 1 taken in brightfield and polarized light microscopy at 25 °C at 30 minutes (A, C), and 60 minutes (B, D). Scale bars = 50 μ m.

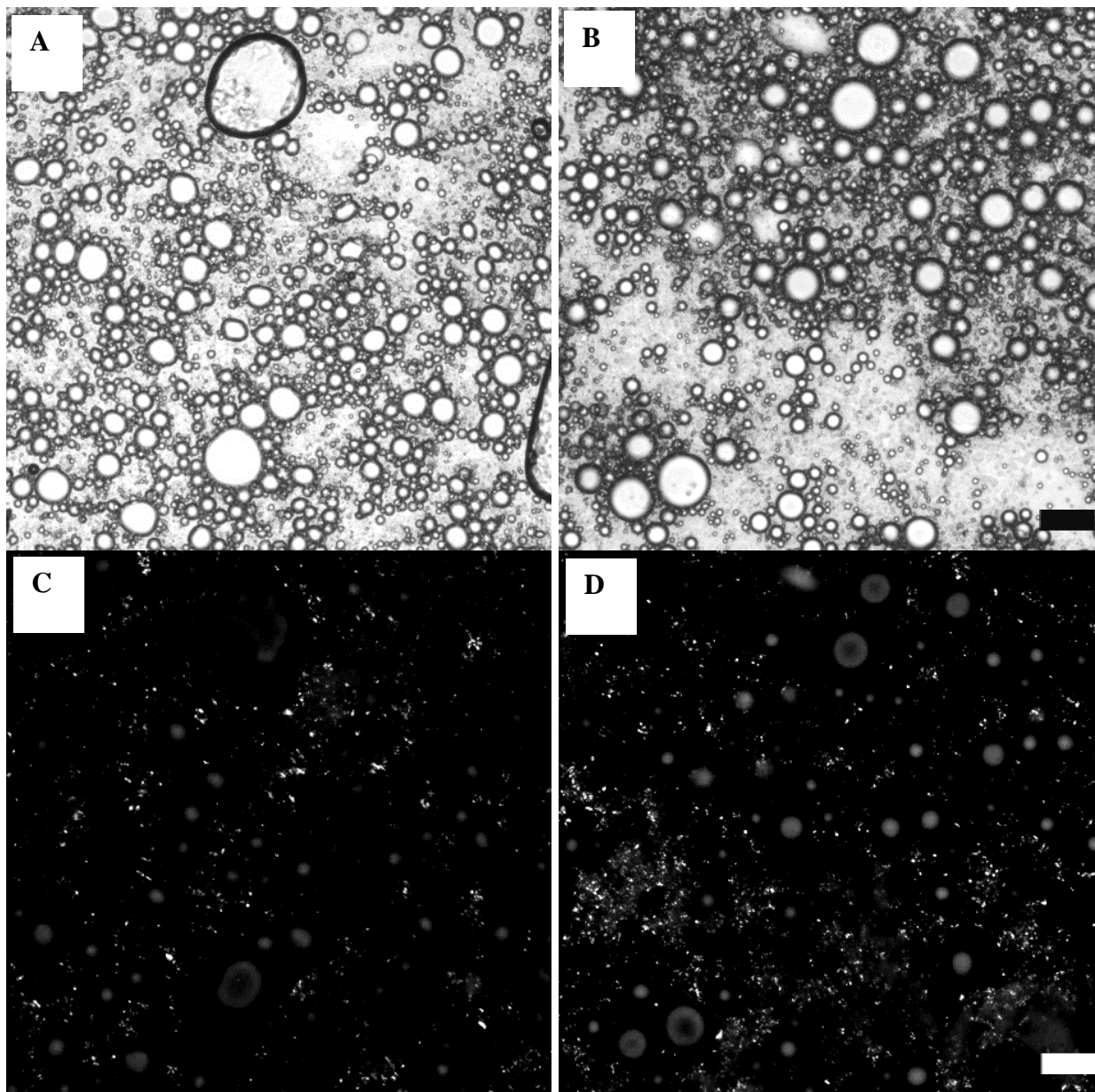


Figure A 7. Microstructure of PGPR-F emulsion in condition 1 taken in brightfield and polarized light microscopy at 25 °C at 30 minutes (A, C), and 60 minutes (B, D). Scale bars = 50 μm

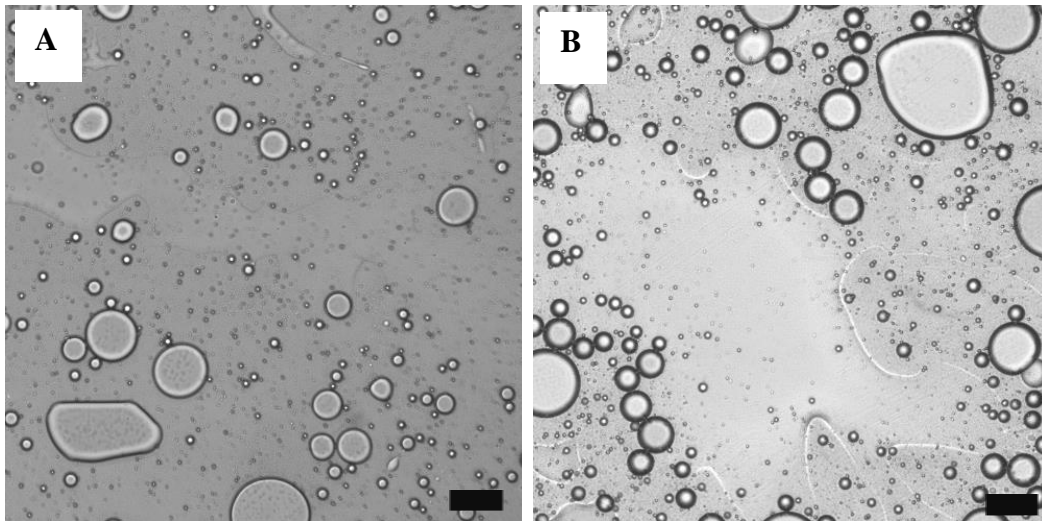


Figure A 8. Microstructure of PGPR emulsion in condition taken in brightfield and polarized light microscopy at 25 °C at 30 minutes (A), and 60 minutes (B). Scale bars = 50 μm .

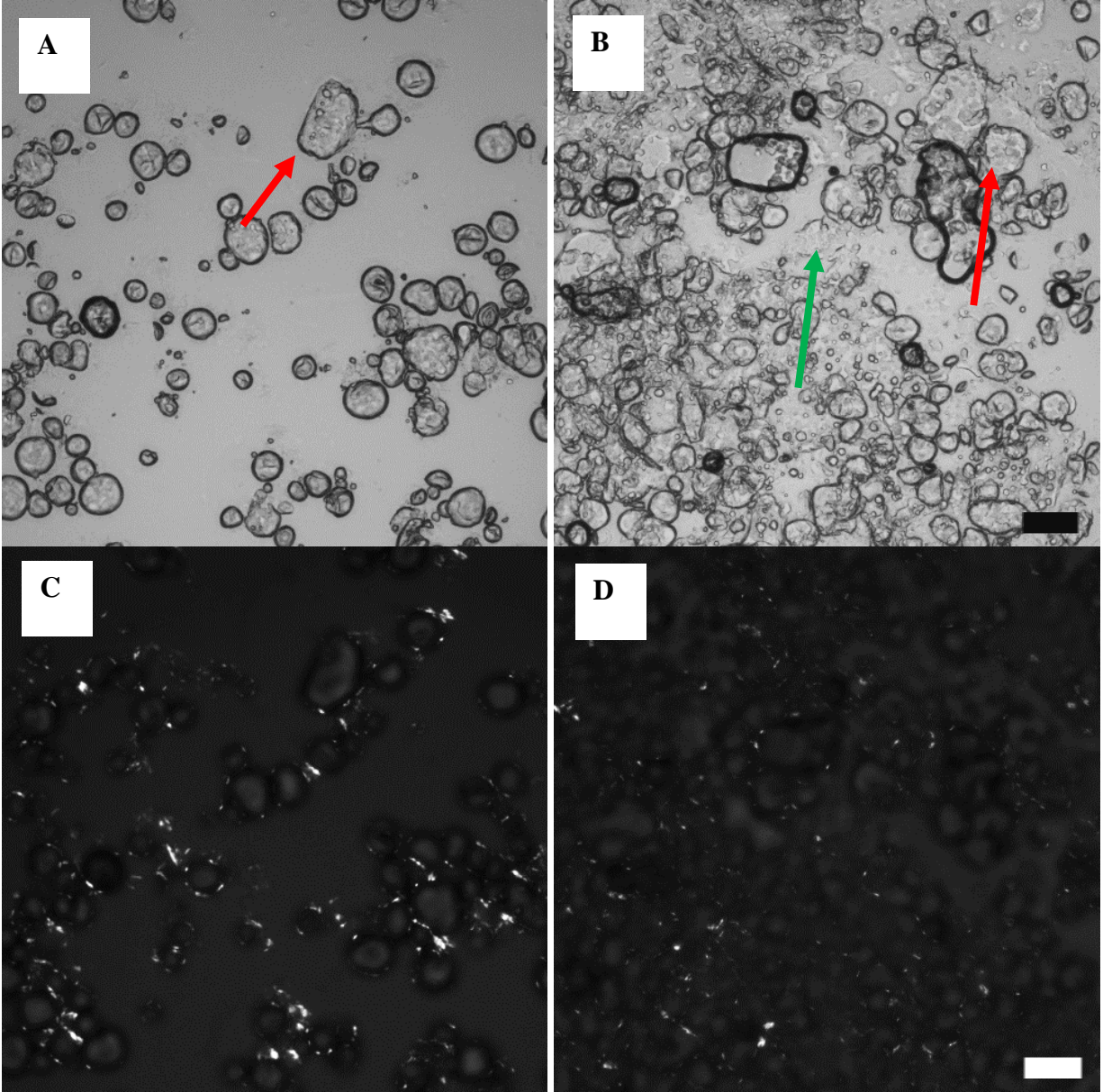


Figure A 9. Microstructure of GMS emulsion in condition 2 – SGF taken in brightfield and polarized light microscopy at 25 °C at 30 minutes (A, C), and 60 minutes (B, D). Scale bars = 50 μm

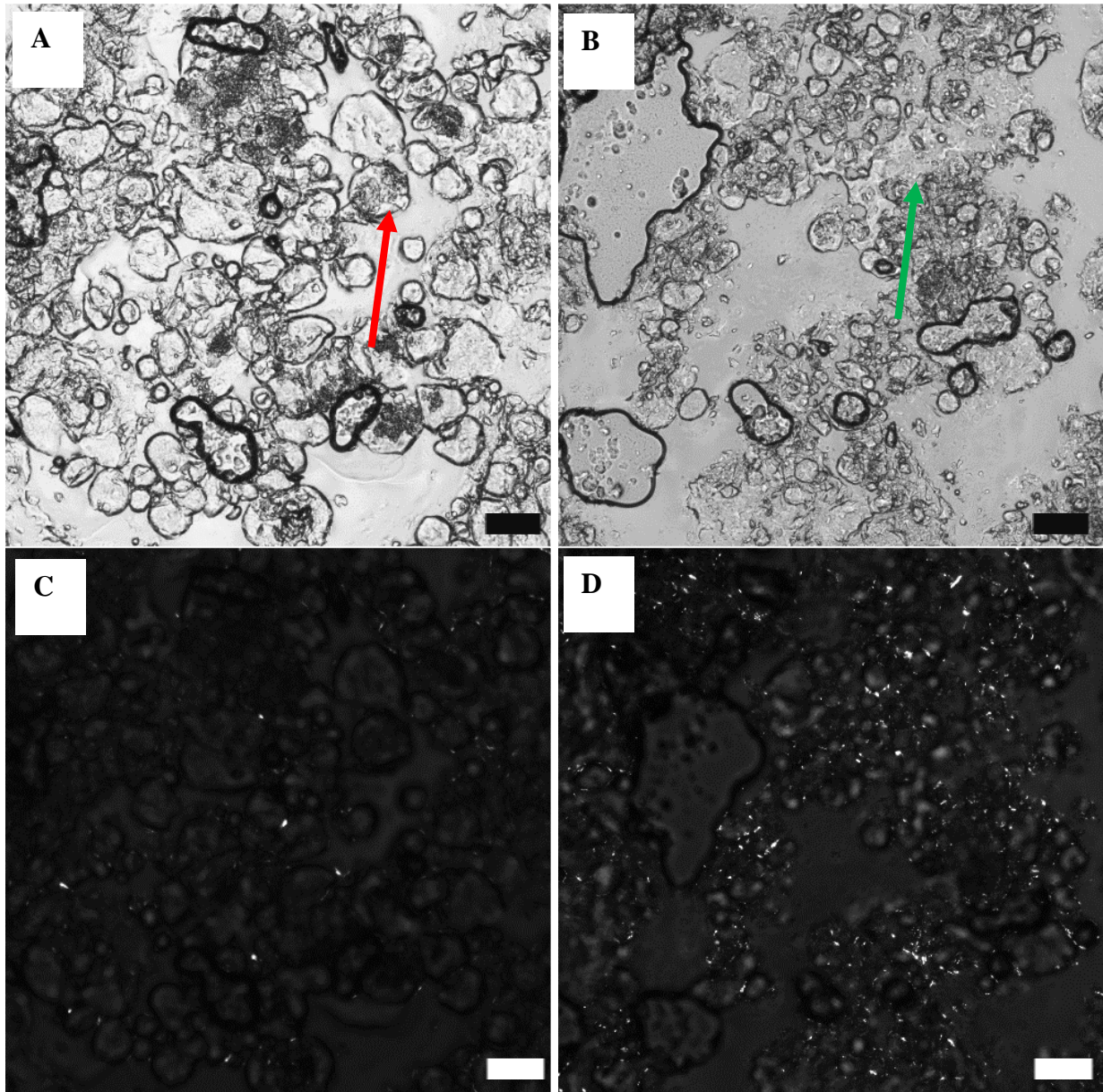


Figure A 10. Microstructure of GMS emulsion in condition 2 – SIF taken in brightfield and polarized light microscopy at 25 °C at 30 minutes (A, B), and 60 minutes (B, D). Scale bars = 50 μm .

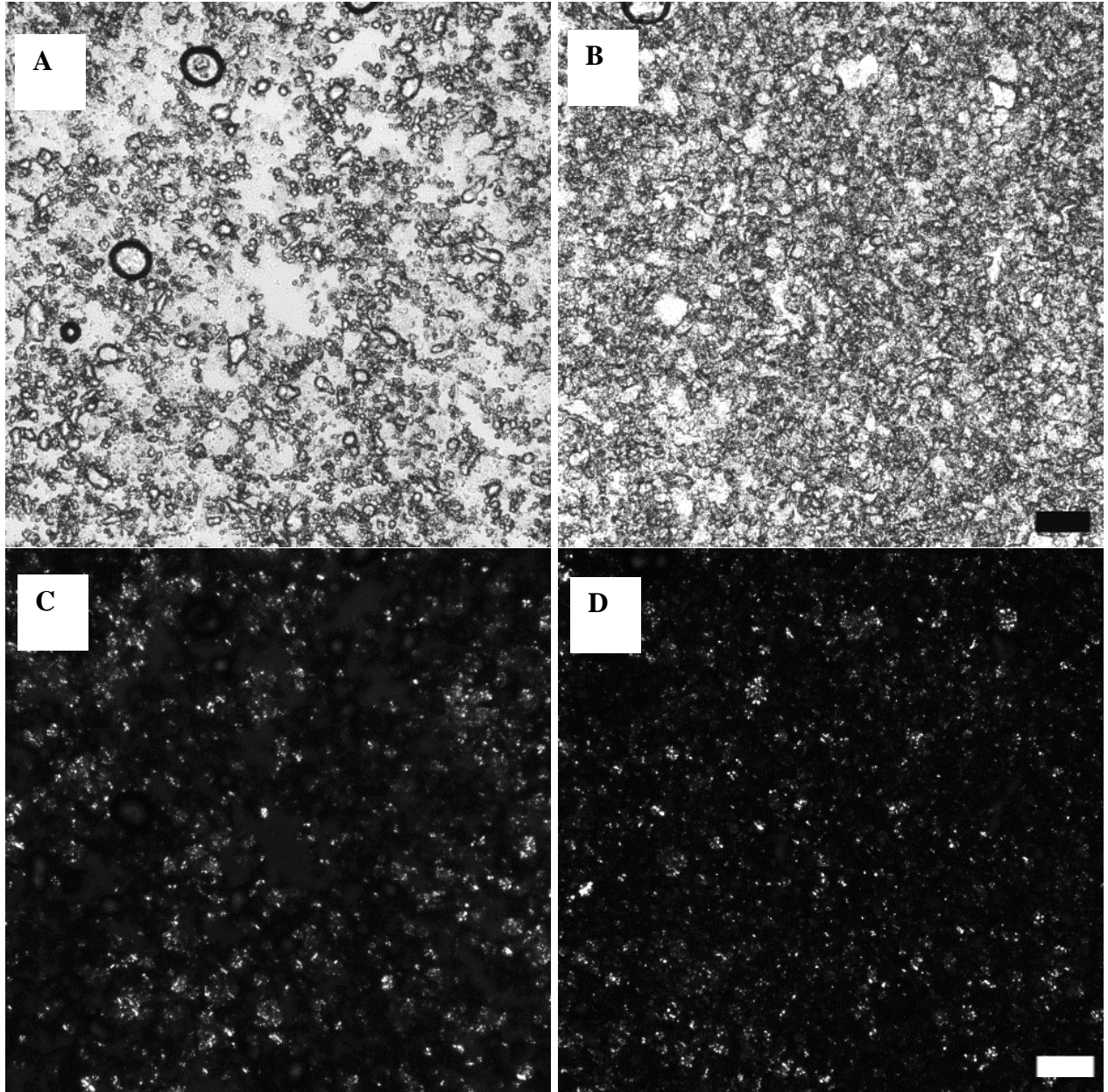


Figure A 11. Microstructure of GMO-F emulsion in condition 2 – SGF taken in brightfield and polarized light microscopy at 25 °C at 30 minutes (A, C), and 60 minutes (B, D). Scale bars = 50 μm .

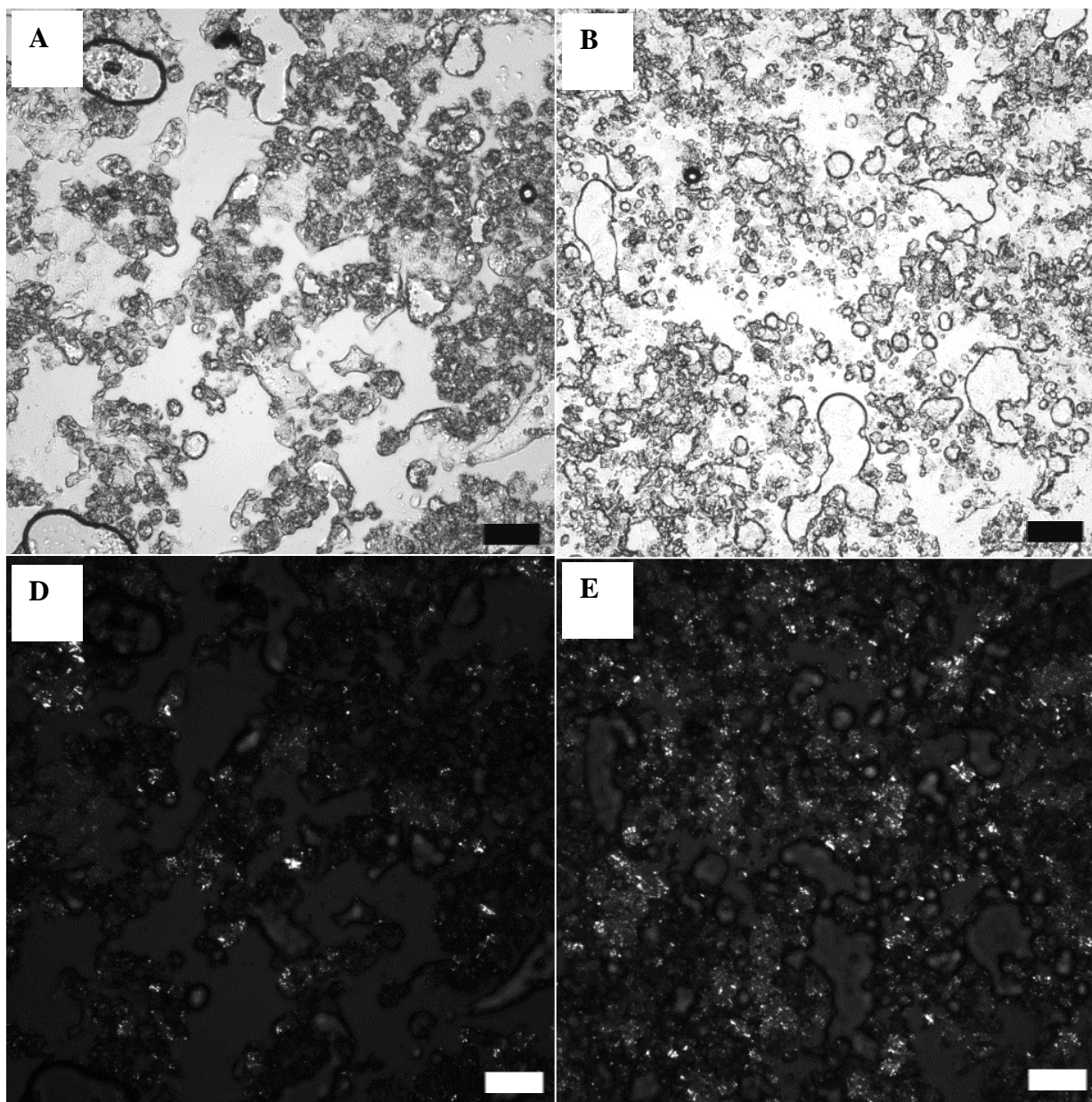


Figure A 12. Microstructure of GMO-F emulsion in condition 2 – SIF taken in brightfield and polarized light microscopy at 25 °C at 30 minutes (A, B), and 60 minutes (B, D). Scale bars = 50 μm .

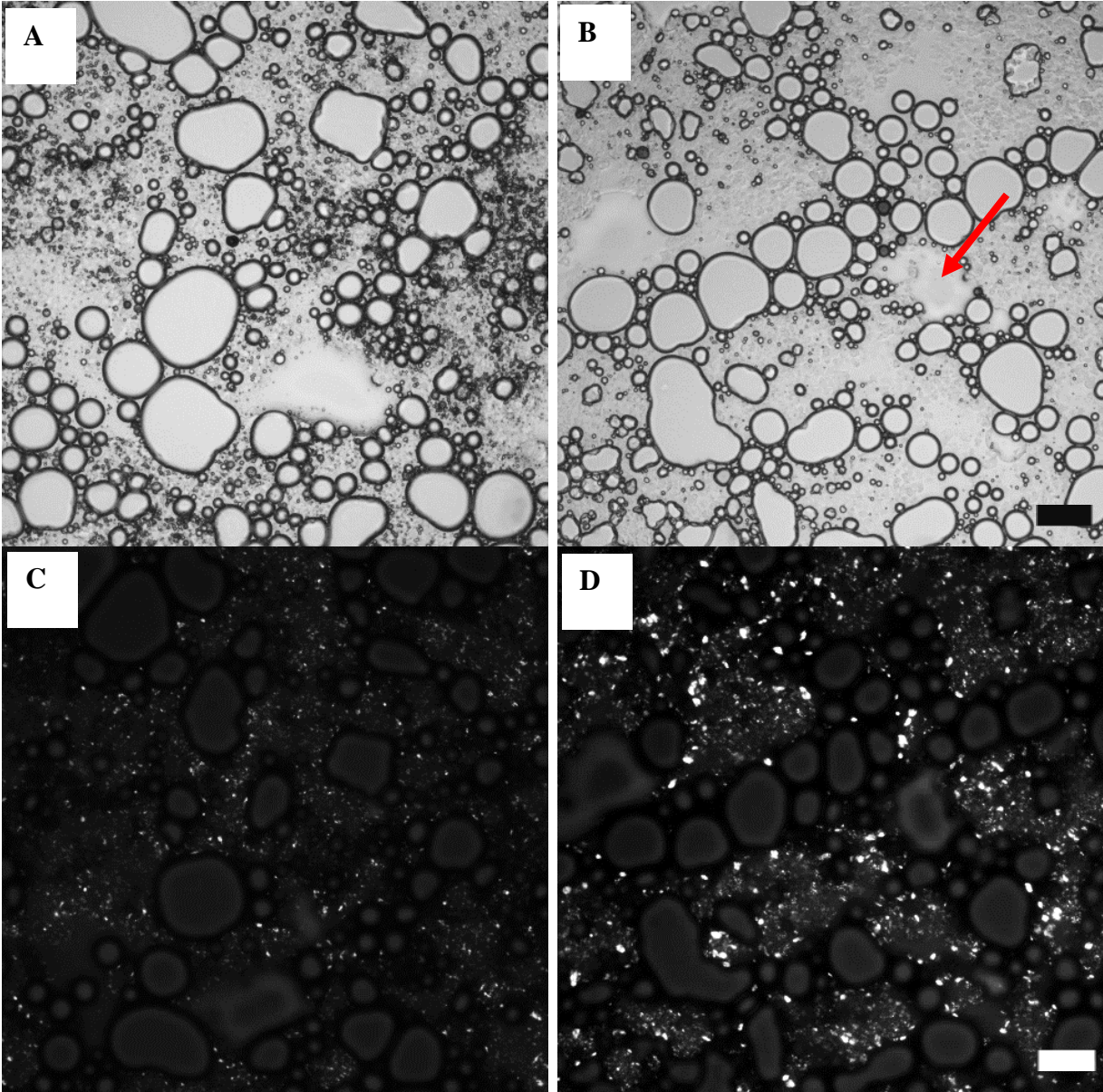


Figure A 13. Microstructure of PGPR-F emulsion in condition 2 – SGF taken in brightfield and polarized light microscopy at 25 °C at 30 minutes (A, C), and 60 minutes (B, D). Scale bars = 50 μm .

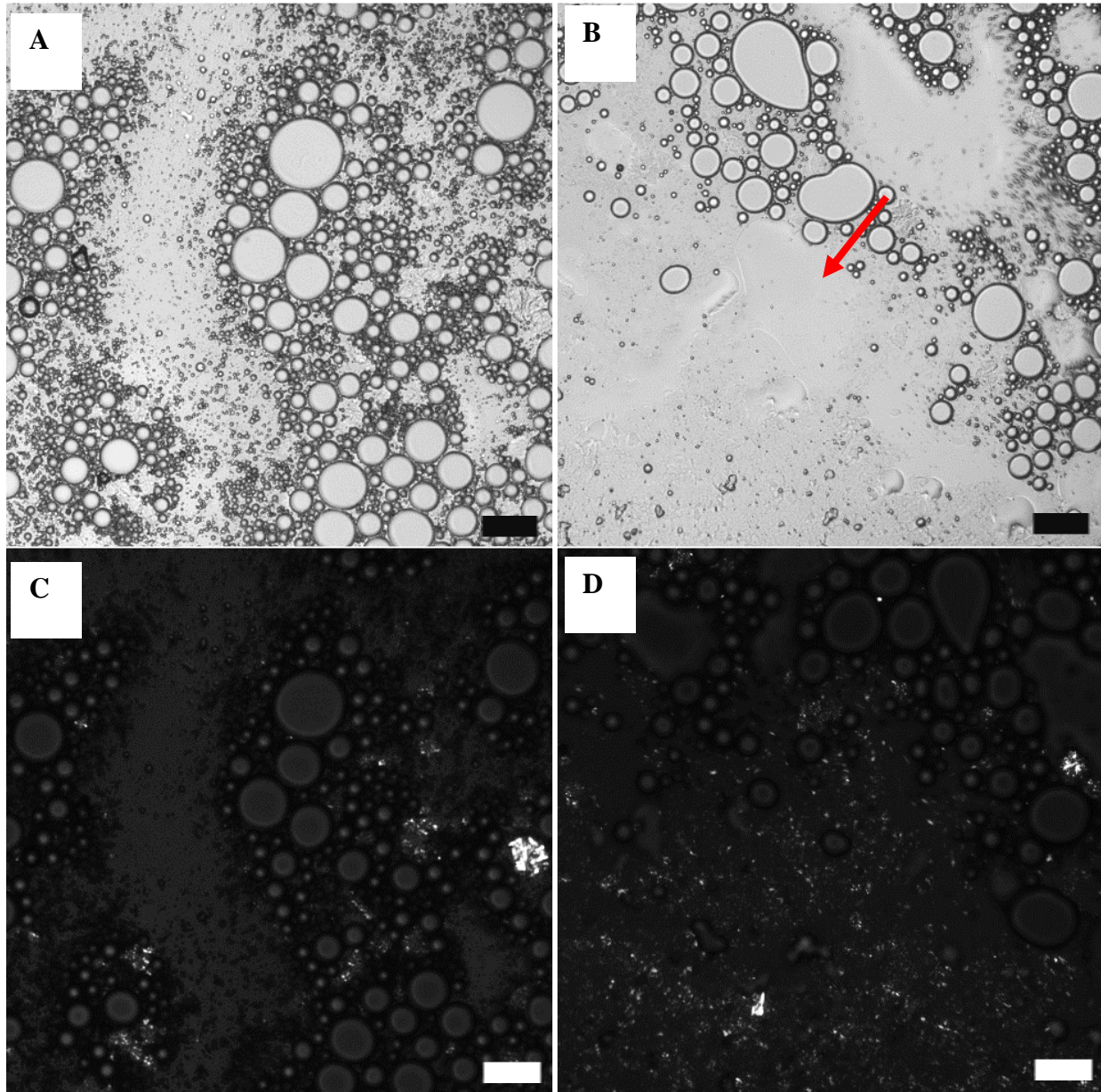


Figure A 14. Microstructure of PGPR-F emulsion in condition 2 – SIF taken in brightfield and polarized light microscopy at 25 °C at 30 minutes (A, B), and 60 minutes (B, D). Scale bars = 50 μm.

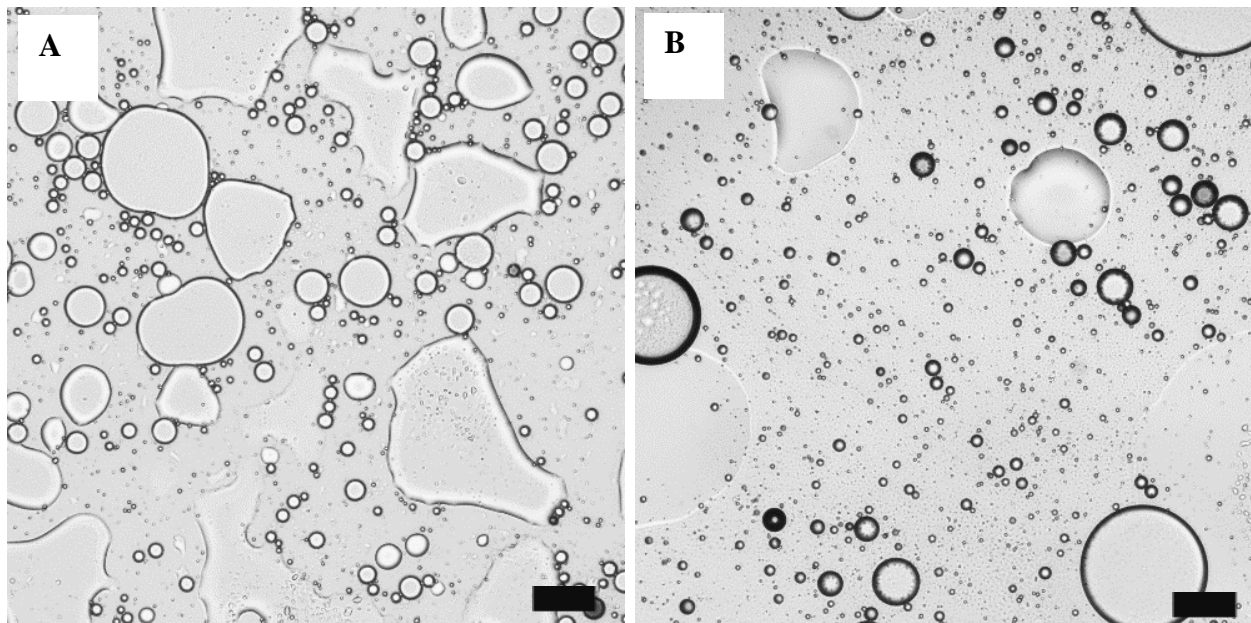


Figure A 15. Microstructure of PGPR emulsion in condition 2 – SGF taken in brightfield and polarized light microscopy at 25 °C at 30 minutes (A, B), and 60 minutes (B, D). Scale bars = 50 μm.

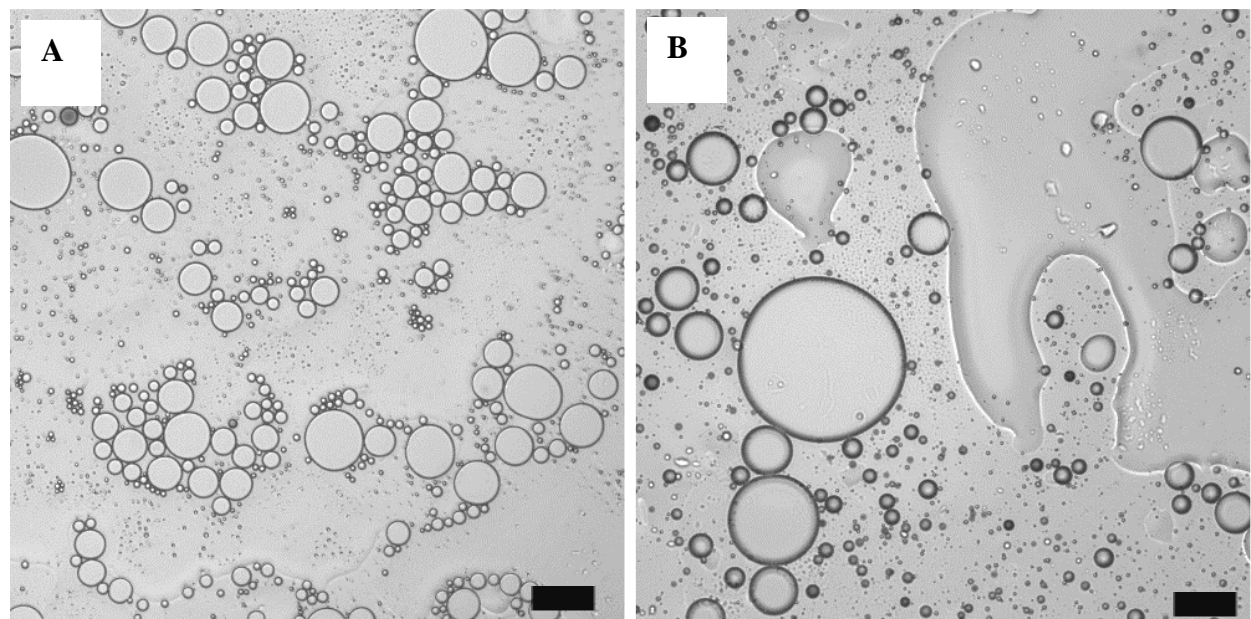


Figure A 16. Microstructure of PGPR emulsion in condition 2 – SIF taken in brightfield and polarized light microscopy at 25 °C at 30 minutes (A, B), and 60 minutes (B, D). Scale bars = 50 μm.

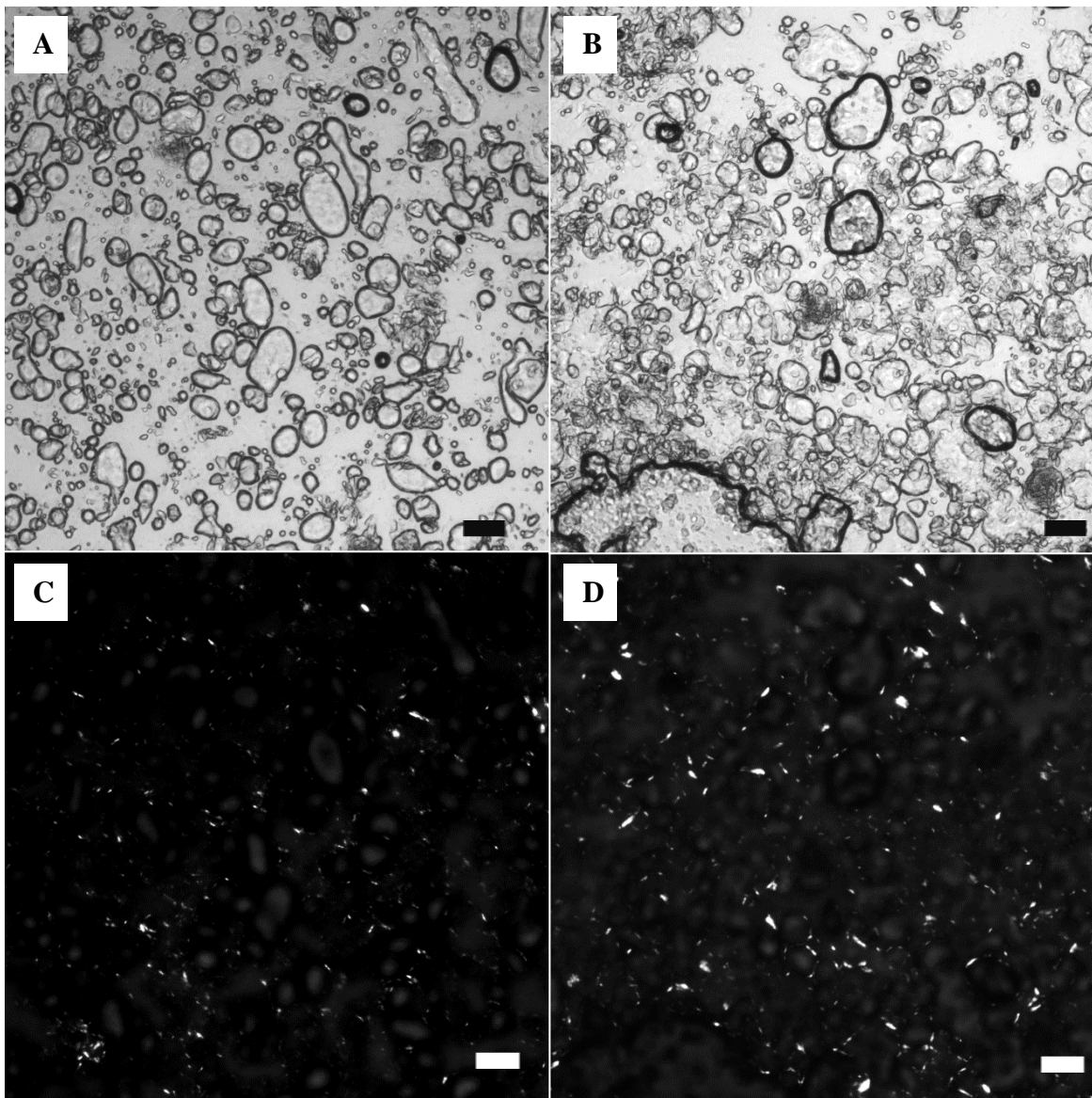


Figure A 17. Microstructure of GMS emulsion in condition 3 – SGF taken in brightfield and polarized light microscopy at 25 °C at 30 minutes (A, B), and 60 minutes (B, D). Scale bars = 50 μm.

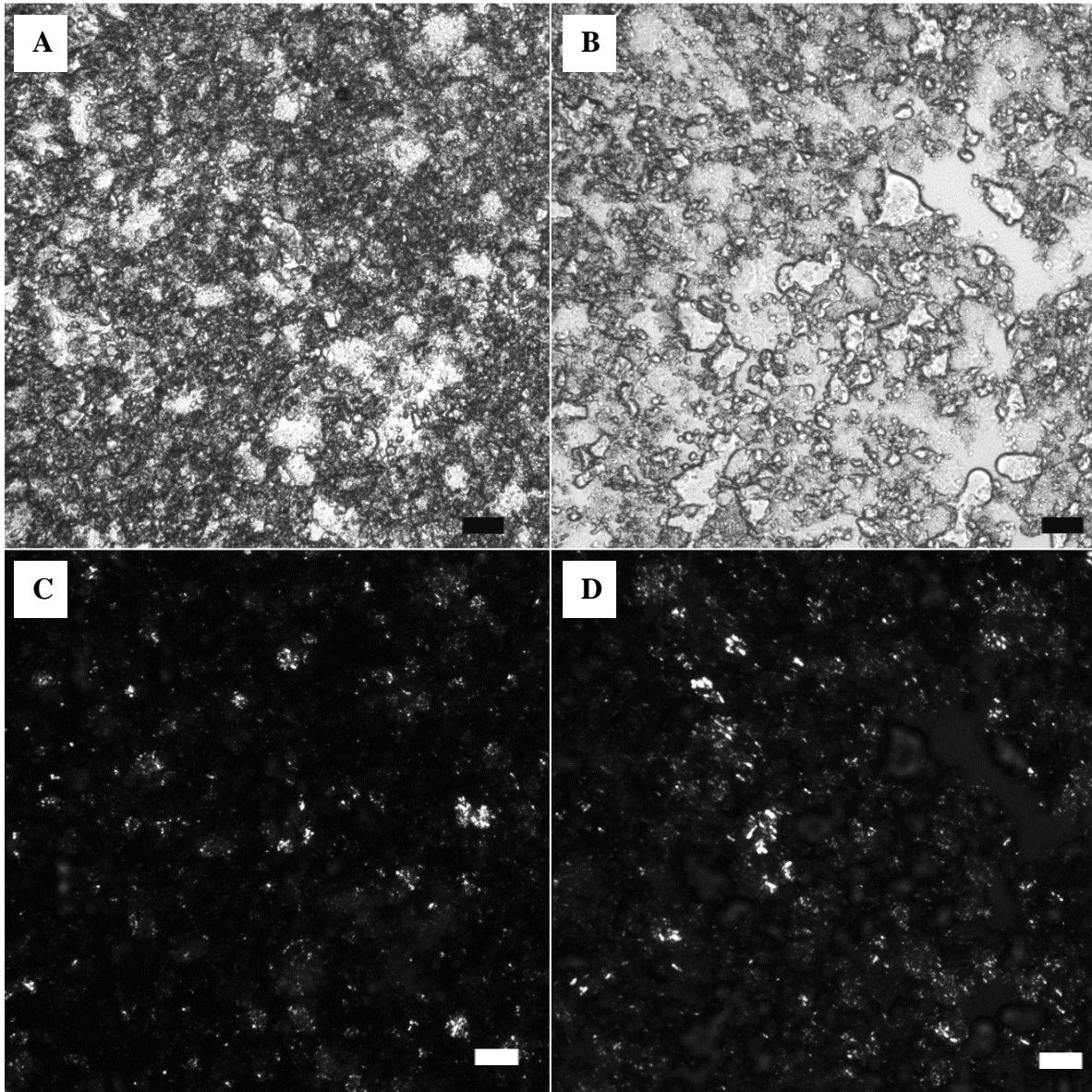


Figure A 18. Microstructure of GMO-F emulsion in condition 3 – SGF taken in brightfield and polarized light microscopy at 25 °C at 30 minutes (A, B), and 60 minutes (B, D). Scale bars = 50 μm .

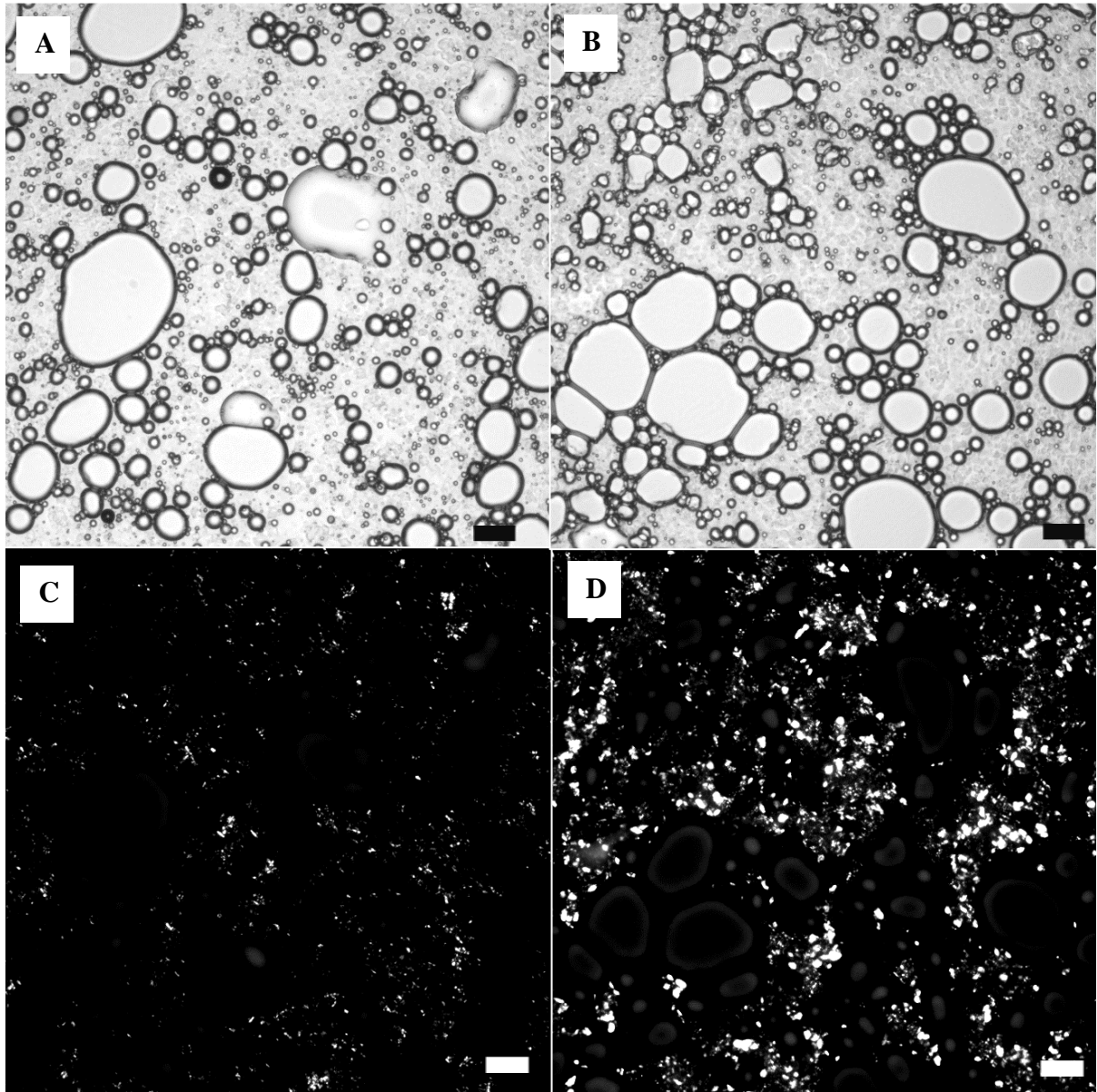


Figure A 19. Microstructure of PGPR-F emulsion in condition 3 – SGF taken in brightfield and polarized light microscopy at 25 °C at 30 minutes (A, B), and 60 minutes (B, D). Scale bars = 50 μm .

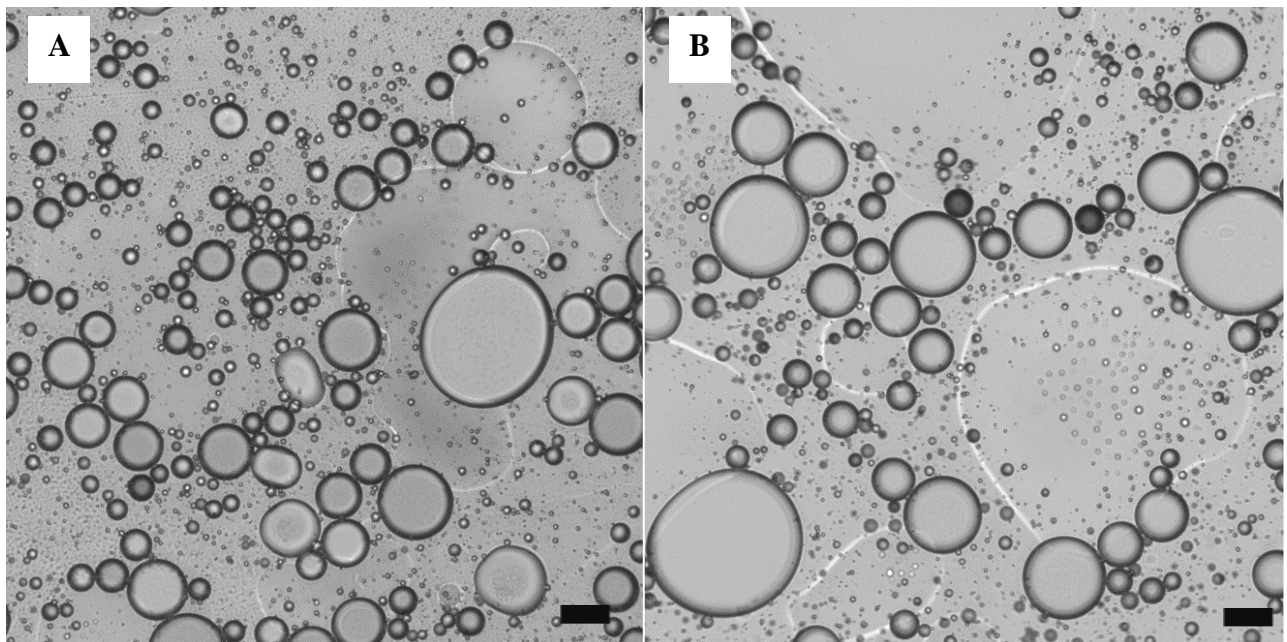


Figure A 20. Microstructure of PGPR emulsion in condition 3 – SGF taken in brightfield and polarized light microscopy at 25 °C at 30 minutes (A, B), and 60 minutes (B, D). Scale bars = 50 μm .

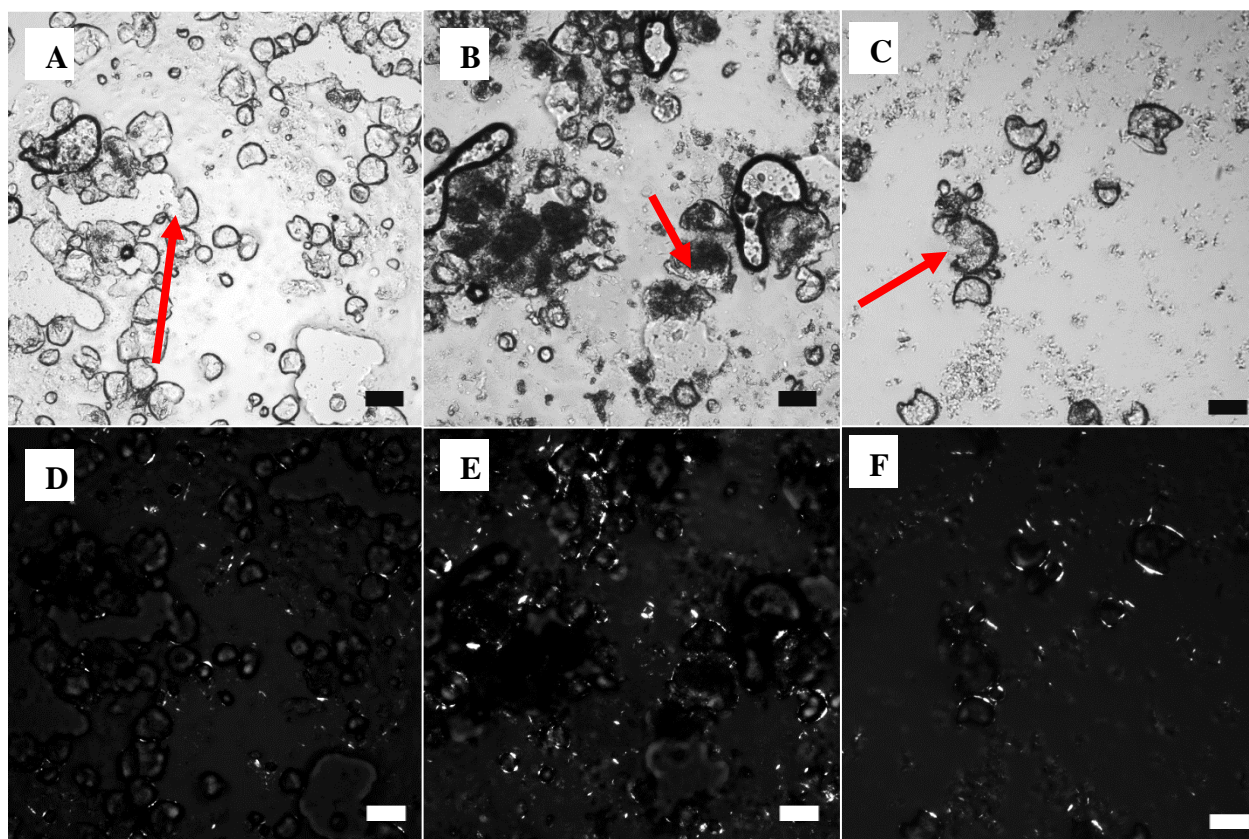


Figure A 21. Microstructure of GMS emulsion in condition 3 – SIF taken in brightfield and polarized light microscopy at 25 °C at 30 minutes (A, D), 60 minutes (B, E), and 120 minutes (C, F). Scale bars = 50 μm .

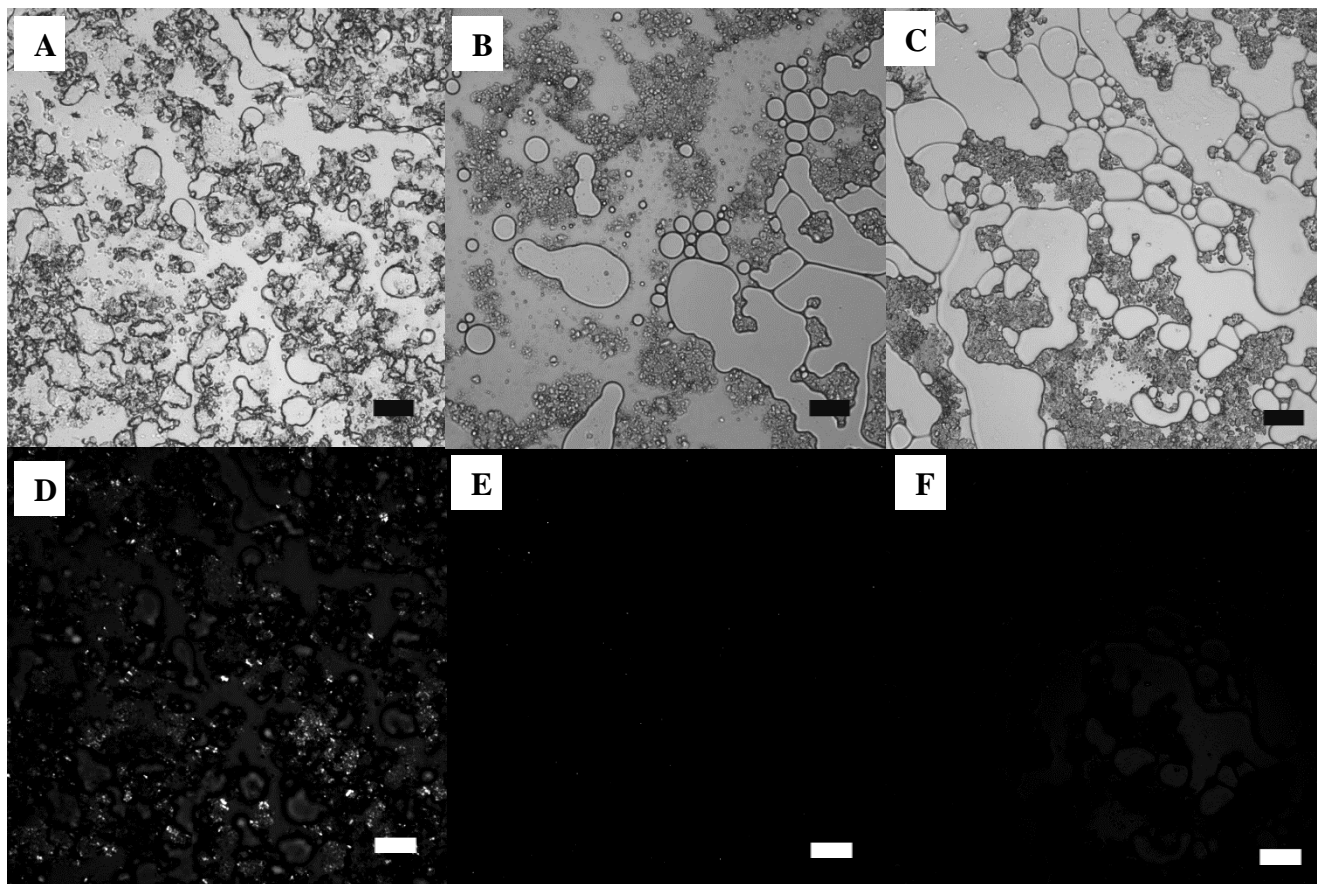


Figure A 22. Microstructure of GMO-F emulsion in condition 3 – SIF taken in brightfield and polarized light microscopy at 25 °C at 30 minutes (A, D), 60 minutes (B, E), and 120 minutes (C, F). Scale bars = 50 μ m.

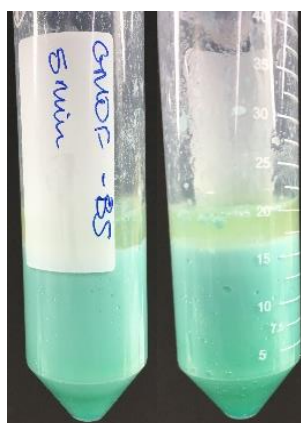


Figure A 23. GMO-F destabilization via condition 3 – SIF showing separation of an oil layer.

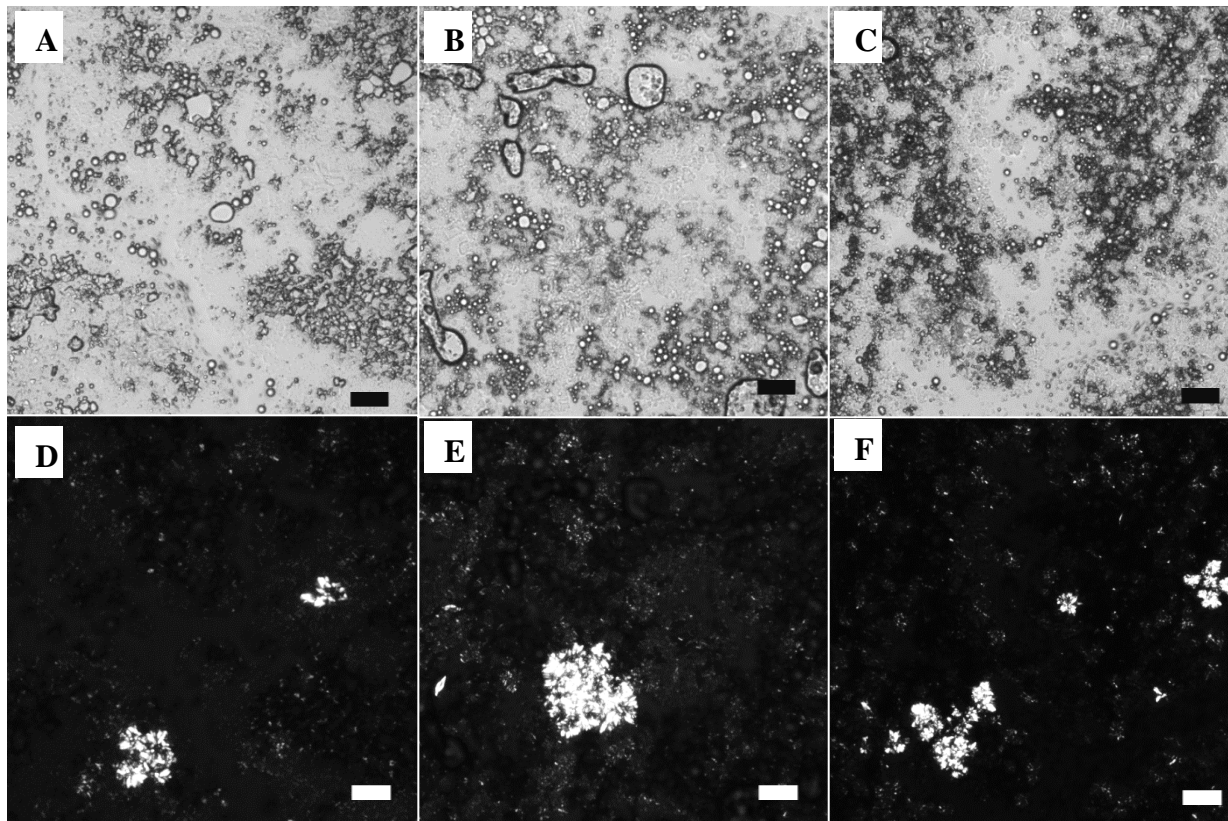


Figure A 24. Microstructure of PGPR-F emulsion in condition 3 – SIF taken in brightfield and polarized light microscopy at 25 °C at 30 minutes (A, D), 60 minutes (B, E), and 120 minutes (C, F). Scale bars = 50 μ m.

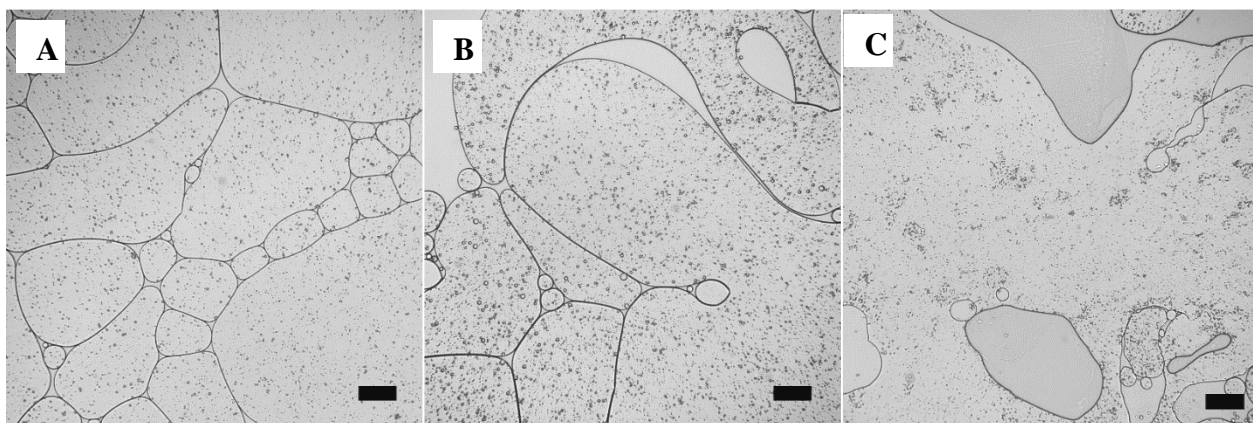


Figure A 25. Microstructure of PGPR emulsion in condition 3 – SIF taken in brightfield and polarized light microscopy at 25 °C at 30 minutes (A, D), 60 minutes (B, E), and 120 minutes (C, F). Scale bars = 50 μ m.

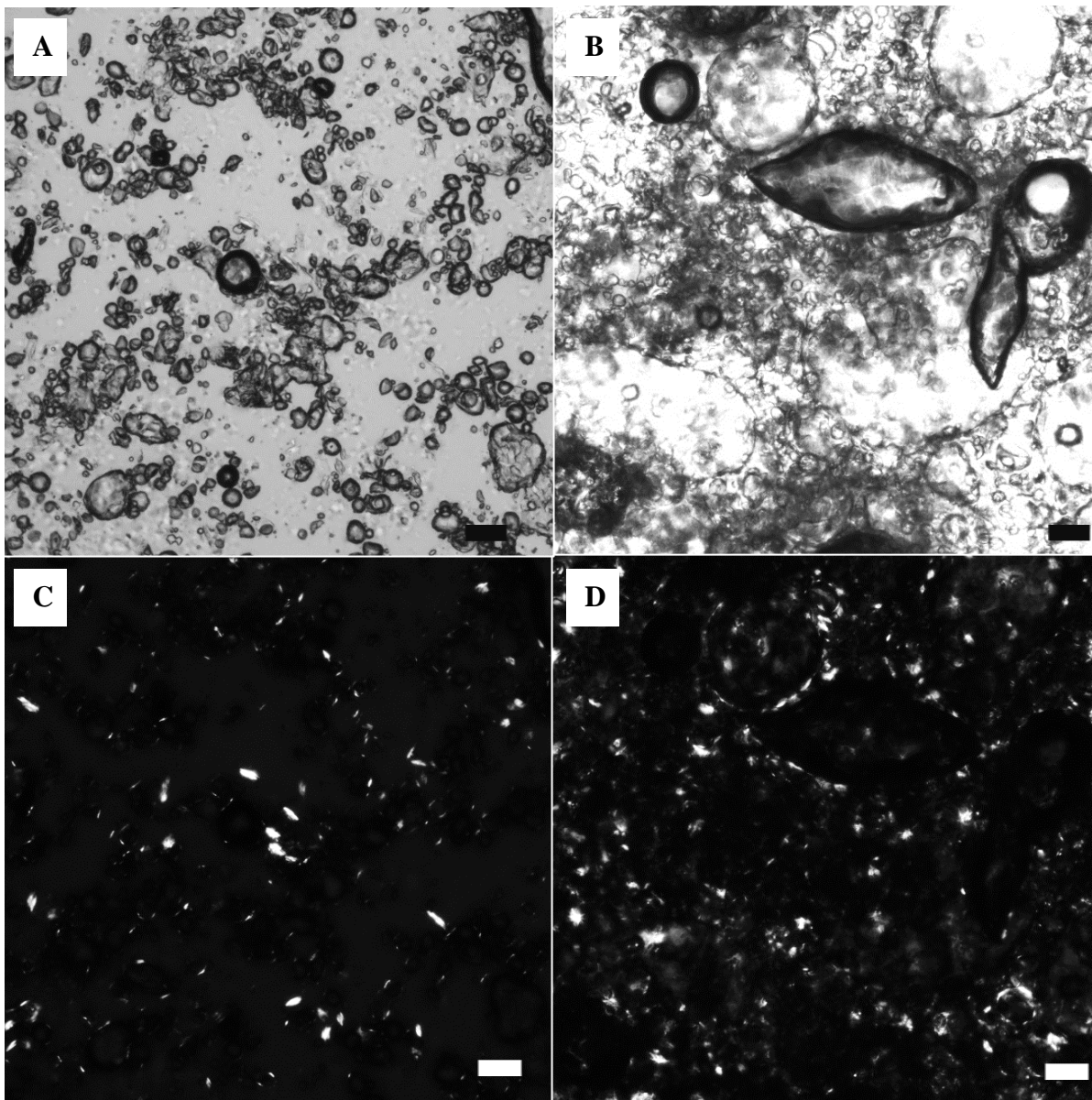


Figure A 26. Microstructure of GMS emulsion in SGF taken in brightfield and polarized light microscopy at 25 °C at 30 minutes (A, C), 60 minutes (B, D). Scale bars = 50 μm .

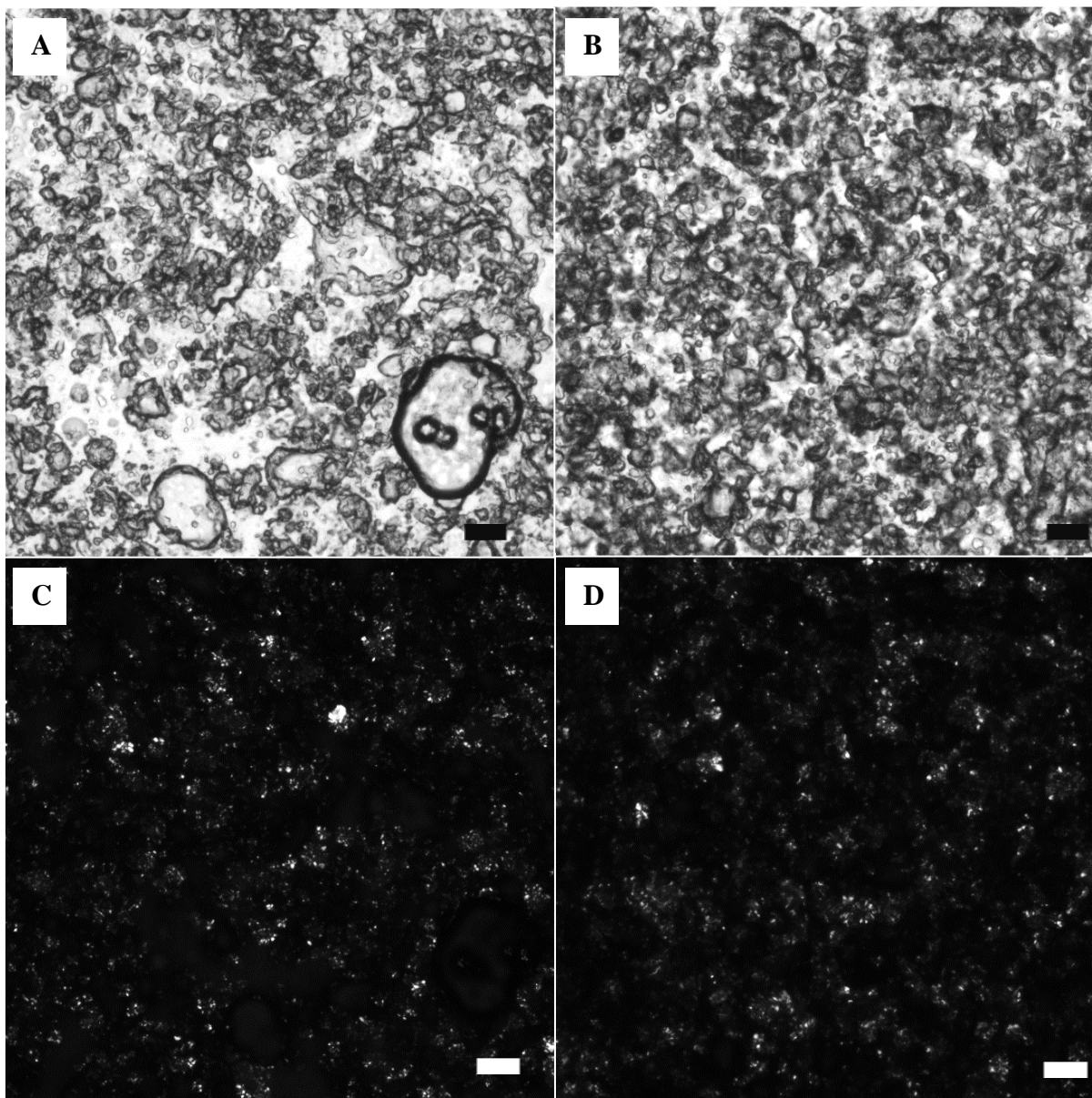


Figure A 27. Microstructure of GMO-F emulsion in SGF taken in brightfield and polarized light microscopy at 25 °C at 30 minutes (A, C), 60 minutes (B, D). Scale bars = 50 μm .

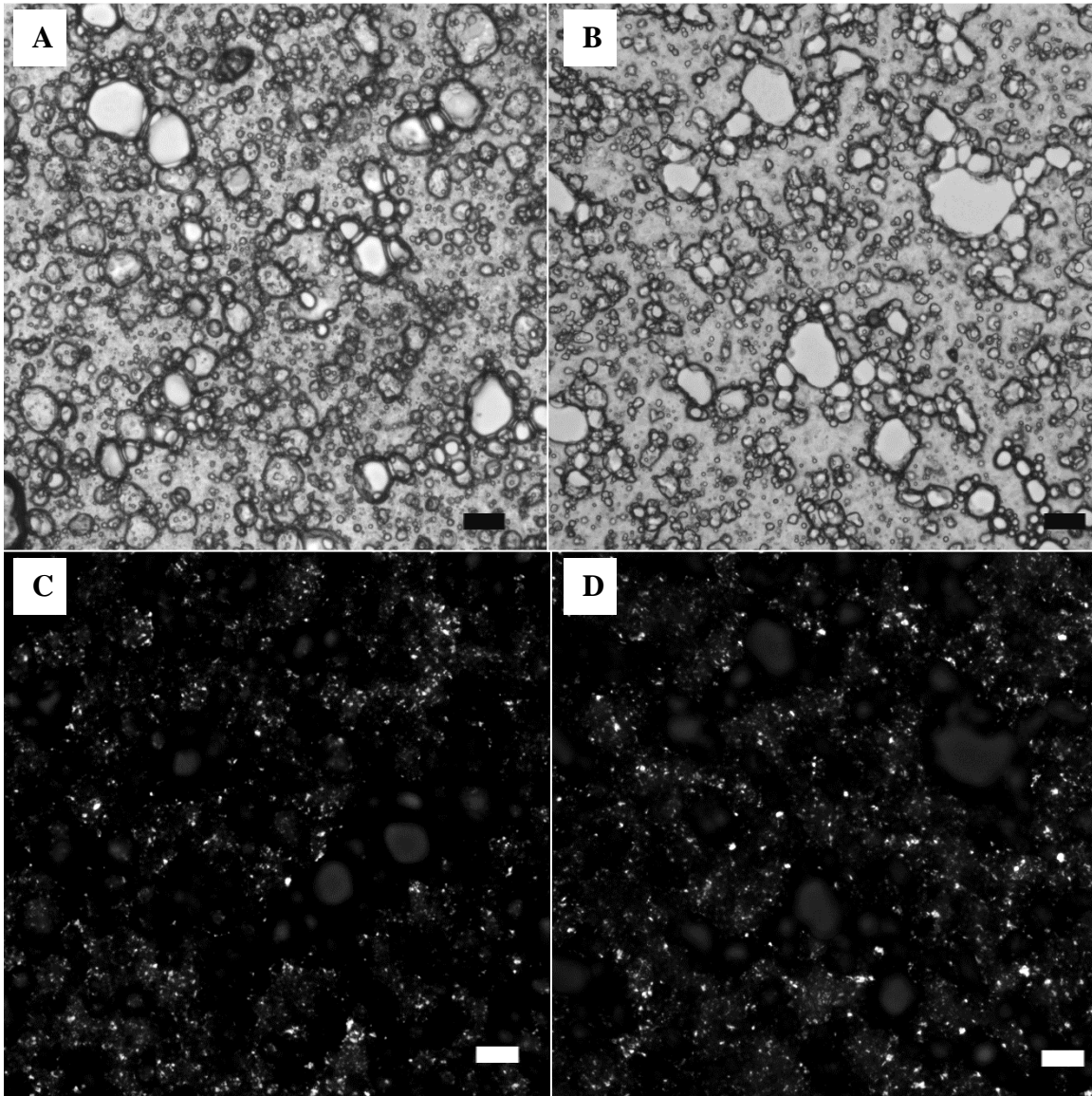


Figure A 28. Microstructure of PGPR-F emulsion in SGF taken in brightfield and polarized light microscopy at 25 °C at 30 minutes (A, C), 60 minutes (B, D). Scale bars = 50 μm .

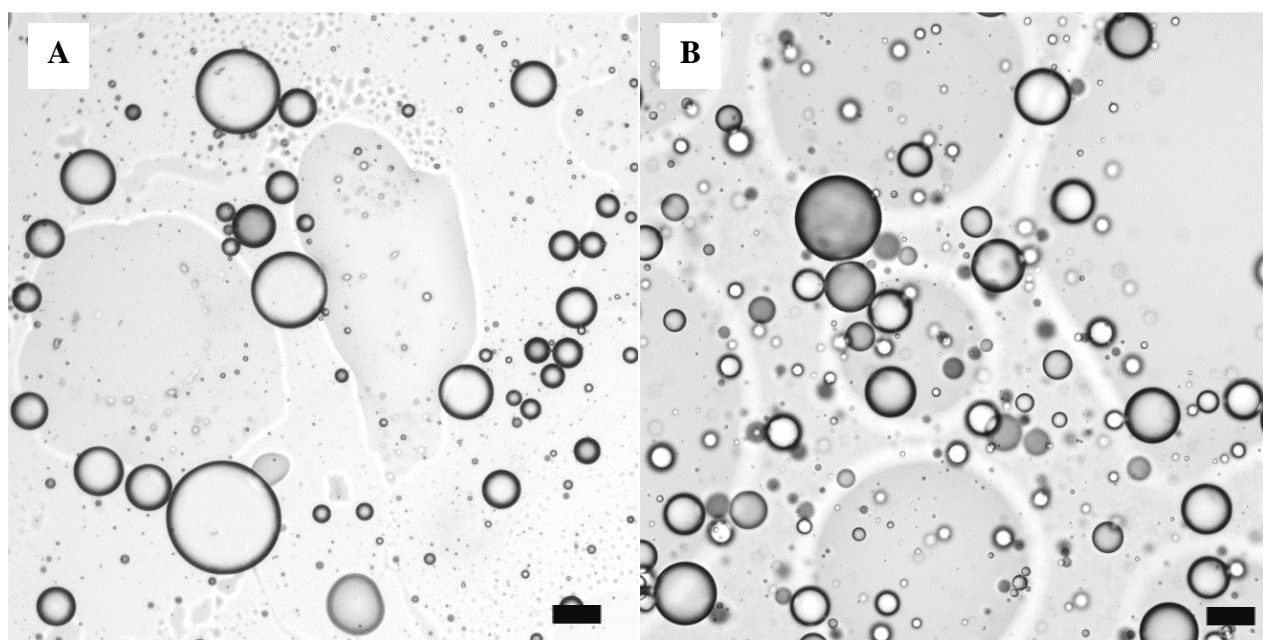


Figure A 29. Microstructure of PGPR emulsion in SGF taken in brightfield and polarized light microscopy at 25 °C at 30 minutes (A), 60 minutes (B). Scale bars = 50 μm .

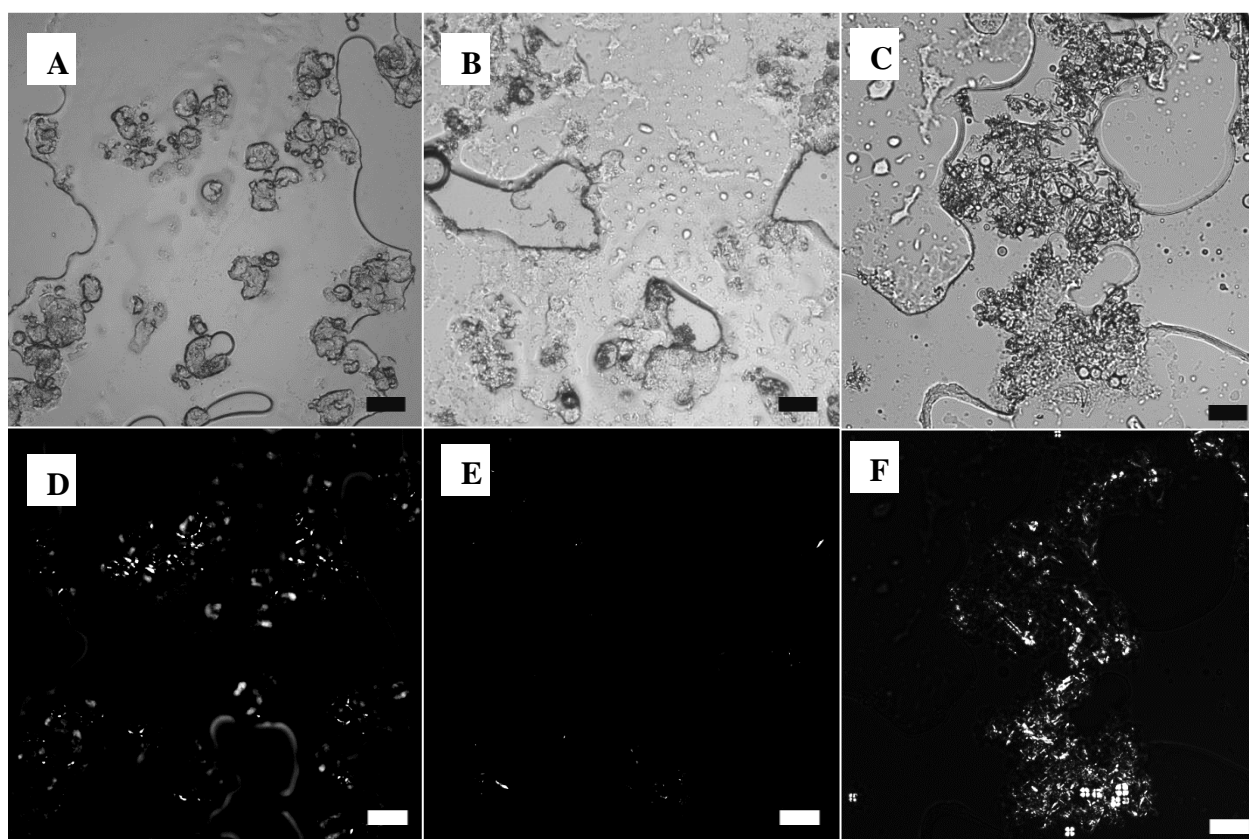


Figure A 30. Microstructure of GMS emulsion in SIF taken in brightfield and polarized light microscopy at 25 °C at 30 minutes (A, D), 60 minutes (B, E), and 120 minutes (C, F). Scale bars = 50 μm .

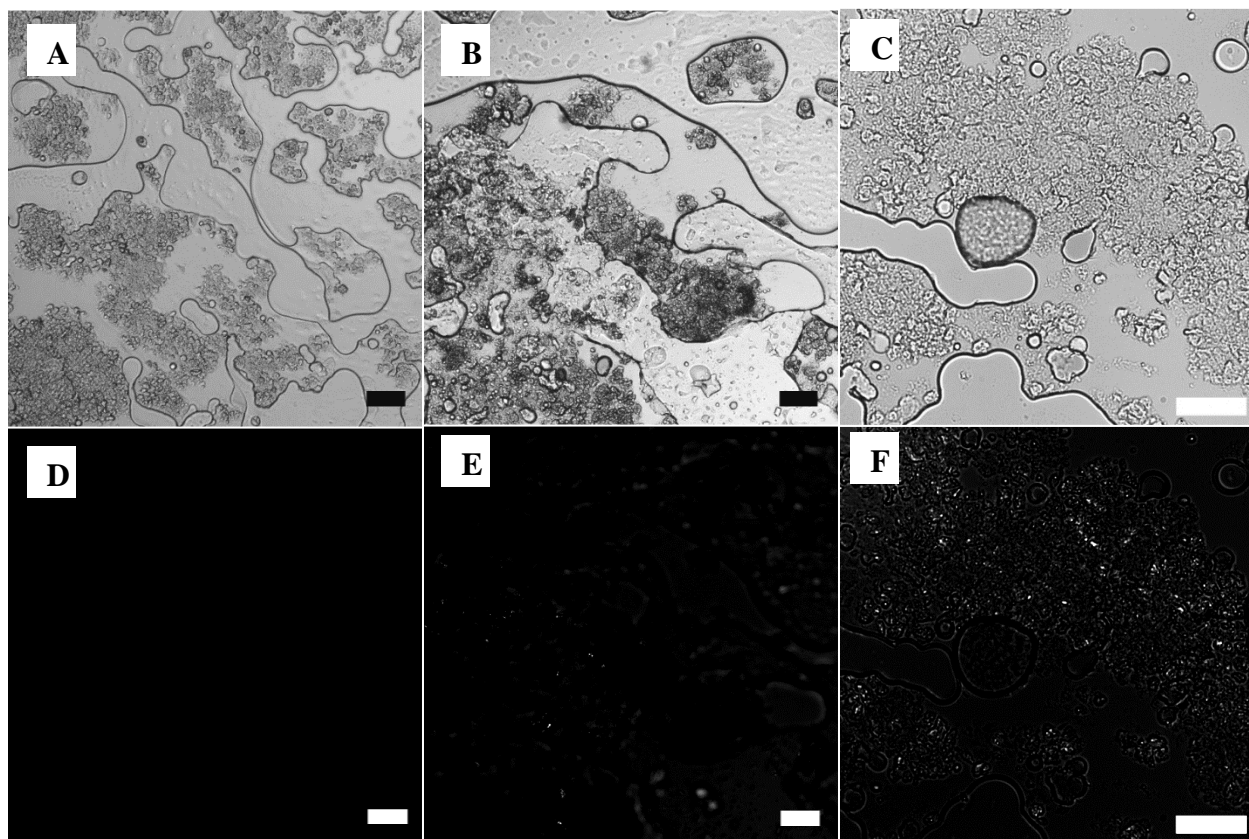


Figure A 31. Microstructure of GMO-F emulsion in SIF taken in brightfield and polarized light microscopy at 25 °C at 30 minutes (A, D), 60 minutes (B, E), and 120 minutes (C, F). Scale bars = 50 μm .

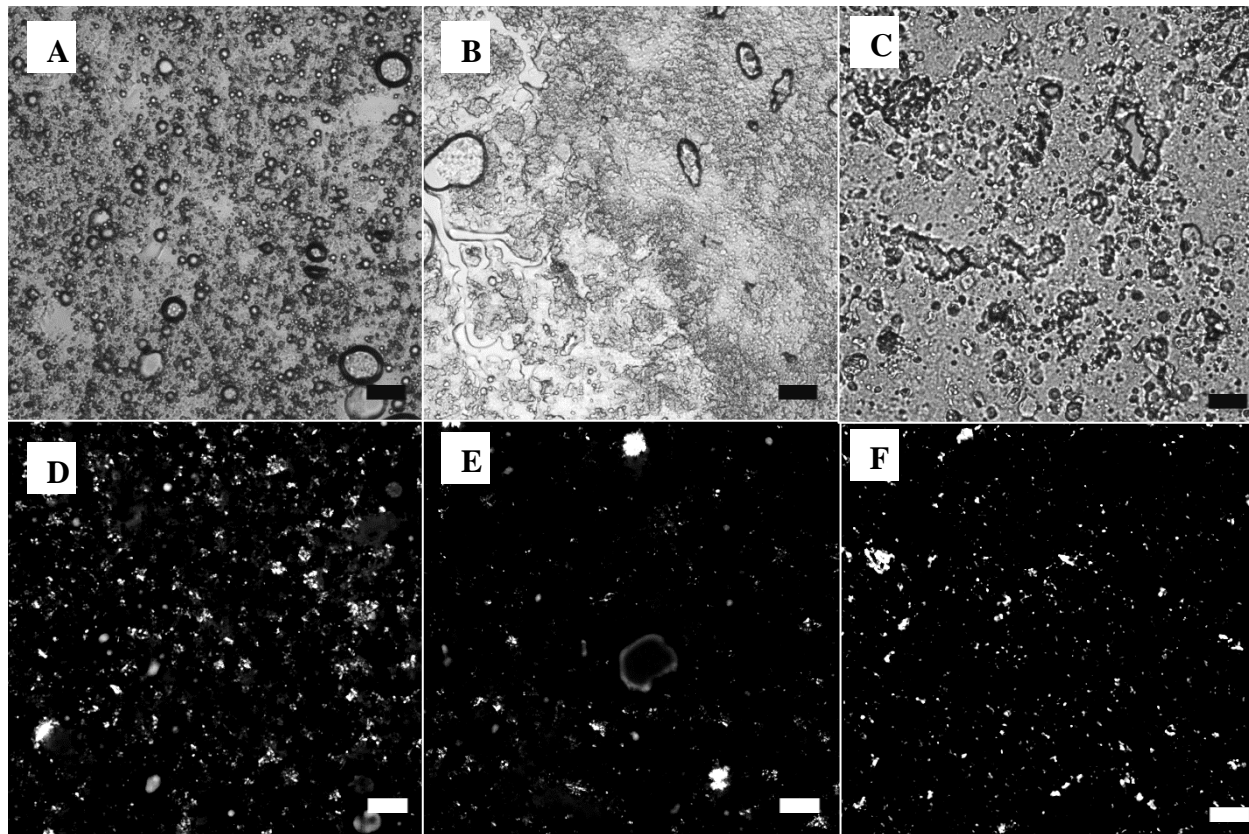


Figure A 32. Microstructure of PGPR-F emulsion in SIF taken in brightfield and polarized light microscopy at 25 °C at 30 minutes (A, D), 60 minutes (B, E), and 120 minutes (C, F). Scale bars = 50 μm .

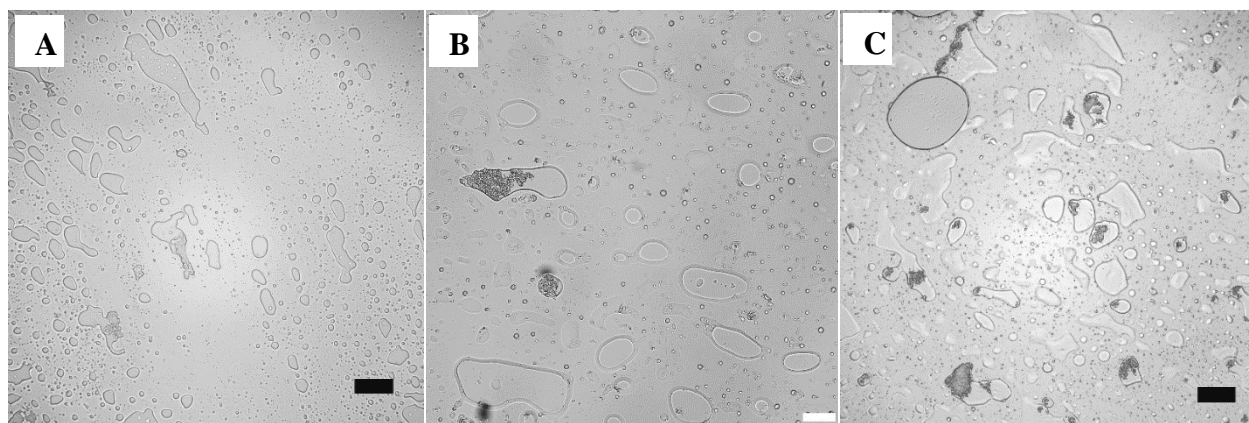


Figure A 33. Microstructure of PGPR emulsion in SIF taken in brightfield and polarized light microscopy at 25 °C at 30 minutes (A), 60 minutes (B), and 120 minutes (C). Scale bars = 50 μm .

References

- (1) McClements, D. J. Emulsion Design to Improve the Delivery of Functional Lipophilic Components. *Annu. Rev. Food Sci. Technol.* **2010**, *1* (1), 241–269.
- (2) Le Révérend, B. J. D.; Taylor, M. S.; Norton, I. T. Design and application of water-in-oil emulsions for use in lipstick formulations. *Int. J. Cosmet. Sci.* **2011**, *33* (3), 263–268.
- (3) Frelichowska, J.; Bolzinger, M. A.; Valour, J. P.; Mouaziz, H.; Pelletier, J.; Chevalier, Y. Pickering w/o emulsions: Drug release and topical delivery. *Int. J. Pharm.* **2009**, *368* (1–2), 7–15.
- (4) Nadin, M.; Rousseau, D.; Ghosh, S. Fat crystal-stabilized water-in-oil emulsions as controlled release systems. *LWT - Food Sci. Technol.* **2014**, *56* (2), 248–255.
- (5) Bhatti, H. S.; Khalid, N.; Uemura, K.; Nakajima, M.; Kobayashi, I. Formulation and characterization of food grade water-in-oil emulsions encapsulating mixture of essential amino acids. *Eur. J. Lipid Sci. Technol.* **2017**, *119* (6).
- (6) Rousseau, D. Fat crystals and emulsion stability - A review. *Food Res. Int.* **2000**, *33* (1), 3–14.
- (7) *Food Lipids - Chemistry, Nutrition, and Biotechnology*, 3rd ed.; Akoh, C. C., Min, B. D., Eds.; CRC Press, 2002.
- (8) Pickering, S. U. Emulsions. *J. Chem Soc.* **1907**, *91*, 2001–2021.
- (9) Pawlik, A.; Kurukji, D.; Norton, I.; Spyropoulos, F. Food-grade Pickering emulsions stabilised with solid lipid particles. *Food Funct.* **2016**, *7* (6), 2712–2721.
- (10) Corstens, M. N.; Berton-Carabin, C. C.; Kester, A.; Fokkink, R.; van den Broek, J. M.; de Vries, R.; Troost, F. J.; Masclee, A. A. M.; Schroën, K. Destabilization of multilayered interfaces in digestive conditions limits their ability to prevent lipolysis in emulsions. *Food Struct.* **2017**, *12* (2017), 54–63.
- (11) Frasc-Melnik, S.; Norton, I. T.; Spyropoulos, F. Fat-crystal stabilised w/o emulsions for controlled salt release. *J. Food Eng.* **2010**, *98* (4), 437–442.
- (12) Corstens, M. N.; Berton-Carabin, C. C.; Elichiry-Ortiz, P. T.; Hol, K.; Troost, F. J.; Masclee, A. A. M.; Schroën, K. Emulsion-alginate beads designed to control in vitro intestinal lipolysis: Towards appetite control. *J. Funct. Foods* **2017**, *34* (2017), 319–328.
- (13) Corstens, M. N.; Berton-Carabin, C. C.; Schroën, K.; Viau, M.; Meynier, A. Emulsion encapsulation in calcium-alginate beads delays lipolysis during dynamic in vitro digestion. *J. Funct. Foods* **2018**, *46* (December 2017), 394–402.
- (14) Muschiolik, G.; Dickinson, E. Double Emulsions Relevant to Food Systems: Preparation, Stability, and Applications. *Compr. Rev. Food Sci. Food Saf.* **2017**, *16* (3), 532–555.
- (15) Frasc-Melnik, S.; Spyropoulos, F.; Norton, I. T. W1/O/W2 double emulsions stabilised by fat crystals - Formulation, stability and salt release. *J. Colloid Interface Sci.* **2010**, *350* (1), 178–185.
- (16) Regan, J. O.; Mulvihill, D. M. Water soluble inner aqueous phase markers as indicators of the encapsulation properties of water-in-oil-in-water emulsions stabilized with sodium caseinate. *Food Hydrocoll.* **2009**, *23* (8), 2339–2345.
- (17) Raviadaran, R.; Ng, M. H.; Manickam, S.; Chandran, D. Ultrasound-assisted water-in-palm oil nano-emulsion: Influence of polyglycerol polyricinoleate and NaCl on its stability. *Ultrason. Sonochem.* **2019**, *52* (August 2018), 353–363.
- (18) Minekus, M.; Alming, M.; Alvito, P.; Ballance, S.; Bohn, T.; Bourlieu, C.; Carrière, F.; Boutrou, R.; Corredig, M.; Dupont, D.; et al. A standardised static *in vitro* digestion

- method suitable for food – an international consensus. *Food Funct.* **2014**, 5 (6), 1113–1124.
- (19) Golding, M.; Wooster, T. J. The influence of emulsion structure and stability on lipid digestion. *Current Opinion in Colloid and Interface Science*. April 2010, pp 90–101.
 - (20) McClements, D. J. Encapsulation, protection, and release of hydrophilic active components: Potential and limitations of colloidal delivery systems. *Advances in Colloid and Interface Science*. Elsevier 2015, pp 27–53.
 - (21) Andrade, J. Food-based multiple emulsions as carriers of bioactive compounds: interactions at the interface and physical and chemical changes during in vitro digestion. **2016**, 124.
 - (22) Hemar, Y.; Cheng, L. J.; Oliver, C. M.; Sanguansri, L.; Augustin, M. Encapsulation of resveratrol using Water-in-Oil-in-Water double emulsions. *Food Biophys.* **2010**, 5 (2), 120–127.
 - (23) Tamnak, S.; Mirhosseini, H.; Tan, C. P.; Tabatabaee Amid, B.; Kazemi, M.; Hedayatnia, S. Encapsulation properties, release behavior and physicochemical characteristics of water-in-oil-in-water (W/O/W) emulsion stabilized with pectin-pea protein isolate conjugate and Tween 80. *Food Hydrocoll.* **2016**, 61, 599–608.
 - (24) Griffin, W. C. Classification of surface-active agents by “HLB.” *J. Soc. Cosmet. Chem.* **1949**, 1, 311–326.
 - (25) Bregni, C. The Studies on Hydrophilic-Lipophilic Balance (HLB): Sixty Years after William C . Griffin ’ s Pioneer Work (1949-2009) The Studies on Hydrophilic-Lipophilic Balance (HLB): Sixty Years. **2016**, 24 (January 2009), 702–708.
 - (26) Binks, B. P. *Particles as surfactants similarities and differences*.
 - (27) Rafanan, R.; Rousseau, D. Effect of shear and interfacial fat crystallization on release of water-soluble dye from water-in-oil emulsions. *Lwt* **2019**, 105 (December 2018), 400–407.
 - (28) Han, L.; Wang, T. Preparation of glycerol monostearate from glycerol carbonate and stearic acid. *RSC Adv.* **2016**, 6 (41), 34137–34145.
 - (29) Alison, L.; Rühs, P. A.; Tervoort, E.; Teleki, A.; Zanini, M.; Isa, L.; Studart, A. R. Pickering and Network Stabilization of Biocompatible Emulsions Using Chitosan-Modified Silica Nanoparticles. *Langmuir* **2016**, 32 (50), 13446–13457.
 - (30) Pantoja-Romero, W. S.; Estrada-López, E. D.; Picciani, P. H. S.; Oliveira, O. N.; Lachter, E. R.; Pimentel, A. S. Efficient molecular packing of glycerol monostearate in Langmuir monolayers at the air-water interface. *Colloids Surfaces A Physicochem. Eng. Asp.* **2016**, 508, 85–92.
 - (31) Carrillo-Navas, H.; Fouconnier, B.; Vernon-Carter, E. J.; Alvarez-Ramírez, J. Shear rheology of water/glycerol monostearate crystals in canola oil dispersions interfaces. *Colloids Surfaces A Physicochem. Eng. Asp.* **2013**, 436, 215–224.
 - (32) Talele, P.; Sahu, S.; Mishra, A. K. Physicochemical characterization of solid lipid nanoparticles comprised of glycerol monostearate and bile salts. *Colloids Surfaces B Biointerfaces* **2018**, 172 (May), 517–525.
 - (33) Lupi, F. R.; Gabriele, D.; de Cindio, B. Effect of Shear Rate on Crystallisation Phenomena in Olive Oil-Based Organogels. *Food Bioprocess Technol.* **2012**, 5 (7), 2880–2888.
 - (34) Lutton E. S. Review of the Polymorphism of : Saturated Chains of Unequal Length. *J. Am. Chem. Soc.* **1950**, 276–281.
 - (35) Vereecken, J.; Meeussen, W.; Foubert, I.; Lesaffer, A.; Wouters, J.; Dewettinck, K.

- Comparing the crystallization and polymorphic behaviour of saturated and unsaturated monoglycerides. *Food Res. Int.* **2009**, *42* (10), 1415–1425.
- (36) Milak, S.; Zimmer, A. Glycerol monooleate liquid crystalline phases used in drug delivery systems. *International Journal of Pharmaceutics*. Elsevier B.V. January 30, 2015, pp 569–587.
- (37) Zeng, F.; Ning, Z.; Wang, Y.; Yang, B.; Liu, H. Application of enzymatic synthesized glycerol monooleate in the manufacture of low fat ice cream. *J. Food Biochem.* **2012**, *36* (1), 116–121.
- (38) Orfanakis, A.; Hatzakis, E.; Kanaki, K.; Pergantis, S. A.; Rizos, A.; Dais, P. Characterization of polyglycerol polyricinoleate formulations using NMR spectroscopy, mass spectrometry and dynamic light scattering. *JAOCS, J. Am. Oil Chem. Soc.* **2013**, *90* (1), 39–51.
- (39) Márquez, A. L.; Medrano, A.; Panizzolo, L. A.; Wagner, J. R. Effect of calcium salts and surfactant concentration on the stability of water-in-oil (w/o) emulsions prepared with polyglycerol polyricinoleate. *J. Colloid Interface Sci.* **2010**, *341* (1), 101–108.
- (40) Su, J.; Flanagan, J.; Hemar, Y.; Singh, H. Synergistic effects of polyglycerol ester of polyricinoleic acid and sodium caseinate on the stabilisation of water-oil-water emulsions. *Food Hydrocoll.* **2006**, *20* (2-3 SPEC. ISS.), 261–268.
- (41) Tran, T.; Green, N. L.; Ghosh, S.; Rousseau, D. Encapsulation of water-in-oil emulsion droplets within crystal spheroids. *Colloids Surfaces A Physicochem. Eng. Asp.* **2017**, *524*, 1–7.
- (42) Ribeiro, A. P. B.; Grimaldi, R.; Gioielli, L. A.; Gonçalves, L. A. G. Zero trans fats from soybean oil and fully hydrogenated soybean oil: Physico-chemical properties and food applications. *Food Res. Int.* **2009**, *42* (3), 401–410.
- (43) Yang, Y.; Fang, Z.; Chen, X.; Zhang, W.; Xie, Y.; Chen, Y.; Liu, Z.; Yuan, W. An Overview of Pickering Emulsions: Solid-Particle Materials, Classification, Morphology, and Applications. *Front. Pharmacol.* **2017**, *8*, 287.
- (44) Rousseau, D. Trends in structuring edible emulsions with Pickering fat crystals. *Current Opinion in Colloid and Interface Science*. August 2013, pp 283–291.
- (45) Hodge, S. M.; Rousseau, D. Continuous-phase fat crystals strongly influence water-in-oil emulsion stability. *J. Am. Oil Chem. Soc.* **2005**, *82* (3), 159–164.
- (46) Ghosh, S.; Tran, T.; Rousseau, D. Comparison of pickering and network stabilization in water-in-oil emulsions. *Langmuir* **2011**, *27* (11), 6589–6597.
- (47) Johansson, D.; Bergenståhl, B. Sintering of fat crystal networks in oil during post-crystallization processes. *J. Am. Oil Chem. Soc.* **1995**, *72* (8), 911–920.
- (48) Ghosh, S.; Rousseau, D. Fat crystals and water-in-oil emulsion stability. *Current Opinion in Colloid and Interface Science*. October 2011, pp 421–431.
- (49) rick Rousseau, D. *Fat crystals and emulsion stability D a review*.
- (50) Rafatullah, M.; Sulaiman, O.; Hashim, R.; Ahmad, A. Adsorption of methylene blue on low-cost adsorbents: A review. *Journal of Hazardous Materials*. May 2010, pp 70–80.
- (51) Selvam, S.; Sarkar, I. Bile salt induced solubilization of methylene blue: Study on methylene blue fluorescence properties and molecular mechanics calculation. *J. Pharm. Anal.* **2017**, *7* (1), 71–75.
- (52) Ghasemi, J. B.; Miladi, M. *Association Equilibrium of Methylene Blue by Spectral Titration and Chemometrics Analysis: A Thermodynamic Study*.
- (53) Balu, S.; Uma, K.; Pan, G. T.; Yang, T. C. K.; Ramaraj, S. K. Degradation of methylene

- blue dye in the presence of visible light using SiO₂@ α -Fe₂O₃ nanocomposites deposited on SnS₂ flowers. *Materials (Basel)*. **2018**, *11* (6).
- (54) Berneth, H. Azine Dyes. In *Ullmann's Encyclopedia of Industrial Chemistry*; Wiley-VCH Verlag GmbH & Co. KGaA: Weinheim, Germany, 2008.
- (55) Douaire, M.; Di Bari, V.; Norton, J. E.; Sullo, A.; Lillford, P.; Norton, I. T. Fat crystallisation at oil-water interfaces. *Adv. Colloid Interface Sci.* **2014**, *203*, 1–10.
- (56) Kurukji, D.; Pichot, R.; Spyropoulos, F.; Norton, I. T. Interfacial behaviour of sodium stearyllactylate (SSL) as an oil-in-water pickering emulsion stabiliser. *J. Colloid Interface Sci.* **2013**, *409*, 88–97.
- (57) Zafeiri, I.; Smith, P.; Norton, I. T.; Spyropoulos, F. Fabrication, characterisation and stability of oil-in-water emulsions stabilised by solid lipid particles: The role of particle characteristics and emulsion microstructure upon Pickering functionality. *Food Funct.* **2017**, *8* (7), 2583–2591.
- (58) Gupta, R.; Rousseau, D. Surface-active solid lipid nanoparticles as Pickering stabilizers for oil-in-water emulsions. *Food Funct.* **2012**, *3* (3), 302–311.
- (59) Di Bari, V.; Macnaughtan, W.; Norton, J.; Sullo, A.; Norton, I. Crystallisation in water-in-cocoa butter emulsions: Role of the dispersed phase on fat crystallisation and polymorphic transition. *Food Struct.* **2017**, *12*, 82–93.
- (60) Ramsden, W. Separation of solids in the surface layers of solutions and “suspensions” - Observations on surface membranes, bubbles, emulsions, and mechanical coagulation. *Proc. R. Soc. London* **1903**, *72* (4), 156–164.
- (61) Melle, S.; Lask, M.; Fuller, G. G. Pickering emulsions with controllable stability. *Langmuir* **2005**, *21* (6), 2158–2162.
- (62) Frascch-Melnik, S.; Norton, I. T.; Spyropoulos, F. Fat-crystal stabilised w/o emulsions for controlled salt release. *J. Food Eng.* **2010**, *98* (4), 437–442.
- (63) Frelichowska, J.; Bolzinger, M. A.; Pelletier, J.; Valour, J. P.; Chevalier, Y. Topical delivery of lipophilic drugs from o/w Pickering emulsions. *Int. J. Pharm.* **2009**, *371* (1–2), 56–63.
- (64) Hendry, C.; Farley, A.; McLafferty, E.; Johnstone, C. The digestive system: part 2. *Nurs. Stand.* **2014**, *28* (25), 37.
- (65) Zhang, Z.; Mei, L.; Feng, S.-S. Paclitaxel drug delivery systems. *Expert Opin. Drug Deliv.* **2013**, *10* (3), 325–340.
- (66) Johnstone, C.; Hendry, C.; Farley, A.; McLafferty, E. The digestive system: part 1. *Nurs. Stand.* **2014**, *28* (24), 37–45.
- (67) Zhang, R.; Zhang, Z.; Zhang, H.; Decker, E. A.; McClements, D. J. Influence of lipid type on gastrointestinal fate of oil-in-water emulsions: In vitro digestion study. *Food Res. Int.* **2015**, *75*, 71–78.
- (68) Amara, S.; Patin, A.; Giuffrida, F.; Wooster, T. J.; Thakkar, S. K.; Bénarouche, A.; Poncin, I.; Robert, S.; Point, V.; Molinari, S.; et al. In vitro digestion of citric acid esters of mono- and diglycerides (CITREM) and CITREM-containing infant formula/emulsions. *Food Funct.* **2014**, *5* (7), 1409–1421.
- (69) Giang, T. M.; Gaucel, S.; Brestaz, P.; Anton, M.; Meynier, A.; Trelea, I. C.; Le Feunteun, S. Dynamic modeling of in vitro lipid digestion: Individual fatty acid release and bioaccessibility kinetics. *Food Chem.* **2016**, *194*, 1180–1188.
- (70) Sarkar, A.; Murray, B.; Holmes, M.; Ettelaie, R.; Abdalla, A.; Yang, X. In vitro digestion of Pickering emulsions stabilized by soft whey protein microgel particles: influence of

- thermal treatment. *Soft Matter* **2016**, *12* (15), 3558–3569.
- (71) Minekus, M.; Alminger, M.; Alvito, P.; Ballance, S.; Bohn, T.; Bourlieu, C.; Carrière, F.; Boutrou, R.; Corredig, M.; Dupont, D.; et al. A standardised static in vitro digestion method suitable for food-an international consensus. *Food Funct.* **2014**, *5* (6), 1113–1124.
- (72) Xiao, J.; Li, Y.; Huang, Q. Recent advances on food-grade particles stabilized Pickering emulsions: Fabrication, characterization and research trends. *Trends in Food Science and Technology*. Elsevier Ltd September 1, 2016, pp 48–60.
- (73) Zhou, Y.; Wang, Q.; Wang, Y.; Xu, H.; Yuan, B.; Li, S.; Liu, H. Biological artificial fluid-induced non-lamellar phases in glyceryl monooleate: The kinetics pathway and its digestive process by bile salts. *Drug Dev. Ind. Pharm.* **2014**, *40* (2), 178–185.
- (74) Venema, K. *The TNO in vitro model of the colon (TIM-2)*; 2015.
- (75) Arranz, E.; Santoyo, S.; Jaime, L.; Fornari, T.; Reglero, G.; Guri, A.; Corredig, M. Improved Bioavailability of Supercritical Rosemary Extract Through Encapsulation in Different Delivery Systems After In Vitro Digestion. *Food Dig.* **2015**, *6* (1–3), 30–37.
- (76) McClements, D. J.; Li, Y. Review of in vitro digestion models for rapid screening of emulsion-based systems. *Food Funct.* **2010**, *1* (1), 32–59.
- (77) Guo, Q.; Bellissimo, N.; Rousseau, D. Effect of Emulsifier Concentration and Physical State on the in Vitro Digestion Behavior of Oil-in-Water Emulsions. *J. Agric. Food Chem.* **2018**, *66* (28), 7496–7503.
- (78) Van Den Enden, J. C.; Waddington, D.; Van Aalst, H.; Van Kralingen, C. G.; Packer, K. J. Rapid determination of water droplet size distributions by PFG-NMR. *J. Colloid Interface Sci.* **1990**, *140* (1), 105–113.
- (79) Giroux, H. J.; Robitaille, G.; Britten, M. Controlled release of casein-derived peptides in the gastrointestinal environment by encapsulation in water-in-oil-in-water double emulsions. *LWT - Food Sci. Technol.* **2016**, *69*, 225–232.
- (80) Rueden, C. T.; Schindelin, J.; Hiner, M. C.; DeZonia, B. E.; Walter, A. E.; Arena, E. T.; Eliceiri, K. W. ImageJ2: ImageJ for the next generation of scientific image data. *BMC Bioinformatics* **2017**, *18* (1), 529.
- (81) Bahtz, J.; Gunes, D. Z.; Syrbe, A.; Mosca, N.; Fischer, P.; Windhab, E. J. Quantification of Spontaneous W/O Emulsification and its Impact on the Swelling Kinetics of Multiple W/O/W Emulsions. *Langmuir* **2016**, *32* (23), 5787–5795.
- (82) Su, J.; Flanagan, J.; Singh, H. Improving encapsulation efficiency and stability of water-in-oil-in-water emulsions using a modified gum arabic (Acacia (sen) SUPER GUM™). *Food Hydrocoll.* **2008**, *22* (1), 112–120.
- (83) Muschiolik, G.; Scherze, I.; Preissler, P.; Weiss, J.; Knoth, A.; Fechner, A. Multiple Emulsions - Preparation and Stability. *Refrig. Food Eng. Process Eur. Masterfoods* **2006**, 37–49.
- (84) Oosterveld, A.; Minekus, M.; Bomhof, E.; Zoet, F. D.; Van Aken, G. A. Effects of inhomogeneity on triglyceride digestion of emulsions using an: In vitro digestion model (Tiny TIM). *Food Funct.* **2016**, *7* (7), 2979–2995.
- (85) Mantovani, R. A.; Pinheiro, A. C.; Vicente, A. A.; Cunha, R. L. In vitro digestion of oil-in-water emulsions stabilized by whey protein nanofibrils. *Food Res. Int.* **2017**, *99*, 790–798.
- (86) Marze, S.; Choimet, M. In vitro digestion of emulsions: Mechanistic and experimental models. *Soft Matter* **2012**, *8* (42), 10982–10993.
- (87) Sarkar, A.; Murray, B.; Holmes, M.; Ettelaie, R.; Abdalla, A.; Yang, X. In vitro digestion

- of Pickering emulsions stabilized by soft whey protein microgel particles: influence of thermal treatment. *Soft Matter* **2016**, *12* (15), 3558–3569.
- (88) Yasmin, R.; Rao, S.; Bremmell, K. E.; Prestidge, C. A. Porous Silica-Supported Solid Lipid Particles for Enhanced Solubilization of Poorly Soluble Drugs. *AAPS J.* **2016**, *18* (4), 876–885.
- (89) Howes, D.; Wilson, R.; James, C. T. The fate of ingested glyceran esters of condensed castor oil fatty acids [polyglycerol polyricinoleate (PGPR)] in the rat. *Food Chem. Toxicol.* **1998**, *36* (9–10), 719–738.
- (90) Aditya, N. P.; Aditya, S.; Yang, H.; Kim, H. W.; Park, S. O.; Ko, S. Co-delivery of hydrophobic curcumin and hydrophilic catechin by a water-in-oil-in-water double emulsion. *Food Chem.* **2015**, *173*, 7–13.
- (91) Werawatganone, P.; Muangsiri, W. Interactions between charged dye indicators and micelles to determine the critical micelle concentration. *Asian J. Pharm. Sci.* **2009**, *4* (4), 221–227.
- (92) Andrade, J.; Wright, A. J.; Corredig, M. In vitro digestion behavior of water-in-oil-in-water emulsions with gelled oil-water inner phases. *Food Res. Int.* **2018**, *105* (November 2017), 41–51.
- (93) Shimoni, G.; Shani Levi, C.; Levi Tal, S.; Lesmes, U. Emulsions stabilization by lactoferrin nano-particles under invitro digestion conditions. *Food Hydrocoll.* **2013**, *33* (2), 264–272.